BASIC PROBLEMS IN THE PHOTOGRAPHIC PHOTOMETRY OF NEBULAE

by

Christopher W. Fraser

A Thesis presented for the Degree of Master of Science in the University of St Andrews

March, 1965

DECLARATION

I hereby declare that the following Thesis is based on the results of experiments carried out by me, that the Thesis is my own composition, and that it has not previously been presented for a Higher Degree. The research was carried out in the University Observatory, St Andrews.

CERTIFICATE

I certify that Christopher W. Fraser has spent four terms at Research Work in the University Observatory, St Andrews, that he has fulfilled the conditions of Ordinance No. 51 (St Andrews) and that he is qualified to submit the accompanying Thesis in application for the degree of M. Sc.

PREFACE

This thesis is concerned with problems which arise in photographic surface photometry using the Cassegrain Schmidt Telescopes at the University Observatory, St Andrews. Photometric investigations are made of different types of objects with telescopes of different apertures and focal lengths, but with approximately the same focal ratios, in order to study the photometric effects in different types of surface distributions and to assess critically the effect of resolution on the photometry. Basic to the problem is the question of the photographic process with its inherent difficulties and limitations. For this reason, detailed consideration is given to those aspects of the process which are particularly relevant to the problem of extended surface photometry. The question of the effect of resolution arose naturally in the course of the investigation when it was possible to extend the observational programme from the 17-inch to the 37-inch telescope when it was commissioned for observational work. This thesis does not aim to obtain a comprehensive set of parameters to describe the surface distributions of a large number of objects, nor to make theoretical deductions from the data, as the emphasis in the work is primarily on basic problems in surface photometry and techniques of data reduction.

CONTENTS

CHAPTER I

1. Introduction

Photometry deals with the measurement of the amount of light falling on a receptor which has the ability to retain information for subsequent reference. The basic assumption in most photometric calculations is the inverse square law for the rate of flow of radiant energy across a unit area of a spherical surface surrounding a point source. The receptor used may take two forms - a photographic plate or a photo-multiplier tube, and it is according to which receptor is used that the terms photographic and photo-electric photometry are derived. Although in recent times there has been an increase in the amount of astronomical photo-electric observations, the ability of a photographic plate to record a great deal of information over its entire surface area makes it an ideal receptor for work on the photometry of extended fields of objects. This feature can only be used effectively if the surface photometry over large areas of the photographic plate can be performed accurately. Success in this direction depends upon a thorough understanding of the photographic process itself and the difficulties which arise in practice. It is therefore appropriate to discuss problems arising in the photographic process, with specific reference to the requirements of extended surface photometry.

2. The Photographic Process

The photographic plate consists of a sheet of flat glass upon which is coated a layer of gelatin. This gelatin layer, which has many silver halide grains suspended within it, is called the emulsion. The silver halide grains are photo-chemically sensitive to light, and when they are exposed to a light source, a latent image is formed, which is then much more readily reduced to silver than unexposed grains when both are subjected to a reducing agent. The agent is called developer and the process development. After a certain development time, the unexposed grains begin to reduce, and the process is then usually terminated by fixation, which removes the remaining silver halide, thus leaving a metallic silver image. The development and fixation of a plate is called processing. The main principle in photographic photometry is the ability of the plate to reproduce equal photographic effects under identical conditions. These conditions, however, are extremely stringent, as the following example will show:-

Supposing we obtain images of galaxies on a photographic plate and then attempt to obtain an identical plate on some future occasion, the chances of so doing are extremely remote because of possible differences in

(i) The temperature and humidity of the air surrounding the plate during exposure;

(ii) The exact properties of the emulsion on each plate;

(iii) Atmospheric conditions;

(iv) The focus of the telescope due to variations in air temperature;

(v) The temperatures and strengths of the developing and fixing solutions;

(vi) The times of development and fixation;

(vii) The method of agitation of the developer;

(viii) The effective times of the telescope exposures;

It will be useful to consider the processing effects in greater detail. The strength of the developing solution depends upon the number of plates it has processed and the length of time for which it has been in use. Hence it would appear that the most satisfactory conditions would exist if a fresh solution were available for each plate. Suppose we attempt to overcome this by obtaining exposures on different nights at the same zenith distance in order to eliminate possible differences in absorption, and then process both plates simultaneously in fresh developer. The resulting photographic effect would still not be identical, because the latent image undergoes certain changes after exposure, and, in this particular case, one image is a multiple of 24 hours older than the other.

Since the necessary development time decreases with increasing temperature of the developing solution, we conclude that even if the development of each plate were undertaken at identical times after exposure, both the temperature of the

developer and the time of development must be identical. Furthermore, the methods of agitation of the solutions are of prime importance.

Tests which will be mentioned at a later stage in the thesis have shown that the dish method of development is extremely unsatisfactory. It consists of immersing the plate in a dish which contains some developer, and agitating the developer in contact with the emulsion by a series of systematic rocking movements of the dish. These movements, however, do not take account of the fact that standing waves may be set up in the liquid, resulting in considerable motion of the developer over one area of the plate, while scarcely any motion may be present in other areas. After many trials, it was found that the only satisfactory way of obtaining a reasonably consistent form of agitation was by means of brush development. In this method, a large badger hair brush was used to draw the developer over the whole plate area, and the movement of the brush was made as gentle and repetitive as possible. Another source of uneven development arises from the fact that it is not physically possible to immerse the entire plate area in the developer simultaneously. These difficulties of immersion could produce faint streaks on the plate due to some areas having been in contact with the developer for slightly longer than others. This effect can be minimized by immersing the plate in water immediately prior to immersion in the developer.

A feature of the photographic plate arises from the fact that it is an integrating device. If a star, assumed to be a point source is imaged on the surface of the emulsion by a high quality objective of large aperture, the light gathered by the objective may be focussed on a spot of smaller dimensions than the silver halide grains. The diagram illustrates how the pencil of rays may be considered as a cone with its vertex touching the emulsion surface. The silver halide grain receiving the light is by no means perfectly absorbing, and a considerable fraction of the total incident radiant energy is transmitted or diffused in all directions and neighbouring particles of the emulsion are consequently affected. Further more, the reaction of a silver halide grain to photons induces certain reactions amongst adjacent grains or clumps of grains. After development, the point will appear as a fuzzy spot (the circle of diffusion), the greater the energy falling on the emulsion, the greater is the diameter of the circle of diffusion.

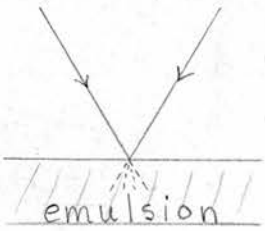

3. <u>The Characteristic Curve</u>

In order to obtain photometric data from a plate, it is necessary to know the relationship between the exposure given to an area of the emulsion, and the transparency produced over that area after processing. The exposure is the quantity of incident light falling on the plate, and is denoted by E. For normal incidence, $E = \int_0^t I\,dt$ or, if I, the intensity of the light, is constant over the time interval, simply It. When

plotting a graph of the density, which is equal to minus the logarithm of the transparency, against exposure, it is convenient to use a logarithmic exposure scale in order to represent the large range of exposure values to which a plate responds. Figure 1 shows the usual result obtained by plotting the density against the logarithm of the exposure, and the curve obtained is called the characteristic curve of the emulsion.

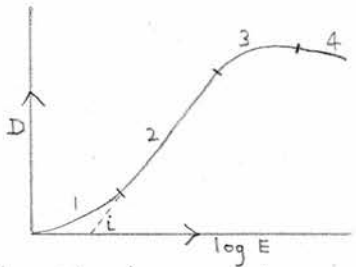

Fig 1. Schematic characteristic curve of a photographic emulsion.

The characteristic curve may be subdivided into the following regions:-

(1) The foot of the curve or the initial period of rising which is essentially a consequence of using the logarithmic exposure scale;

(2) A region containing a point of inflexion, normally called the region of constant slope. On producing this line, the value of the x-intercept is called log i, and this quantity is a measure of the sensitivity of the emulsion;

(3) The shoulder of the curve which is caused by the asymptotic approach to completion shown by most chemical reactions;

(4) The solarization area where the density falls off with increasing exposure. This effect, however, is extremely difficult to produce in practice due to the very high exposure value required.

The calibration of a plate involves constructing the characteristic curve of that plate, and then relating certain densities on the plate to the exposure values which have produced those densities. In this connexion, the characteristic curve is often referred to as the calibration curve.

4. Sensitometry

Sensitometry is concerned with the measurement of sensitivity of photographic materials; the simplest method is to impress upon the plate a series of graduated exposures and then observe which exposure just produces a visible deposit after development. Photometric calibration is the method by which the relation between photographic blackening and intensity is established. An instrument which can give a series of differing yet pre-determined exposures to photographic materials, in such a way that they will be exactly repeatable at any time is called sensitometer. It consists of a light source of constant intensity and a light modulating device. Since the exposure may be varied by changes in either the light intensity or the time of exposure, sensitometers are said to employ either an intensity scale or a time scale.

In the intensity scale method neutral wedges are used and the object is to modify the intensity is a known manner through a wide range without impairing the quality of the transmitted light. The wedge may be continuous, producing a smooth gradation of intensity across the calibration area, or stepped, giving several well-defined areas of constant intensity. The continuous wedge has the advantage that there is no lower limit for the increments chosen for log E, but the disadvantage that the measurements on the exposed on processed strip may be more difficult in the absence of a fiducial mark. A refinement of the continuous wedge is the crossed wedge; in this system the material to be tested is exposed behind the continuous wedge, whose transmission at any point is accurately known, and is then fully developed. The negative obtained is placed over the same wedge, but at right angles to the former position of the wedge, thus making lines of constant density lie at 90^{o} to each other. If another photographic plate is now exposed behind both the wedge and the negative, a sharp boundary which defines the characteristic curve is obtained when the plate is developed.

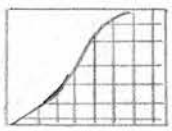

In the time scale method, a time scale is impressed by either continuous or intermittent exposures. The continuous exposure method has the major disadvantage that the light source

must be kept constant throughout the time of exposure. This difficulty would apparently be overcome by the use of intermittent exposures, because any long-period variations in the intensity of the light source would be of minor importance, since they would act over the whole exposed area. Intermittent exposures can be obtained by using a rotating sector, which has different areas cut out of it, as in the diagram; the sector is situated between the light source and the photographic material and a lens images the sector on the photographic plate. In the particular sector illustrated, three rectangular areas would be produced on the photographic plate, each area having a different intensity of light. There is, however, a serious limitation on the use of rotating sectors for calibration purposes, namely that the intermittent exposure is not integrated by photographic materials. The underlying explanation for this phenomenon is reciprocity failure, which is discussed in the next section with specific reference to the step-wedge method of calibration. It is, naturally, of fundamental importance that the intensity of the illumination over the slit area should be uniform.

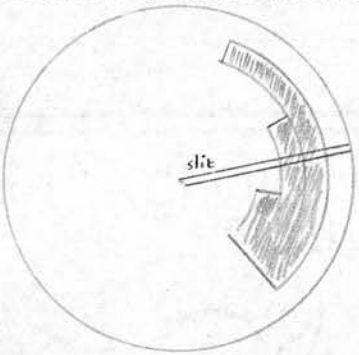

5. Calibrating Step-Wedge

After having noted some of the general techniques used for plate calibration; a detailed account will now be given of the method of calibrating the plates obtained during the course of the work on surface photometry.

The calibrations were made using a Hilger and Watts rhodium step-wedge, with density steps of 0.2, 0.4, 0.6, 0.8, and 1.0, together with clear glass strips at each end, the width of each step being approximately 1.8 mm. The wedge was in the form of an achromatic prism which was mounted in a cell in one corner of a square metal plate; when the metal plate was inserted in the plateholder, light passed through the wedge and on to the photographic plate, the wedge being located almost in contact with the emulsion surface. A schematic illustration of the sensitometer assembly is shown in Figure 2

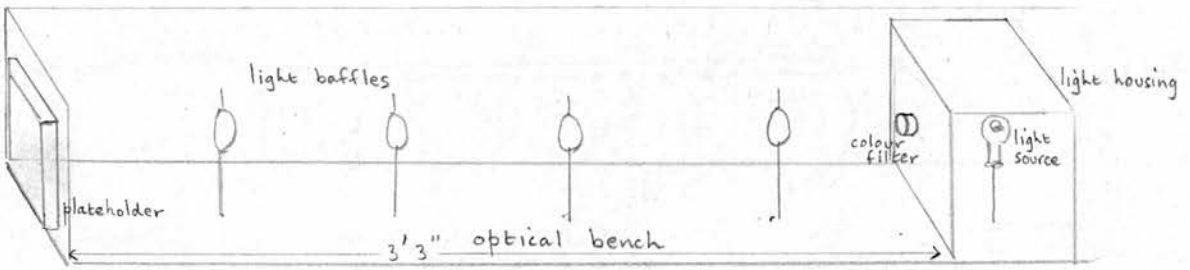

Fig 2. Schematic illustration of sensitometer assembly.

A few of the more important features of the assembly are as follows:- The baffles were inserted in order to prevent light striking the walls of the sensitometer and then being reflected back on to the wedge; a colour filter was inserted at the front of the light-tight housing of the light source in order to raise the colour temperature of the calibrating illumination. These components of the sensitometer were located on an optical bench. The mounting of the lamp was such that the plane of the filament, coiled and shaped like an inverted

capital V, lay along the line drawn from the wedge to the lamp filament in order to reduce the effective area of the source as seen from the wedge. The plateholder assembly, which could be rotated and clamped in positions separated by a right angle, was constructed so that when the dark slide was drawn, the light was incident upon the wedge after passing through a small baffle A approximately twice the size of the wedge thereby avoiding specular reflection near the wedge cell. All surfaces in the assembly were painted matt black in order to reduce to a minimum the amount of reflected light.

After one calibration, the plateholder was rotated through a right angle, the wedge plate being rotated through the same angle in order to re-align the wedge with the baffle A so that another corner of the plate could then be calibrated. The intensity of the lamp was kept as constant as possible by using a power supply of eight volts, taken from two twelve volt high-duty batteries connected in parallel.

Ideal plate calibration could only be obtained if the intensities were produced in exactly the same manner as those from the galaxy on the plate. These conditions are impossible to recreate in the laboratory, but by observing the following precautions, a satisfactory calibration may be obtained. The corners of the plate were masked off during exposure in the telescope and immediately after exposure the mask was removed together with the filter, if any, and the wedge was inserted in

the plateholder and the area of the plate behind the wedge was then exposed in the sensitometer. If a filter had been used during the telescope exposure, it was interposed in the calibrating beam. Although the surrounding conditions of temperature and humidity during calibration should be as close as possible to those encountered during the telescope exposure, this is rather difficult to achieve. However, it is not only desirable but it is possible to overcome an important effect due to the reciprocity failure of the emulsion by making the exposure times of both the telescope and the calibration exposures identical.

Let us suppose that a plate is exposed to radiation of intensity 5 units for a period of 20 minutes on the telescope to give a photographic density on the straight line portion of the characteristic curve. It might be considered that a calibration exposure using a higher intensity of 20 units for a shorter exposure of 5 minutes would produce the same density since in both cases the overall exposure value would be 100 units. However, the photographic effect in each exposure is not the same due to the phenomenon of reciprocity failure of the emulsion; for identical photographic effects for the telescope and calibration exposures, the times should be nearly the same. This is because the density is, in fact, not equal to the product of the intensity and the time, but to the product of intensity and time, the time being raised to a power p, the Schwarzschild index which is usually less than one. Since the

wedge has a clear glass area and a maximum density step of 1.0, this means that the maximum intensity ratio of light reaching the photographic plate is 10:1 and since the sensitivity of the emulsion has a response far in excess of an intensity ratio of 10:1, the corresponding densities produced on the plate will only cover a small portion of the characteristic curve. For this reason, it is necessary to make several exposures identical in time, but with different intensities of the light source, in order to obtain the entire characteristic curve. The first exposure, found by trial, was for a time t such that the resulting densities were on the shoulder of the calibration curve, as in Figure 3.

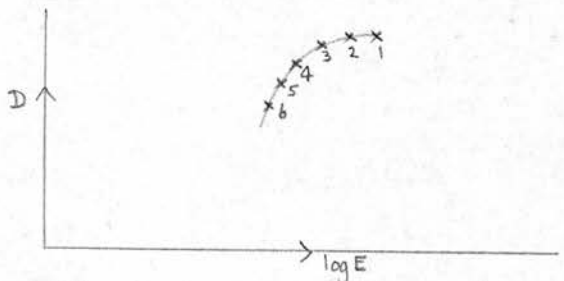

Fig.3. Sketch of a typical set of points resulting from a calibration exposure using the highest light value.

In order to obtain the straight line portion of the curve, we require smaller exposure values. It is possible to take a smaller exposure time in the second calibration such that the first step of the second exposure would correspond to the sixth step of the first exposure, and since the density on the first exposure was 1.0, this would only require an exposure time on the second of t/10. On account of reciprocity failure, this method would fail. Furthermore, an overlap of only one

step in the curves obtained from the first and second exposures would not provide an adequate check on the gradients of the two curves.

Due to these difficulties, the only available method of obtaining the next section of the calibration curve is by reducing the intensity of light reaching the emulsion. This reduction in the intensity could be effected by moving the light source farther away from the emulsion and using the inverse square law to calculate the modified flux, but the length of the optical bench would not permit the use of this method. Therefore, in these calibrations, the light reduction was accomplished by placing neutral density filters into the beam, which were not quite at right angles to the beam in order to prevent multiple reflections occuring between the interposed neutral density filters and other filters nearer the light source. In order to obtain a comparison between the slopes of the resulting curves representing sections of the calibration curve, a neutral density of 0.5 was used. This filter then increased the effective density steps of the wedge by 0.5, thus placing the first step in the second exposure mid-way between the third and fourth steps of the first exposure. On account of uncertainties as to the density of the neutral density filters, the points derived from the second exposure did not always match the slope of the first curve, but it permissible to shift each abscissa by a small amount in order to obtain continuity of the gradient. A third exposure was made using a neutral density

filter of 1.0, in preference to a pair of 0.5 filters. After a fourth exposure in which a neutral density filter of 1.5 was used, a composite characteristic curve was then constructed. These four exposures utilized the four corners of the plate masked during the telescope exposure, and also enabled a quantitative estimation of the uniformity of plate base fog (density produced by development of an unexposed plate) to be made. Although the neutral density filters were stated to have an accuracy of one per cent in transmission over each filter area, they were placed as close as possible to the light source in order to reduce to a minimum any variation in the flux incident upon the wedge due to non-uniformity in transmission.

6. Tube Sensitometers

The step-wedge method of calibration, as described in the previous section, requires a total calibration time which is four times as long as the actual exposure on the telescope. Whereas this is not particularly disadvantageous for short telescope exposures, it is overwhelmingly disadvantageous for longer exposures of an hour or more. For this reason, consideration has been given to an alternative method of plate calibration which would provide a complete coverage of the calibration curve in one exposure.

It is proposed that density spots should be located around the circumference of a circle on the plate corresponding to the 4^{o} angular field of the Schmidt telescopes.

If the order in which the spots were arranged around the circumference were chosen at random, any surface variations in the sensitivity of the emulsion would be smoothed out in obtaining the calibration curve, in much the same way as such variations were averaged by step-wedge calibration in all four corners of the plate. In addition, it is proposed that all the calibrating spots should be impressed on the plate in one exposure, thereby avoiding the difficulties associated with building up the entire calibration curve from segments of the curve obtained with separate exposures in the step-wedge method. In connexion with these proposals, it was decided to investigate the theory, design, and construction of a tube sensitometer.

A tube sensitometer is a light modulating device which produces densities on a plate by the passage of light through tubes which may have either fixed length and varying apertures, or fixed aperture and varying lengths. There are three main requirements: the light entering each tube should have the same intensity within the solid angle which it accepts; there should be no internal reflections within the tubes; and the geometry of the tubes should be such that there is no significant variation in the solid angle which the entry aperture of each tube subtends at any point on a calibrating spot on the photographic plate.

Since we are concerned with the blackening produced on a photographic plate by light incident within a given solid

angle, it is necessary to consider the physical quantities which the photographic emulsion records. Let us consider first the interaction between the silver halide grains and the incident photons. We ask the following two questions:- Will a photon incident upon the emulsion necessarily strike a silver halide grain and be absorbed by it; will an interaction necessarily occur when a photon strikes a silver halide grain? Since the emulsion consists of several layers of silver halide grains suspended in gelatin, a photon incident normally upon the emulsion, even if it were to pass through one of the uppermost layers, would still almost certainly be absorbed in its passage through subsequent layers. Suppose that the path of the photon was not in line with one of the silver halide grains, the scattering properties of the gelatin would probably divert the photon so that it did ultimately strike a silver halide grain. Suppose a photon arrived in a direction which was nearby, but not quite perpendicular to the emulsion, the same argument would be valid, because we can still consider the layers of grain to be, not parallel to the emulsion surface as before, but in any orientation which happens to be perpendicular to the direction of incidence of the photon.

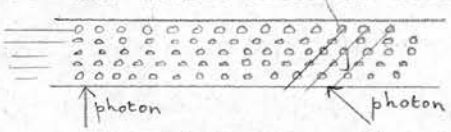

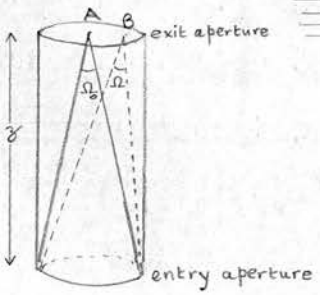

Consider now the geometry of a sensitometer tube. In the diagram, A and B are points on the exit aperture; Ω_0 and Ω are the solid

angles subtended at A and B respectively by the entry aperture. The primary requirement is that the intensity of light over the exit aperture should be practically uniform, and therefore it is necessary to calculate the limiting size of the exit aperture.

Let z be the length of a tube of unit radius, x being the distance from A to B. Since the illumination at a point on the exit aperture depends upon the solid angle subtended at that point by the entry aperture, computed values of solid angles will represent the distribution of the illumination at every point on the exit aperture. Now the solid angle Ω subtended at B by the entry aperture may be shown to be

$$2\gamma\left[\frac{\pi}{(\gamma^2+x^2)^{1/2}} - \frac{2}{\{\gamma^2+(x+1)^2\}^{1/2}} \cdot K\left(\sqrt{\frac{4x}{\{\gamma^2+(x+1)^2\}}}\right)\right]$$

where K(k) is the elliptic integral of the first kind defined by

$$K(k) = \frac{\pi}{2}\left[1+2\left(\frac{k^2}{8}\right)+9\left(\frac{k^2}{8}\right)^2+\cdots\right].$$

Substitution of x=o in the above formula gives the value of Ω_o, the central illumination as

$$2\pi\left(1-\frac{\gamma}{\sqrt{\gamma^2+1}}\right).$$

A meaningful and concise form in which to calculate the values of the solid angles seems to be in terms of Ω_o, the on-axis illumination. This method provides an immediate visual check on the percentage error present in each value compared with the on-axis value for increasing distance from the centre of

the exit aperture.

The following Fortran programme was written for evaluating the ratio Ω_o/Ω_x , where Ω_x is the solid angle subtended at a distance x from the centre of the exit aperture.

```
    PRINT 9
  9 FORMAT(42X,39HILLUMINATION ACROSS A SENSITOMETER SPOT)
  1 READ 100, Z
    IF(Z-30.)2,8,8
  2 PI=3.1415927
    OMEGAC=2.*PI*(1.-Z/(SQRTF(Z**2+1.)))
    DIMENSION X(20),OMX(20),RATIO(20)
    READ 101,(X(I),I=1,18)
    DO 5 I=1,18
    SMK=SQRTF(4.*X(I)/(Z**2+(X(I)+1.)**2))
    SMK2=SMK**2/8.0
    ELLPK=PI*(((50.0*SMK2+9.0)*SMK2+2.0)*SMK2+1.0)/2.0
    OMX(I)=2.*Z*(PI/(SQRTF(Z**2+X(I)**2))-2.*ELLPK/(SQRTF(Z**2+(X(I
   4+1.)**2)))
  5 RATIO(I)=OMEGAC/OMX(I)
    PRINT 102,Z,OMEGAC
    PRINT 103,(X(I),RATIO(I),I=1,18)
    GO TO 1
100 FORMAT(F4.1)
101 FORMAT(18F4.2)
102 FORMAT(6H  Z = ,F5.1,10X,21HCENTRAL ILLUMINATION=,F10.7)
103 FORMAT(10X,6H  X = ,16X,8HRATIO = ,/(11X,F5.2,14X,F10.7))
  8 STOP
    END
```

Z=10 CENTRAL ILLUMINATION=0.0311821

x	RATIO
0.05	1.0000382
0.10	1.0002627
0.15	1.0006415
0.20	1.0011748
0.25	1.0018246
0.30	1.0026492
0.35	1.0036328
0.40	1.0047427
0.45	1.0059810
0.50	1.0074240
0.60	1.0106762
0.70	1.0146727
0.80	1.0191791
0.90	1.0242071
1.00	1.0299310
1.25	1.0470850
1.50	1.0682564
2.00	1.1235368

Z=20 CENTRAL ILLUMINATION=0.0078395

x	RATIO
0.05	1.0000012
0.10	1.0000320
0.15	1.0000931
0.20	1.0002973
0.25	1.0004505
0.30	1.0006548
0.35	1.0009103
0.40	1.0011660
0.45	1.0014729
0.50	1.0017801
0.60	1.0026513
0.70	1.0036268
0.80	1.0048103
0.90	1.0060482
1.00	1.0074693
1.25	1.0117089
1.50	1.0168530
2.00	1.0302158

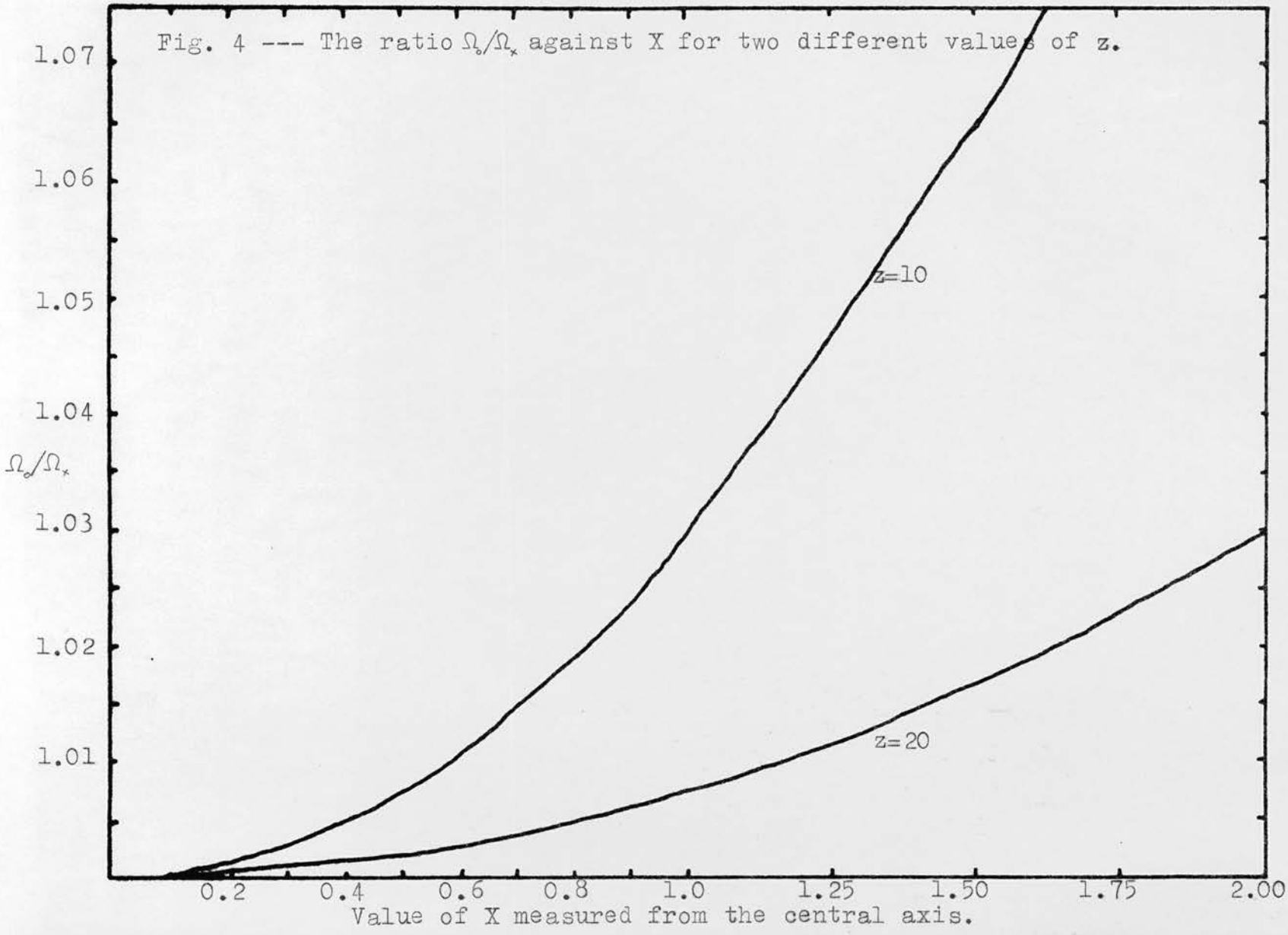

Fig. 4 --- The ratio Ω_o/Ω_x against X for two different values of z.

The computer programme was run on the IBM 1620 Model II computer of the St Salvator's College Computing Laboratory recently established in the University Observatory. It was the first programme compiled and executed in the laboratory.

The results show that at the edge of a tube (where x=1) whose length is ten times its radius, the ratio of the solid angles Ω_o/Ω_x is 1.029, i.e. a 3% error, while at the edge of a tube whose length is twenty times its radius, the error is only 0.7%. Values of $x > 1.00$ give the ratio of the illumination when the entry aperture is smaller than the exit aperture. In this case, a 12% error is introduced when x=2.00 and γ=10, whereas it is only 3% when γ=20. From these results, it is evident that a sufficiently uniform distribution of illumination exists, for calibration purposes, across the exit aperture, even when the exit aperture is larger than the entry, providing $\gamma \sim 15.0$.

The reason for the variation in illumination across the exit aperture is that although the entry aperture, when viewed from the centre of the exit aperture, appears as a circle, when looking from any other point on the exit aperture the entry aperture appears, not as a circle, but as a distorted ellipse.

Having considered the basic theoretical problem in the design of a sensitometer tubes, it is now appropriate to consider the construction and design of the instrument. Two

of the most important points to consider are the diffusely reflecting properties of the surface which provides the illuminating radiation, and the possibility of internal reflections in the tubes themselves.

In the past some investigators appear to have been satisfied with using tube sensitometers which consisted of a box employing a light source near one end, a set of tubes at the other end, with a diffusing screen inserted between the two to provide uniform illumination of the entry apertures of the tubes. The idea is only practical if the diffusing screen has a perfectly uniform transmission of light over its entire surface area; this is one of the most serious difficulties present in such an arrangement. Other investigators have used a variation on this theme whereby they arrange a battery of sensitometer tubes so that the tubes, instead of facing a diffusing screen, face a perfectly uniformly reflecting surface facing a light source, as shown in the diagram. This method is, in fact, satisfactory provided that the reflecting surface obeys Lambert's law; one such surface is a thin coating of magnesium oxide. Some investigators have obtained results using other surfaces, such as blotting paper, but it is pertinent to enquire if their results could be regarded as meaningful without some detailed proof that such a surface obeys Lambert's law.

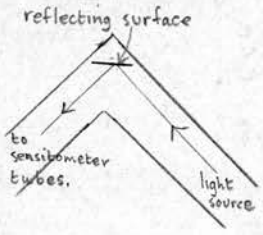

Realization of these difficulties has prompted

consideration of a simple and novel idea for the production of the uniformly reflecting surface in a tube sensitometer. Consider the primary property of an integrating sphere - when a source of light is placed inside a hollow sphere coated internally with a perfectly diffusing material, such as magnesium oxide, the luminance of any part of the surface due to light reflected from the remainder of the sphere is the same and is proportional to the total flux emitted by the light source. Suppose now that a set of tubes are just inserted inside the surface, the entry apertures of each tube would then face identically bright surfaces. Hence if it were possible to insert a set of tubes into the surface of an integrating sphere so that the entry apertures are close to the spherical surface, and if a screen could be fitted over the light source in order to prevent direct rays from reaching the entry apertures, the sensitometry would probably be more reliable than some of the other methods. This important property of the integrating sphere has been incorporated in the design of a tube sensitometer under development at the University Observatory and shown in the diagram. Some features of the design which merit some detailed description are the following:

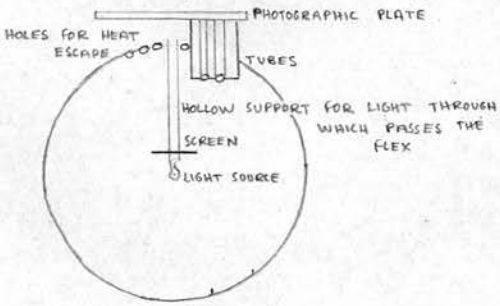

(i) The tubes are arranged so that their entry apertures face those emitting areas on the internal surface

of the sphere which make the angle between the direct ray from the light source to the emitting area XY, and the reflected ray from the emitting area XY to the entry aperture approximately equal to 45^{o} in order to prevent specular reflections. (ii) At least twelve tubes would be required to cover adequately the complete density range of the calibration curve in one exposure, preserving the feature present in the step-wedge method, whereby we obtained a check the uniformity of the plate base fog. The arrangement of twelve tubes could be such that the density spots would be distributed in a circle round the outer regions of the plate. Alternatively, four batteries of three tubes could be used, each battery of three tubes having the same length, but the length of each battery being different, the reasons for which will be given in the next paragraph. (iii) At any point on the internal surface of the sphere, a ray of light is diffusely reflected; there are an infinite number of such points. A screen is necessary to prevent direct rays from the light source from reaching the entry apertures of the tubes; the screen, of course, reduces the useful internal surface area of the sphere, but in the case where four batteries of tubes are used, the screen need only consist of four squares supported by metal rods. (iv) All internal surfaces are painted matt white, including the outside of the sensitometer tubes within the sphere, and the surface of the sphere is coated with magnesium

oxide. (v) The light source is supported by a hollow rod, through which the flex passes.

Since the design of the tubes themselves is of fundamental importance, it is appropriate to give an account of their construction. It is, of course, necessary that the interior of the tubes be painted matt black, so as to prevent internal reflections. As a means of varying the intensity at the exit apertures of the tubes, it was originally intended to have tubes of different lengths and fixed apertures; this idea was not possible because, as indicated in the sketch, it is possible for rays from the magnesium oxide surface of the

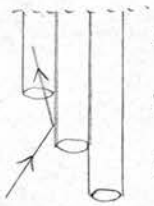

sphere to strike the external walls of one tube, whence they are reflected into the entry apertures of an adjacent tube. It was therefore necessary to consider an alternative arrangement whereby the tubes have fixed lengths and varying apertures.

A further detail is concerned with the shape of the entry apertures. Consider what happens when a ray of light reaches the squared-off aperture edges of the tube as in Figure 5. The ray of light is reflected off the entry aperture edge,

Figure 5. The effect of square aperture edges on the path of a ray of light.

Figure 6. The effect of bevelled aperture edges of a sensitometer tube on the path of a ray of light.

up to the exit aperture edge and hence on to the emulsion.

Turning now to Figure 6, a ray of light may pass through the entry aperture but it is then absorbed by the black walls of the tube. However, even if a ray were to reach the exit aperture edge, it would be reflected back down the tube, and not on to the emulsion. For these reasons, it was decided that the edges of both the entry and exit apertures should be bevelled as in Figure 6. The insertion of light baffles at various distances along the tubes would also eliminate some of the unwanted reflections; these baffles would also be painted matt black (Redman and Shirley, 1936).

Another consideration is the vignetting effect which can occur at the emulsion if the exit aperture is not situated close to it; Figure 7 illustrates this effect, together with the resulting effect on a photographic plate. Of the three regions indicated, (1) represents the region of zero intensity, (2) represents the area of vignetting, and (3) is the area of constant intensity.

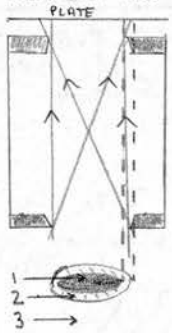

Figure 7. Vignetting effect in a sensitometer tube.

Since the tube sensitometer has been designed with the aim of retaining a few of the features of the step-wedge method of calibration, it would be desirable to have the same intensity ratio produced between adjacent tubes in the sensitometer as that given by each density step on the step-

wedge so that a comparison of the resulting intensities could be made. What then is the ratio of apertures of tubes such that the intensity ratio at the exit apertures corresponds to the interposition of a neutral density of 0.2 over clear glass. Since clear glass gives 100% transmission, and a 0.2 density step gives 62.5% transmission, consequently 62.5% of the illumination striking the density step is transmitted.

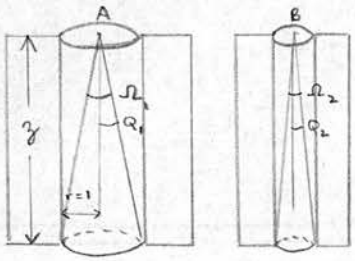

In the diagram, A and B represent two sensitometer tubes, each of length z. The radius of A is unity, and the radius of B is such that

$$I_1/I_2 = 100/62.5 = 1.6 .$$

Now $I_1/I_2 \propto \Omega_1/\Omega_2 = \left[2\pi(1-\cos Q_1)\right]/\left[2\pi(1-\cos Q_2)\right]$, so that

$$1-\cos Q_1 = 1.6(1-\cos Q_2).$$

Hence $1-z/\sqrt{1+z^2} = 1.6(1-z/\sqrt{r^2+z^2})$.

By a previous calibration, $z \geq 10$ gives an accurate representation of uniform distribution of illumination over the exit aperture. With $z = 10$ in the above equation, we have

$$1-0.99504 = 1.6(1-10/\sqrt{r^2+100}).$$

The solution is $r = 0.7892$.

Hence the radius of B must be 0.7892 times the radius of A in order to produce the same intensity ratio reaching the photographic plate as is produced by a density step in the wedge of 0.2.

8. Microphotometry

Although the subject of microphotometry may appear to be outside the scope of a chapter devoted to the study of problems arising in the photographic process, its inclusion at this stage may be justified by two factors. In the first place, an extremely important photographic effect became apparent during microphotometry of preliminary calibration exposures. Secondly, the reduction of the calibration exposures necessarily involved the use of the Hilger microphotometer for the density measurements, and it was used to check the transmission properties of the step-wedge.

Microphotometry deals with the measurement of density of small areas on the photographic plate. The instrument available for use at the University Observatory was a Hilger and Watts L 470 Recording Microphotometer. In this instrument, the plate rests on a moveable carriage, so that any particular area of the plate may be scanned while several drive speeds are available to suit different requirements. Light from a 12 volt 36 watt filament lamp is projected on to a slit which is focussed on the plate by a microscope objective; after passing through the plate, the light is collected by a second microscope objective and is focussed on to a second slit, the purpose of this slit being to reduce to negligible properties any scattered light in the system. A sphero-cylindrical

optical system then produces a patch of light on the cathode of a photomultiplier, the output current from which is then a measure of the light transmitted through the plate. Accordingly, the machine does not measure density, but transmission. Another photomultiplier receives a small quantity of light direct from the measuring lamp to give a reference signal proportional to the light source, thereby eliminating any variations in its intensity. The first slit has a graduated scale for width with a range from 0 to 100 in 0.02 mm divisions, reduced by a factor of 7 at the plate. The photomultiplier output operates a Brown "Electronik" Recorder, which employs a slide wire on which is attached a small pen which records on graduated paper fed over a metal drum. The paper has a scale ranging from 0 to 100 and the tracings give a continuous record of density variations, the scale value of 5 normally being used for zero transmission, and 95 being used for 100% transmission. For an intermediate scale value, the density is readily obtained. For example, for a scale value of 48, the transmission factor is 43/90 = 1/2.092, the opacity being 2.092 and the density $\log_{10}2.092$ = 0.321.

The Hilger microphotometer was also used to check the uniformity of transmission across the width of each step of the wedge. In doing so, some difficulty was encountered

in focussing the microphotometer slit on the wedge since by virtue of its glass mounting, the rhodium layers of the wedge lay much nearer to the microscope objective than the emulsion of a normal photographic plate. The variation in the transmission of any of the steps was found to be not greater than one quarter per cent.

Several difficulties arose in the interpretation of the microphotometer tracings. The first of these difficulties, which became apparent after preliminary scans of calibration exposures, revealed the drawbacks of the dish method of development. Figure 8 illustrates the form of tracing which was anticipated after a run along the calibrated area of the plate, while figure 9 shows the form of tracing which was actually obtained. At the boundary between a light and dark area on the plate, the dark area adjacent to the boundary shows a density level higher than that over the remaining area, and the light area adjacent to the boundary shows an even lower density than the plate base fog level. This increase in density is called the border effect, the decrease in density is called the edge effect while the combined effect is simply called an edge effect. The photographic explanation

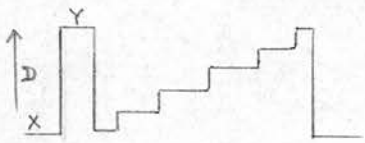

Figure 8. Anticipated form of tracing after run across wedge.

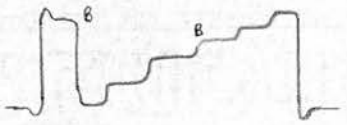

Figure 9. Resulting form of tracing after calibration run across wedge.

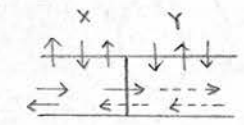

Figure 10. Diffusion of developer and reaction products across boundary between X and Y.

is that the developer has relatively little silver halide to reduce to silver in the plate base fog area, while at the same time it is being exhausted by reduction taking place in the heavily exposed area. Figure 10 shows the fresh developer and the reaction products diffusing backwards and forwards across the boundary between areas X and Y. The influx of relatively fresh developer into area Y from X accelerates the growth of density of Y, and consequently the image near the boundary is more dense than elsewhere. Similarly, the diffusion of the retarding reaction products from Y to X retards development, giving a lower than in the surrounding area.

After considering whether this effect could in any way be attributed to the dish method of development, it became apparent that the careful agitation of the developer over the emulsion at the boundary, referred to in the previous paragraph, was not sufficiently rapid. In an attempt to eliminate the edge effects, further plates were agitated with the aid of a four-inch wide badger-hair brush which drew developer over the whole plate in one movement. Subsequent microphotometer tracings showed that this method was successful in overcoming the earlier development difficulties.

Another effect evident in Figure 9, but one not due to photographic causes, is that in the regions marked B, where

a sharp point is expected, a smoothing off occurs, due mainly to the following two reasons:- (i) The light source is nearly, but not quite a point source, and since the wedge must be protected by its glass mounting, the density steps cannot touch the emulsion, so that when light passes through the wedge on to the photographic plate, a penumbral shadow effect is set up at each sharp edge, resulting in a small area of intermediate light intensity occuring between successive steps on the plate. (ii) The size of the micro-photometer slit used affects the resulting profile. In the diagram, an intensity distribution profile on the plate is represented by a dotted line. It is appreciated, of course, that the larger the slit the greater will be the smearing of the sharp edges in the diagram and that the slit width should be kept as small as possible, though not so small that an insufficient number of photons would reach the photomultiplier. There is also a lower limit to the slit area that can be used, and this is set by the plate grain. At low densities, only a few of the available silver halide grains have been developed, and for even larger slit areas, these grains still produce irregularities in the level obtained on the tracing of the plate base fog. In order to obtain an assessment of where exactly the plate base fog level lies, a large slit would be desired so as to

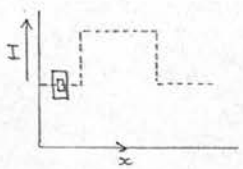

encourage smoothing. Clearly, a compromise is required between having a slit area which is so small as to create undesirably large fluctuations in the tracings and a larger area, which although efficient for smoothing purposes, inevitably means too much loss of resolution.

After considering the distortion of intensity profile by different slit sizes, it is now useful to derive some corresponding analytical results. Consider an intensity distribution $I(x)$ and a scanning aperture of width Δx in the figures by ▨ . Let us denote by $R(x)$ the tracing produced by scanning with this aperture, where

$$R(x)=\int_{x}^{x+\Delta x} I(x)dx \ .$$

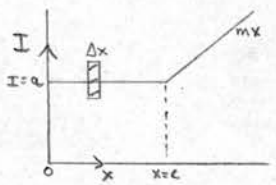

Figure 11.

In Figure 11, the scanning aperture covers the region from X to $X + \Delta X$, and the scan is made from X=O to X=K. It is convenient to divide the scan into three separate parts:-

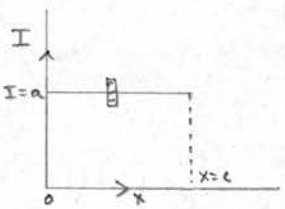

Figure 12.

(i) In Figure 12, the scanning aperture is restricted to the region of the intensity distribution where $0 \leq x \leq c$. In these circumstances, we have

$$R(x)=\int_{0}^{c-\Delta x} I(x)dx=ac.$$

(ii) In Figure 13, the region is given by

$c < x < c + \Delta x$ and we have

$$R(x) = \int_{x}^{c} a\,dx + \int_{c}^{x+\Delta x} mx\,dx = \frac{m}{2}x^2 - ax + c\left(a - \frac{mc}{2}\right).$$

The scanning effect of the aperture thus gives rise to a quadratic trace.

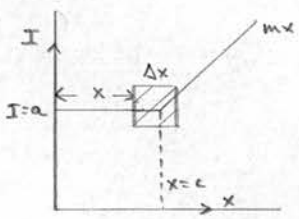

Figure 13.

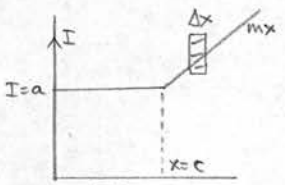

Figure 14.

(iii) In Figure 14, the region is given by

$$c + \Delta x < x \leq k$$ and we have

$$R(x) = \int_{c}^{k-\Delta x} mx\,dx = \frac{m}{2}(k+c)(k-c).$$

This schematic example illustrates that the smearing effect only occurs when there is a change in the gradient of the intensity distribution $I(x)$.

Turning now to the general problem of microphotometry of an extended object, such as a galaxy, several tracings would have to be taken and then assembled to give an isophotal representation of the distribution. However, if the intensity across the major axis of a galaxy were required, it would only be necessary to make a single scan along the major axis using a small square slit, as in Figure 15, or alternatively, one scan could be made using a slit whose width was small but whose height was greater than the minor axis of the galaxy as in Figure 16. The effect of smearing would be present in both cases, but would be more complicated in the latter.


Figure 15.

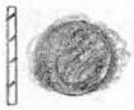
Figure 16.

CHAPTER II

1. Introduction

The telescopes available for use at the University Observatory were two Cassegrain Schmidt telescopes, with apertures of 17-inches and 37-inches respectively. The 17-inch telescope was constructed in 1950 in order to serve as a half-scale pilot model for a 37-inch telescope, which was completed and commissioned for use in the winter of 1963. The 17-inch and the 37-inch telescopes, called the Scott Lang Telescope and James Gregory Telescope respectively, are designated in this work as SLT and JGT.

Before describing the optical system of a Cassegrain Schmidt telescope in detail, it is first necessary to give an account of some of the limitations, in the surface photometry of fields of galaxies, which occur in other types of telescope and to show how particular limitations are overcome in the design of a Cassegrain Schmidt system.

As the photometry was performed using B and V-filters, it is appropriate to consider the optical and photographic effects produced by interposing these filters in the light beam.

2. Cassegrain Schmidt Telescope

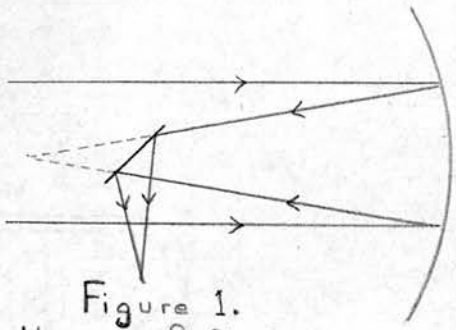

Figure 1.
Newtonian Reflector

Figure 1 shows schematically the optical arrangement in a Newtonian reflector; when it is used as an astrographic instrument, the light collecting power for photographic use is high, but the inherent resolving power of the primary mirror is not fully utilized. Such full use would only be possible if the focal length of the primary mirror were chosen so that the size of the diffraction pattern formed on the plate was of the same order of magnitude as the limit set by the scattering of the grains in the photographic emulsion. This choice would require a very small aperture which would lead to excessive exposure times for faint extended objects. A Cassegrain arrangement with a large focal ratio makes it possible for the light, after reflection by the primary mirror, to fall on a convex mirror. The Cassegrain telescope, like the Newtonian, has a parabolic mirror. However, the field of a parabolic mirror showing good resolution is small, and therefore unsuitable for fields of galaxies, especially if the focal ratio is large. Why, then, cannot the mirror be made aplanatic in order to increase the field? In this connexion, let us consider a spherical mirror with a stop in

the plane of its centre of curvature. Since the whole system has axial symmetry for all incident pencils of rays, aberrations arising from the lack of symmetry cannot be present, and this means that the system is free from astigmatism and coma. The one defect, however of the resulting image is spherical aberration, illustrated in Figure 2; this aberration is considerable when the focal ratio is large and must obviously be corrected. This correction is achieved by placing a plate of low dispersion glass in the aperture of the diaphragm. This method, introduced by Schmidt, makes very large focal ratios possible, but the two disadvantages of a Schmidt telescope are the curvature of the field, the inaccessibility of the curved focal surface and the difficulties arising from the necessity of bending the plates. The Cassegrain Schmidt system overcomes these difficulties by having a convex mirror between the focus of the primary and the primary mirror itself, enabling light to be reflected off the convex secondary mirror through a hole in the primary mirror to the focus. The focal surface is flat and the field covered by the two St Andrews telescopes is four degrees square, while the plateholder assembly is also more readily

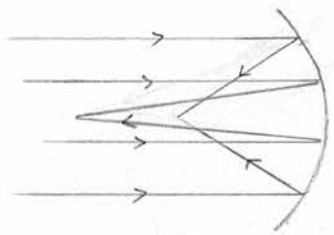

Figure 2. Spherical aberration.

accessible. The dimensions of the plateholders for the SLT and the JGT are four and eight inches square respectively, and when in focus, these telescopes produce good images over the entire circular area, with no vignetting of the beam.

3. The Effect of Filters on the Focus

The observational work with the St Andrews Schmidt telescopes on surface photometry of galaxies reported in this thesis has been limited to photographic work in B and V-wavelengths. In these observations, B and V-filters were inserted in the plateholders so that they were enclosed in the plateholder when the dark slide was closed. Before considering the properties and transmission curves of the filters used, it is appropriate to study the effect on the focus by interposing a filter of thickness t in the converging light beam.

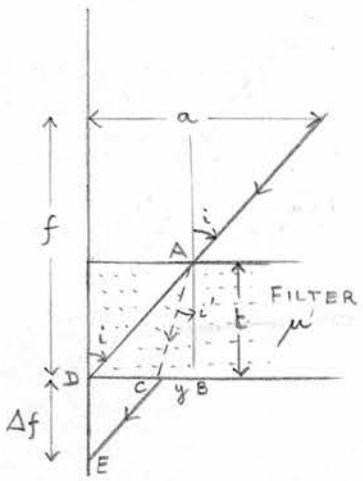

In the diagram, D represents the focus before inserting a filter of thickness t, and XAD is a particular ray, inclined at an angle i to the vertical, passing through air with refractive index

unity. After the filter of refractive index μ is inserted, the ray in question is deviated and travels via AC and CE to a new focus at E. We wish to calculate Δf, the change in focus, in terms of the quantities μ, i and t.

We have $\tan i = a/f = x/t$, so that $x = at/f$. We also have $\sin i = \mu \sin i'$ hence

$$x/\sqrt{x^2+t^2} = \mu y/\sqrt{y^2+t^2}.$$

$$y = xt/\sqrt{(x^2+t^2)\mu^2 - x^2}.$$

From the triangle DEB, DE is the focal shift Δf given by DC/tan i. The change in focus Δf is $t\left[1-\left(t/\left(\sqrt{(x^2+t^2)\mu^2-x^2}\right)\right)\right]$ This form satisfies the requirements that Δf tends to zero when t tends to zero and μ tends to unity. Since $x = at/f$, we have $\Delta f = t\left[1-\left(t/\sqrt{\left((a^2t^2/f^2)+t^2\right)\mu^2-(a^2t^2/f^2)}\right)\right]$ The focal shift in terms of the angle of incidence i and the refractive index μ of the filter is $t\left(1-\left(\cot i/\sqrt{\operatorname{cosec}^2 i\,\mu^2-1}\right)\right)$. Consequently

Focal Shift/Thickness of Filter $= 1-\left(\cot i/\sqrt{\mu^2\operatorname{cosec}^2 i-1}\right)$.

In order to find the focal shift, we need some knowledge of the values of i which may be expected in a Cassegrain Schmidt system, before substitution of i and μ in the above formula. For this reason, both the dimensions of, and the distances between the optical components of the St Andrews telescopes were ascertained in order to

construct scale diagrams of the optical systems for graphical ray tracing. The following are the requisite data:-

	SLT	JGT
Radius of curvature of primary mirror	49.00"	116.45"
Radius of curvature of secondary mirror	47.00"	111.72"
Diameter of primary mirror	18.81	37.00
Diameter of secondary mirror	9.60	18.75
Distance between the vertices of mirrors	13.16	33.19
Overall length from Schmidt plate to focus	62.00	141.5

On the scale diagrams, the paths of extreme rays were traced geometrically from the primary mirror to the secondary mirror and thence to the focus and it was found that for on-axis rays, the angles ranged from 6 ° to 9 °. The refractive index of the glass filters is not listed accurately in the catalogues, but an approximate value of 1.52 is given and it is using this value that the following table has been compiled, using the formula derived for $\Delta f/t$:-

Values of focal shift with angles of incidence

i	$\Delta f/t$	i	$\Delta f/t$	i	$\Delta f/t$
1°	0.3421	5°.25	0.3436	7°.75	0.3455
3°	0.3427	5°.75	0.3440	8°.25	0.3458
3°.75	0.3429	6°.25	0.3443	8°.75	0.3465
4°.25	0.3431	6°.75	0.3447	10°.0	0.3478
4°.75	0.3434	7°.25	0.3451	15°.0	0.3456

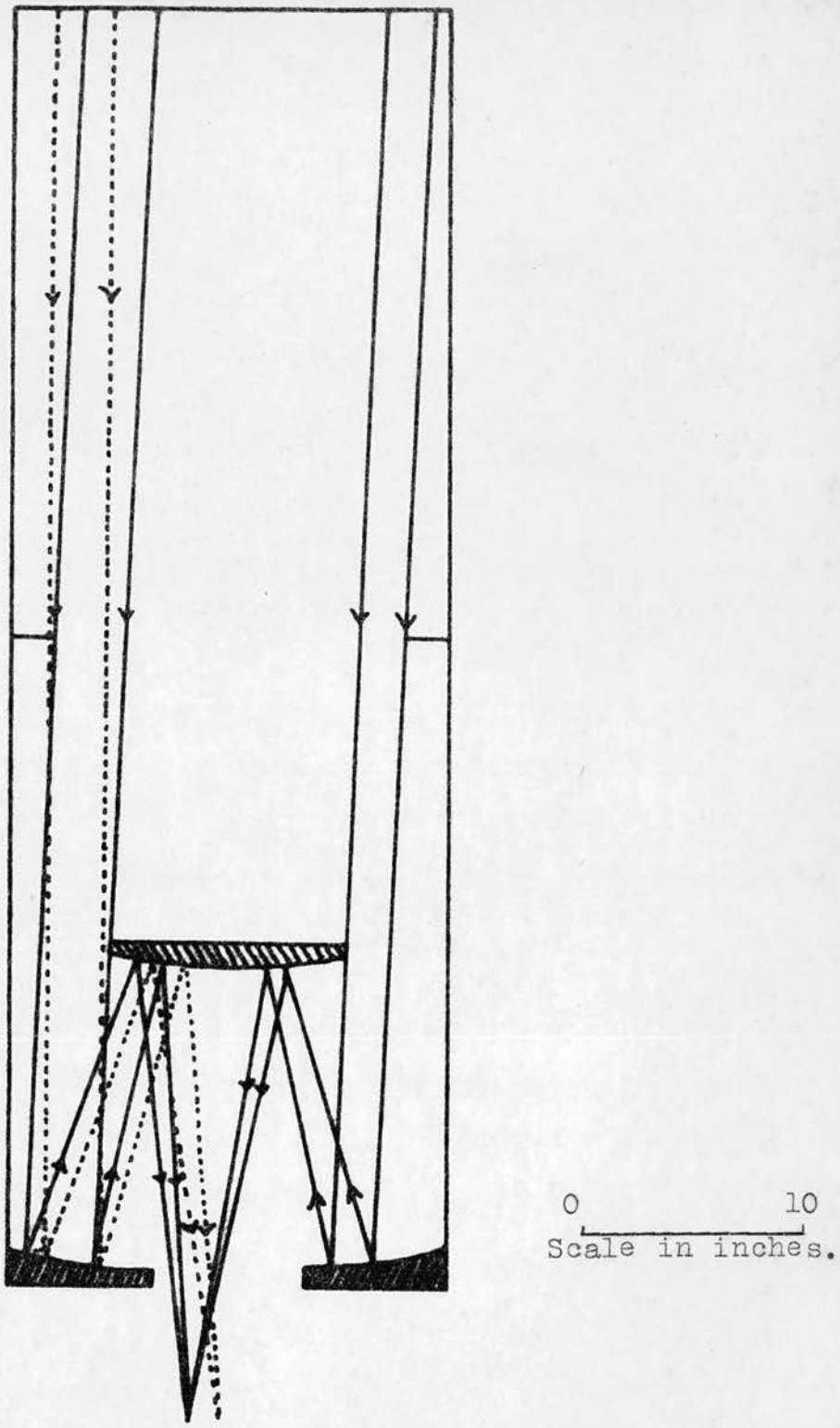

Ray tracing diagram for the 15-18 - inch Cassegrain Schmidt Telescope at the University Observatory.

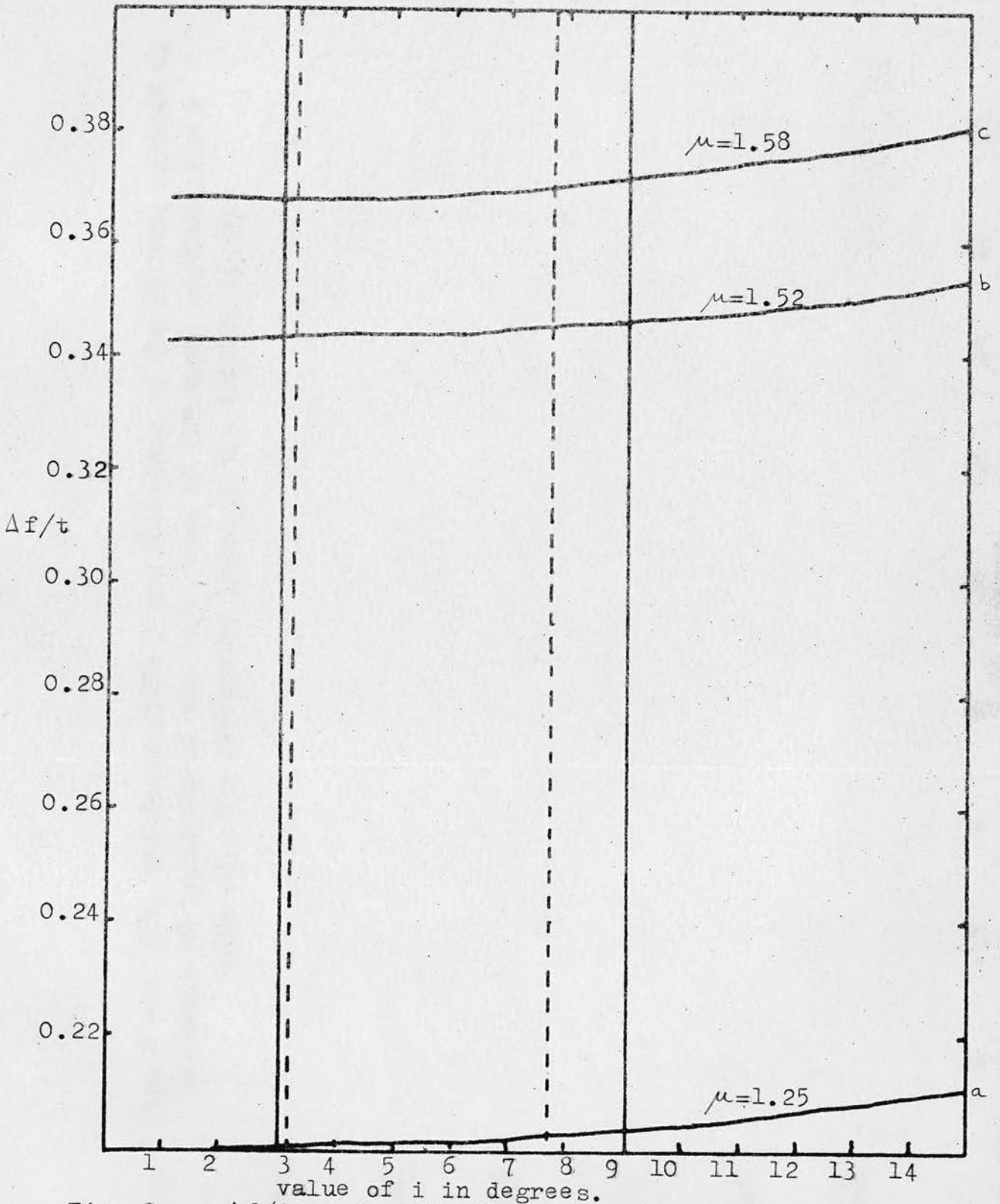

Fig. 3 --- $\Delta f/t$ against i, the angle of incidence, for three different values of μ, the refractive index of the filter.

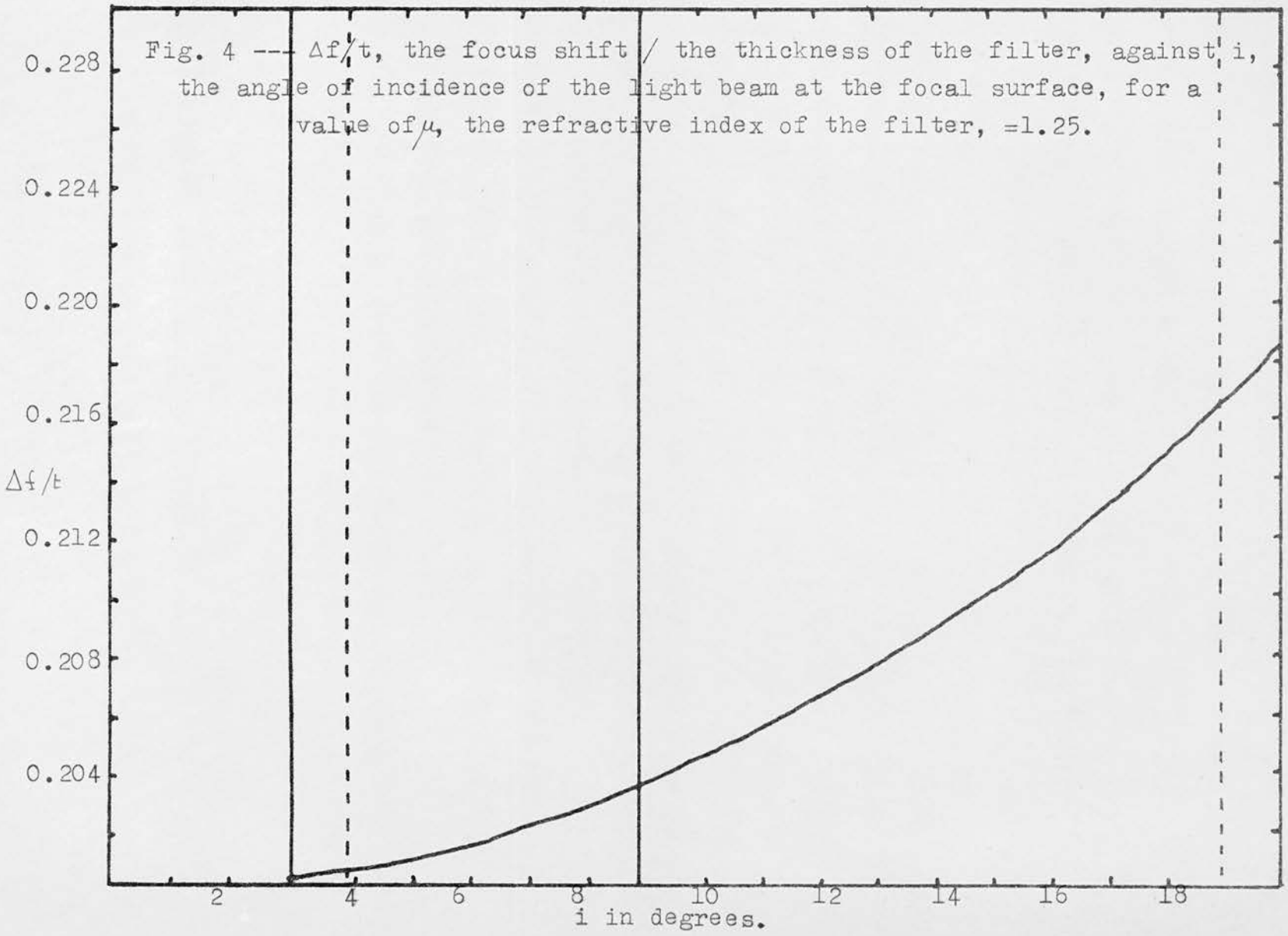

Fig. 4 --- Δf/t, the focus shift / the thickness of the filter, against i, the angle of incidence of the light beam at the focal surface, for a value of μ, the refractive index of the filter, =1.25.

Figure 3 a, b and c illustrates the values obtained when $\Delta f/t$ is plotted against i for three different values of the refractive index of the filter. The outer solid lines indicate the extreme values of the angles of incidence obtained on the scale diagram of the JGT while the dotted lines denote the corresponding values for the SLT.

Figure 4 is constructed using the same data as was used for Figure 3 a, but the scale has been considerably enlarged on this occasion. The solid lines correspond to the extreme angles of incidence on the JGT, as before, but the dotted lines in this case are values of angles which may be found in classical Schmidts. These values were found approximately by constructing a scale diagram of a classical Schmidt in the same manner as was used for the Cassegrain Schmidt drawings. From this graph, it is apparent that the focal shift at the centre of a plate on the JGT is 0.2004 t, while at the edge of the plate, where larger angles of incidence are encountered, this value is 0.2036 t. This means that the focal surface, instead of lying in a plane, as is the case without any filter in the beam, now lies between two values; in this particular case, the difference in these values is 0.0032 times the thickness of the filter in use. The average thickness of the filters

is 1.95mm., therefore Δf = 0.00624mm. = 0.00025 inches. In comparison, on a classical Schmidt, where larger angles of incidence may be found, these values may be proportionately larger, and an appreciable difference in focus over the field may result, but for work on surface photometry of galaxies, where a critical focus is not essential, it suffices to remark that this effect will not impair the quality of the resulting plates obtained with a Cassegrain Schmidt telescope.

It is of interest to reverse the calculation and find the refractive index of the filter by using the formula

$$\mu = \sin i \sqrt{1 + \left(\cot^2 i / (x^2 - 2x + 1)\right)},$$

where $x = \Delta f / t$, if we measure the actual change in focus and select an appropriate value for i, the angle of incidence. How are we to select this value for i. A good choice would appear to be the average value of the incident light falling on the plate, that is, the average value of i between two cones of semi-vertical angles 6° and 9°.

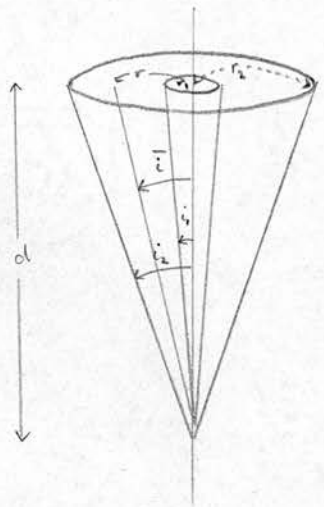

Let us define the average angle of incidence i in the accompanying diagram by $\bar{i} = \int_{r_1}^{r_2} i(r) r^2 dr \Big/ \int_{r_1}^{r_2} r^2 dr$,

where r_1 and r_2 are the radii of the secondary and primary mirrors respectively. Let d be

the distance from the secondary mirror to the focal surface then

$$\sin i = r/\sqrt{r^2+d^2}.$$

Since i is small and not more than 10^o, and since the error in approximating sin i = i is less than 1% for i less than 10^o, we may assume sin i = i. This gives

$$\bar{i} = \int_{r_1}^{r_2} \left(r^3/\sqrt{r^2+d^2}\right).dr \Big/ \int_{r_1}^{r_2} r^2\,dr$$

$$= \left\{\left(r^2\sqrt{r^2+d^2}\right)_{r_1}^{r_2} - \int_{r_1}^{r_2} 2r\sqrt{r^2+d^2}\,dr\right\} \Big/ \left[r^3/3\right]_{r_1}^{r_2}$$

$$= \left[r^2\sqrt{r^2+d^2} - \tfrac{2}{3}\left(r^2+d^2\right)^{3/2}\right]_{r_1}^{r_2} \Big/ \left[r^3/3\right]_{r_1}^{r_2}.$$

Inserting the appropriate numerical values in this expression, the equation reduces to $\bar{i} = \sin^{-1} 0.139$, hence $\bar{i} = 8^o$. It is interesting to note that this average value is not much greater than the median angle of incidence. Using a value of $i = 8^o$, the change in focus by inserting a filter of thickness 1.97mm was found to be 0.026 inches. Substitution of these values in the formula for μ gives a value of 1.46 for the refractive index of the filter glass.

4. Glass Filters

The effect of the filters on the photographic systems is now investigated, together with the appropriate filter and emulsion combinations used in B and V-photometry.

Photographic surface photometry of NGC 4111 and

NGC 4258 has been performed using the following filters:-

Scott Lang Telescope	B-filter	PILKINGTON	OY 10
" " "	V-filter	PILKINGTON	OY 6
James Gregory Telescope	B-filter	SCHOTT	GG 13
" " "	V-filter	SCHOTT	GG 14

The transmission curves of each filter are shown in Figures 5 to 8, while Figures 9 and 10 show the wavelength/sensitivity curves of the emulsions used in the work.

In B and V-photometry, certain wavelength ranges are isolated by using certain filters with different types of photographic emulsion. Although the emulsion is sensitive to wavelengths below those of the given wavelength range, the filter does not transmit these wavelengths, but the region where the filter has appreciable transmission defines a possible pass-band. Similarly, although the filter transmits light, the wavelengths of which are far in excess of the required range, the sensitivity of the emulsion falls off and this area of declining sensitivity delimits the range of the actual pass-band. B-photometry is achieved by using a B-filter with a Kodak OaO emulsion while an OaD emulsion and a V-filter produce the V-wavelength range. The emulsion type OaO as opposed to IIaO is used for the work because although it is slower than other emulsions for exposures

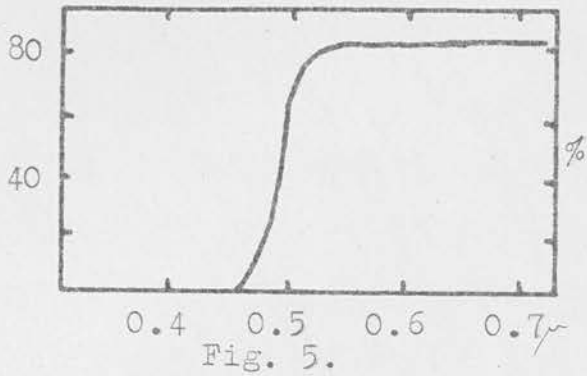

Fig. 5.

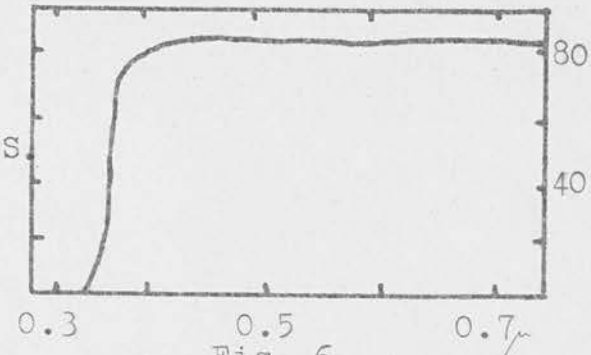

Fig. 6.

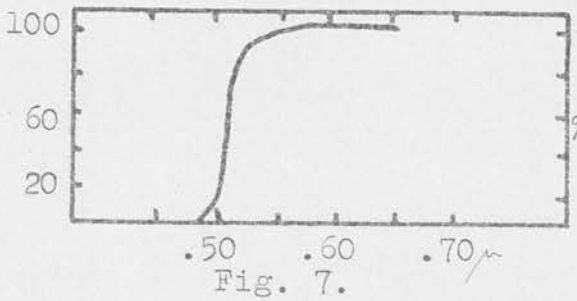

Fig. 7.

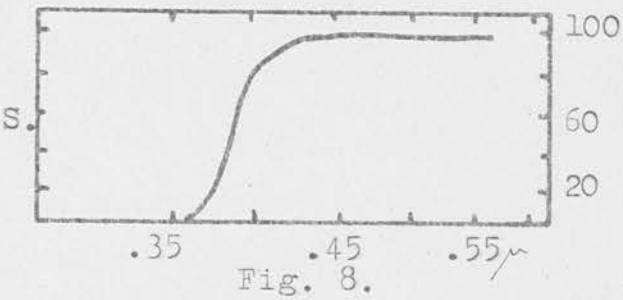

Fig. 8.

Fig. 5 --- Transmission curve of Pilkington OY 6 filter.
Fig. 6 --- Transmission curve of Pilkington OY 10 filter.
Fig. 7 --- Transmission curve of Schott GG14 filter.
Fig. 8 --- Transmission curve of Schott GG13 filter.

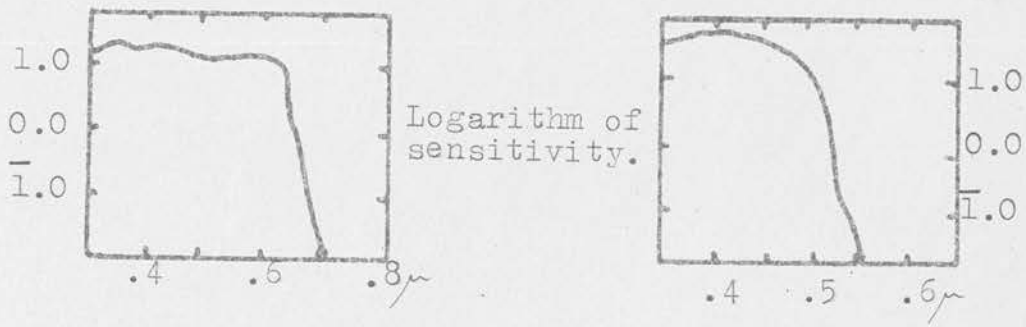

Fig. 9 --- Wavelength/sensitivity curve of Kodak OaD emulsion.
Fig. 10 --- Wavelength/sensitivity curve of Kodak OaO emulsion.

of the order of a fraction of a second, it is of the highest possible speed to exposures of several minutes or longer. The uniformity of transmission of the filters is an important factor in successful photometry; their transmissions were tested using the Hilger microphotometer. Systematic runs were made in two directions at right angles to each other across the filter and the analyses of the resultant tracings showed that the filters were all almost perfectly uniform, with the exception of the Pilkington OY 10 filter, which exhibited small areas where the transmission was not quite as high as that over the rest of the filter; these dark areas had differences of around 0.75%, compared with the normal transmission value of the filter.

5. Interference Filters

A photometric study of the planetary nebulae NGC 6720 and NGC 6543 was made using interference filters, to isolate emission lines in their spectra.

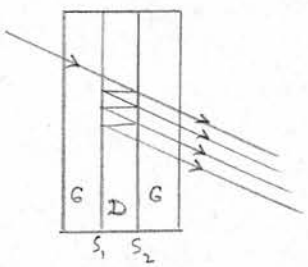

G – glass slabs.

D – di-electric layer of magnesium fluoride.

$S_1 S_2$ – layers of silver.

The isolation of the wavelength band is achieved by inserting a di-electric layer of magnesium fluoride between

two glass slabs, which have a layer of silver on the surfaces which are in contact with the magnesium fluoride; the thickness of the di-electric layer determines the exact position of the transmission peak. The di-electric coating is deposited by an evaporation process. If the transmission peak of a filter occurs on the long wavelength side of the desired part of the spectrum, it may be tilted slightly to shift the peak to a shorter wavelength. In most applications, interference filters are used in parallel light. At the present time, precision interference filters cannot be made much larger than six inches square, consequently observations on the JGT have been carried out using filters two inches in diameter; these filters screwed into a hole in a metal plate, and this plate was fitted to the telescope instead of the eight-inch square plateholder. Provision was made on this metal plate for attaching a four-inch plateholder.

Tests for the uniformity of transmission of the interference filters have been carried out using a different procedure from that used for the glass filters. The interference filters, because of their large thickness and the thickness of the cells in which they are mounted, were unable to rest on the plate carriage of the microphotometer without obstructing the movement of the plate carriage. It was therefore necessary to test the uniformity of the filter

transmission by another method. Several plates were exposed to a fairly bright sky in which neither clouds nor stellar images could be detected with the naked eye; these plates were taken on the JGT with interference filters. The resulting plates showed areas of blackening corresponding to the position of the filter, and the degree of blackening was thus a measure of the uniformity of transmission of the filter; subsequent microphotometry of these plates confirmed that the filters transmitted light uniformly over their entire surface area to an accuracy better than one per cent. By way of comparison with glass filters, it is interesting to note that the change in focus due to an interference filter was 0.092 inches whereas the B-filter changed the focus by 0.026 inches.

The filters supplied by Grubb Parson and used in this work were an $H\beta$ with a peak wavelength transmission at λ 4864 and an N_1+N_2 filter with a transmission peak centred on N at λ 5012. These filters were designed to operate in an f/3 cone, the HB filter having zero transmission at the N_1+N_2 wavelength, the N_1+N_2 filter having inappreciable transmission at the $H\beta$ wavelength. Now the wavelengths of the forbidden oxygen lines N_1 and N_2 are λ 4950 and λ 5007 respectively, and the average angle of incidence, derived in the previous section of this chapter, is 8°. Consequently when the interference filter is situated parallel to the

photographic plate, this is equivalent to tilting it 8° in parallel light, hence the peak transmission would fall below λ 5012. Accordingly, during the calibration of the photographic plate, it is necessary to tilt the filter so that it is at an angle of 8° to the calibrating beam of approximately parallel light.

In the present study of planetary nebulae, OaO plates have been used, but an examination of Figure 10 shows that the sensitivity of the OaO plates begins to decrease over the wavelength range λ 4864 to λ 5012, although it does not decrease rapidly until λ 5150, and so for equal intensities of light falling on the plate at both the Hβ and N_1 tN_2 wavelengths, the Hβ image will be slightly brighter than the N_1 $+N_2$ image. Since OaJ plates have a much more uniform sensitivity over this particular wavelength range, they will be used in preference to OaO plates in future work on planetary nebulae.

6. Instrumental Profile

The telescope does not produce a point source image of a star on the photographic plate largely due to the scattering of light within the photographic emulsion which results in the spreading of the image; other reasons include atmospheric tremor and the scattering of the light during its transmission through the Schmidt plate and its subsequent reflection off two mirrors. The form of the

resulting distribution function is called the instrumental profile. After microphotometry of a plate which has been exposed to a star, the resultant tracing is representative of the instrumental profile, if the scanning aperture were so small that it did not cause appreciable distortion. It is important to calculate the effect of this instrumental profile on the surface photometry of a galaxy with high central condensation. Let T represent the true distribution across a galaxy, I the instrumental profile and M the measured distribution. The integral equation for the true distribution T is as follows

$$M(x) = \int_{-\infty}^{+\infty} T(y)\, I(x-y)\, dy \,.$$

In this section, we are concerned with the determination of I(x-y), the instrumental profile. For this purpose, a set of exposures was taken of β Ursae Majoris on both the SLT and JGT with a B-filter. In order to eliminate scattering in the emulsion, and to make the interpretation of the microphotometer tracings more accurate, Ilford N 25 fine grain plates were used; these plates are considerably slower than other emulsion mentioned in this thesis. The exposure times ranged from one second to twenty minutes; guiding during these exposures is particularly important, since observational errors can be enlarged greatly because of instrumental distortion. In the microphotometry

of the plates, the size of the slit was the same as that used in the microphotometry of the plates taken of galaxies, as this scanning aperture introduced very little distortion of the instrumental profile. After the reduction of the tracings, the intensity profile of each plate was plotted and then the composite instrumental profile was assembled by superimposing on the intensity profile of the longest exposure that of the second longest, then superimposing the third longest on the combined profile already obtained etc., right down to the shortest exposure.

The stellar images on the plates of longest exposure contain four spikes which are caused by the diffraction of the light beam at the four metal supports for the secondary mirror. The microphotometry of the images was performed at 45^{o} to the direction of any of these spikes to avoid undue complication.

r"	JGT^{m}	SLT^{m}
0	0	0
5	0.25	0.20
10	2.75	0.45
15	3.50	1.20
20	4.25	2.45

The table shows the observed instrumental profiles of both the SLT and JGT. The distance from the centre of the image is r and the intensities of the images have been converted into magnitudes, taking the central intensity as the zero magnitude m in each case. The values of the magnitudes show that the JGT has a greater resolving power than the SLT; some of this difference could be due to the

plate scale, because although the microphotometer produces little distortion, the size of the scanning aperture is, in angular measure on the plate, 2.2 times larger on the SLT than on the JGT plates. An example of the application of the JGT instrumental profile to correct an observed distribution for a galaxy is given in the following chapter.

CHAPTER III

1. Introduction

The photographic surface photometry of galaxies described in this chapter has been confined to two galaxies of different types, an elliptical galaxy and a spiral galaxy. The choice of the objects was made with due regard to their accessibility during the observing season, their apparent brightness and angular size as well as the desirability of examining the photometric effects which arise in the study of objects with different types of surface distribution of intensity. The galaxies chosen were the E7 elliptical galaxy NGC 4111 and the Sb spiral NGC 4258.

Photographic surface photometry of NGC 4111 with the Scott Lang and James Gregory Telescopes has been carried out during the first few months of 1964. Prior to deriving the photometric parameters, we shall describe the basic method used throughout the work for plotting isophotes of an extended object, in addition to giving attention to associated problems which arise in the work, such as pre and post-exposure.

2. Reduction Method

2.1. Plate Selection

Usually, at least two plates of a galaxy must be obtained, because the intensity range from the wings to the central nucleus of a galaxy may be greater than that to which the photographic emulsion will respond. Figure 1 shows a possible shape of a galaxy on a plate of long exposure (i), while Figure 2 shows the corresponding density distribution on the plate for the major axis. The density distribution from A to B can be related to the corresponding intensity distribution from A to B by converting densities to intensities; the calibration curve for such conversions is shown in Figure 3. It shows that the density at B is the highest density value for which we can accurately assign a corresponding intensity

Figure 1.

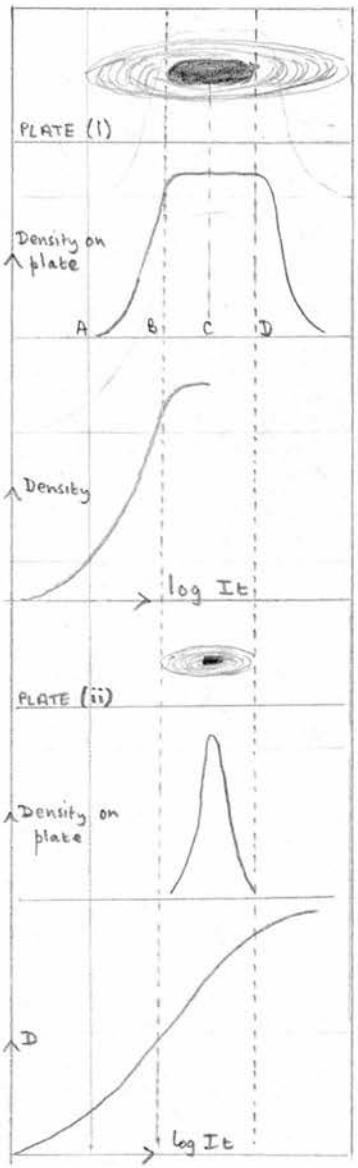

Figure 2.

Figure 3.

Figure 4.

Figure 5.

Figure 6.

value. In order to obtain the density distribution from B to D, it is necessary to take a plate of shorter exposure (ii) than before, and in this case, the weak intensities in the wings of the galaxy will be unable to produce any measurable density on the emulsion while the central nucleus produces a continuously varying distribution; the resulting form of the density distribution is shown in Figure 5. Using Figures 5 and 6, an intensity distribution can be assembled by means of the calibration curve shown in Figure 6; on this occasion, the density area of the calibration curve corresponding to the densities found in areas B to C can be related to intensity. By plotting the two intensity distributions obtained from plates (i) and (ii) and displacing the ordinates of the intensity distribution obtained from plate (ii) so as to continue the slope of the intensity distribution for the region outside BC of Plate (i), a composite intensity distribution curve may be drawn up; this distribution is referred to as the intensity profile of a galaxy.

It is important to describe the major difficulties present in obtaining a definitive set of plates of a galaxy. Normally, one attempts to obtain a set of plates, covering an exposure range of 1, 2, 5, 10, 20, 40, and 80 minutes. This is because only two of these plates may be required to cover

the intensity range of the galaxy, although several plates must be taken to allow a wider choice from which the ultimate selection of these two plates is made. Furthermore, guiding difficulties are more likely with plates of long exposure, although they can also be present on short exposure plates, and hence the selection, in the first place, is cut down to a selection from those plates which are as perfect as possible. Difficulties in selection occur after the elimination of plates with guiding errors; this is due to variations in the sky brightness, the temperature, the zenith distance, and also to the period of time which elapses while the plate material is being gathered. It is considered for the current programme that the unexposed plates used for the photometry of each object are better to be taken, not even from the same batch of plates, but, even better still, from the same box of plates, since variations in the emulsion characteristics do occur from box to box.

Each calibration cannot, as one would wish, be carried out immediately after the telescope exposure, since valuable observing time would be lost in so doing. They are, however, performed as soon as the remaining observations are completed, and in the same order in which the telescope exposures were taken. By following this procedure, each plate could be subject to a time lag from the end of the exposure to the commencement of calibration of around three

hours, but to offset this unavoidable delay, at least 60 hours were allowed to elapse before processing the plate, in order to minimize the latent image decay times of the galaxy and calibration images. Some investigators make the calibrations on separate plates, and process the two simultaneously, but this procedure is open to question, as errors could arise from variations in certain emulsion properties of each plate and in their processing conditions; in this work, each plate was calibrated for the same time as the telescope exposure.

2.2. Pre and Post-Exposure

The reason for taking each image on a separate plate is to eliminate difficulties caused by pre and post-exposure. Other investigators have often obtained several images on the same plate, and it is useful to try to describe the shortcomings of such a method. Suppose two separate images of a galaxy are made on the same plate, with exposure times t_1 and t_2 respectively, then the first image has a post-exposure time t_2, while the second image has a pre-exposure time t_1; the pre and post-exposures refer to the sky background.

In the early stages of a photographic exposure, a stable product called the sub-image is formed which is later built up to form the latent image. The sub-image itself,

however, does not cause a photographic grain to be developable, but the sub-image can be turned into a full latent image by a process whereby developing a sub-image for a longer time than usual may make it developable. An easier method of rendering developable a sub-image is to give it a carefully controlled exposure to very low level intensities of light; the sub-image grains utilize the low intensity light with full efficiency and they could almost regarded as hypersensitized particles.

Figure 7. 

Figure 8. 

In Figure 7, an image of a galaxy is obtained and a second exposure of uniform light intensity is impressed upon it; this low level is the sky background. The final image is a result of the fact that the extreme wings of the galaxy had probably formed a sub-image, and the weak intensities of the sky background had probably converted the sub-image into a full image. In Figure 8, the whole plate has a sub-image on it, and the addition of the galaxy only means that the area underneath the otherwise undevelopable low intensity areas of the wings are now full images. If the two exposure times t_1 and t_2 were equal and sufficiently

small to produce low levels of intensity of sky background, we could reasonably expect to obtain similar images. If $t_1 \neq t_2$, for any effect to be produced, either t_1 or t_2 must be small enough so that the two low levels of intensity can be added together. Supposing $t_1 \gg t_2$, then in the case of Figure 7, extra density would be produced by the exposure t_2 in the wings of the galaxy, while in Figure 8, no effect would be produced because t_1 has been so long that the sky background would no longer have been at a lower level. We may conclude from these comments that the effect produced by pre and post-exposure is, in some cases, an alteration of the density distribution due to the presence of extra density in the wings compared with that density which would have been obtained had there only been one exposure; removal of these distortions is only achieved by the removal of the cause, that is, by dispensing with pre and post-exposures and taking each image on a separate plate.

With regard to the sky background, when an exposure of a galaxy is made, the resulting image on the plate after processing is not a black galaxy on a clear plate, but a black galaxy on a grey plate. This is because the sky itself is not completely dark, because of scattering in the atmosphere due to urban lights etc., and the light emitted

from the sky is sufficient to produce measurable density on the plate, especially after long exposure times. This means that the intensity range of the galaxy on a plate with a large amount of sky fog is much smaller than we had previously outlined. From Figure 9 it is apparent that with the given level of sky fog density, the intensity range, instead of running from A to C, now only runs from B to C.

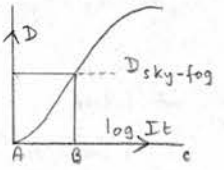

Fig. 9. Effect of sky fog on intensity range.

The set of plates for each galaxy photographed on any one night is processed simultaneously to ensure uniform development of each.

2.3. Scale Factors

Turning now to the method used for construction of the isophotes, a large grid of intensities throughout the entire surface of the galaxy is drawn up, and the isophotes are then constructed by interpolation in the X and Y directions between each grid point. Before the plates are measured on the Hilger microphotometer, the exact plate scale must be determined. This quantity was calculated by measuring accurately the distance on a plate between two stars in the Pleiades whose co-ordinates are precisely known.

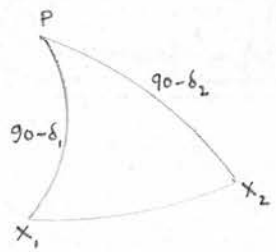

Let the stars be X_1 and X_2 with co-ordinates for the epoch in question $\alpha_1\ \delta_1$ and $\alpha_2\ \delta_2$.

$\alpha_1 = 3^h38^m6^s.8$, $\delta_1 = 24^\circ52'56"$,

$\alpha_2 = 3^h40^m42^s.7$, $\delta_2 = 23^\circ47'33"$.

The cosine formula gives

$$\cos X_1X_2 = \cos(90-\delta_1)\cos(90-\delta_2) + \sin(90-\delta_1)\sin(90-\delta_2)\cos(\alpha_1-\alpha_2),$$

whence $\cos X_1X_2 = \sin 24^\circ52'56".\sin 23^\circ47'33" + \cos 24^\circ52'56".$

$\cos 23^\circ47'33".\cos (2^m35^s.9)$.

The measured distance is 26.173mm. and the value of X_1X_2 bycalculation is 74'.3; this gives a plate scale of

1mm. = 170".328 for the SLT and a similar calculation gives a plate scale of 1mm. = 76".4116 for the JGT.

After determination of the plate scales, we now require to know the distance scale on the microphotometer tracing in terms of the angular distance on the plate. Since a driving speed of 0.25mm./min. was used throughout the work, a run of 25 millimetres was made. The run was timed accurately over 1 hour 40 minutes; the distance travelled by the carriage was measured and found to be 25mm. which proved that the driving rate was, in fact, 0.25mm./minute. Knowing the plate scale, the distance scale on the tracing paper was established and, in particular, the distance corresponding to 5 seconds of arc. A template with

divisions corresponding to 5" of arc on the plate was constructed to assist in the X direction analyses of the tracings. Furthermore, we require a Y shift for successive runs across a galaxy, and as the microphotometer has no Y co-ordinate measuring facility, a dial test indicator was fitted to the plate carriage assembly so that the distances such as the necessary 0.029mm. shift for SLT plates could be performed.

For accurate results, the size of the scanning aperture limiting the measuring beam is important. A small scanning aperture gives good resolution throughout the image, but too small a scanning aperture gives a very irregular tracing due to plate grain. However, small variations in the intensity of the galaxy require a very small scanning aperture. The optimum size of the scanning aperture which gives somewhat irregular tracings at low densities due to plate grain but yet resolves small variations in the surface density of the galaxy seemed to be 0.004mm. square as projected on the plate corresponding to a scanning aperture of 0.46 square seconds of arc on the SLT plates, and 0.09 square seconds of arc for the JGT plates.

2.4. Microphotometry and Data Reduction

The microphotometry of the image of a galaxy involves making a series of scans across the image, beginning each scan from a fixed value, and moving the ordinate a

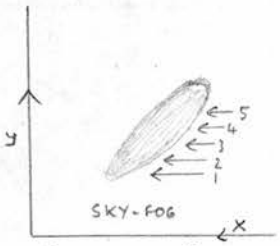

Figure 10. Scans across a galaxy.

constant value before commencing succeeding scans. The wedge steps were scanned, and this data was used for plotting the characteristic curve for the plate. It was found advisable to make scans across the wedge both before and after the galaxy scanning as this procedure served as a useful check on the sensitivity of the microphotometer throughout the scanning. A series of tracings was thus produced. An example of one such tracing is shown in Figure 11 which would correspond qualitatively to the form obtained from scan 3 in Figure 10. The next step was to mark off the tracing in steps of X=5" using the template. The sky-fog level was found by measuring the average transmission at a series of points on the tracing extended well outside the galaxy area, each point being the average of the transmissions of ten points in a small range of the trace. The values on the paper tracing of 0% and 100% transmission were known for each X value along a scan. The following set of calculations was performed in order to obtain the intensity at any point:-

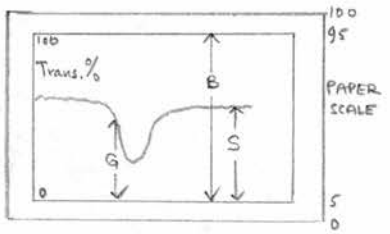

Figure 11. Example of a tracing produced after a scan across a galaxy.

(1) note the number of the X value being dealt with, the initial X and Y co-ordinates of that run, and B, the range.

(2) Measure the sky-fog transmission value S and the galaxy transmission G

(3) Calculate the sky-fog opacity B/S and the galaxy opacity G/S

(4) Find the sky-fog density D_s=log (B/S) and the galaxy density D_g=log(G/S)

(5) Use the characteristic curve to find log intensities I_s and I_g corresponding to D_s and D_g respectively

(6) Calculate log I_g-log I_s=log I_g/I_s=log I, following the definition of de Vaucouleurs and Page (1962)

(7) Plot the value of log I on the appropriate grid point.

Each plate was scanned on the one complete run, since variations in the sensitivity of the microphotometer could occur if the machine had not been reset accurately. The main difficulty, as mentioned previously, was balancing the reference and test amplifier circuits in the absence of any input signal, and it is for this reason that the whole galaxy was scanned on the one fixed setting of controls.

Since the evaluation of several thousand intensity values would have proved extremely time consuming, the following computer programme, based upon a detailed investigation of the best numerical procedures, was written to calculate the intensity values, given data for the characteristic curves and transmission values at each point.

```
C       ISOPHOTES OF NGC 4111
        DIMENSION D(452),F(452),TX(96),REIN(96)
        READ 100, (D(I),I=1,452)
        READ 101, (F(I),I=1,452)
   33 READ 102,KPL,Y,X,SKY,DR,L
        IF(KPL-9)7,8,8
    7 PRINT 103,KPL,Y,X
        KPL=KPL-5
        READ 104, (TX(M),M=1,L)
        M=1
   35 IF(TX(M))10,10,11
   11 Z=100.*(LOGF(DR/TX(M))/(LOGF(10.)))
        GO TO (12,13,14),KPL
   12 I=1
        GO TO 18
   13 I=126
        GO TO 18
   14 I=223
        GO TO 18
   18 IF(D(I)-Z)4,6,6
    4 I=I+1
        GO TO 18
    6 XIN=F(I-1)+(F(I)-F(I-1))*(Z-D(I-1))
```

```
    9 REIN(M)=1000.*(XIN-SKY)
      M=M+1
      GO TO 35
   10 J=M-1
      PRINT 105,(REIN(M),M=1,J)
      GO TO 33
  100 FORMAT (18F4.0)
  101 FORMAT (18F4.3)
  102 FORMAT(I1,1XF5.0,1XF5.0,1XF5.0,1XF5.0,1X12)
  103 FORMAT(4HPL =,I1,9X2HY=,F6.1,9X2HX=,F6.1)
  104 FORMAT(24F3.1)
  105 FORMAT(11HINTENSITIES/(10F8.0))
    8 STOP
      END
```

The isophotes were obtained by joining points with a given value of log I; these points were found by linear interpolation in both the X and Y directions. An alternative method suggested by F. Bertola at the sub-committee meeting of commission 28 on galaxy photometry at the I.A.U. (Hamburg 1964), would be to select a given value of log I, and determine what transmission factor on the microphotometer tracing would be required to produce the corresponding density for the given value of log I. The isophote would then be obtained by manipulating the X and Y co-ordinates on

the microphotometer so that the transmission value on the tracing would remain constant. The number of values defining the isophote would depend on the number of X and Y co-ordinates noted during manipulation; such a method, however, would require extremely accurate X and Y scales, with a vernier attachment a necessary feature.

2.5. Isophotometers

According to information communicated to me privately by de Vaucouleurs, a commercial version of the machine now in use at the McDonald Observatory, Texas, for drawing isophotes automatically is shortly to become available at a purchase price of approximately 20,000 dollars. Dr D. Koelbloed, of the University of Amsterdam, has recently designed and developed a machine for plotting isophotes. The instrument, based on an idea by Mohler and Pierce (1957), recently became operational, and it is claimed that it could be manufactured at a cost of about 1000 dollars. An invitation was kindly extended by Dr Koelbloed to use this machine at the Astronomical Institute, Amsterdam.

The main mechanical constructional work in his isophotometer involves a conversion of a Hilger and Watts H825 microphotometer. Instead of the output being relayed to a Brown recorder, it is relayed to a pen which is in

contact with a drum. The pen and drum are arranged so that the rotation of the drum gives the X movement on the plate and the rotation of the lead screw to which the pen is attached gives the Y movement. The main difficulty involved in such a construction is the ability of the machine to reproduce accurately the Y shift, where Y is measured in the same units as the X movement. The speeds of the motors controlling the X and Y movements are variable, thus enabling different magnifications of the plate scale to be used. For plotting a particular isophote, there must be some device between the photomultiplier output and the pen for recognizing the given transmission. There must also be an automatic device so that the operation

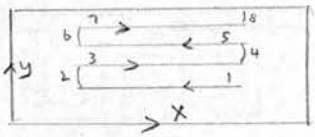

displayed on the diagram takes place--limit switches at the end of the X runs serve this purpose. The method by which the transmission at any point is recognized is extremely simple and overcomes any electronic difficulties due to photomultiplier noise in distinguishing the transmission. The current from the photomultiplier of the Hilger is fed into a Kipp Stylo galvanometer with a full scale deflection time of 1/20 sec. Light passes through a slit on to the galvanometer mirror and is reflected against a board containg many slits. When a transmission of 50% is desired, it is ascertained where the clear plate value of the light reflected from the

galvanometer mirror lies, and where the dark slide value appears. At the half-way point, a slit is opened and when the motor is set running, the current from the photomultiplier causes a rotation of the galvanometer mirror, and when the scanning aperture passes over an area having 50% transmission, the light source is reflected by the galvanometer mirror through the open slit, and the light then passes through a lens which focusses the beam on a photomultiplier. The current from the photomultiplier is then amplified and relayed to the pen which gives a slight spark. Teledeltos paper has been wrapped round the drum and this spark causes a mark to be left on the paper. Each time the plate transmission measured by the microphotometer is 50%, a spark is obtained and by joining up all the marks on the paper, the isophote is produced. Since there are difficulties in the backlash in the gearing system driving the drum recorder, alternate runs are omitted by fitting a switch over the amplifier-pen wire.

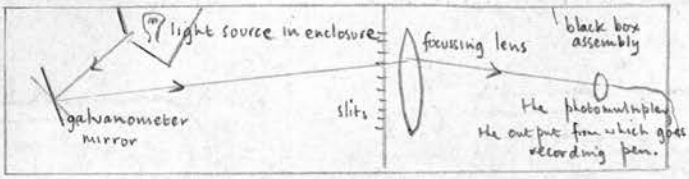

Figure 12. Schematic arrangement of part of Dr Koelbloed's isophotometer.

The isophotes obtained using Dr Koelbloed's isophotometer will be shown in connexion with the photometry of NGC 6720, when they can be compared with the corresponding

isophotes obtained at St Andrews.

Another type of isophotometer is described in this section, the Joyce-Loebl Isodensitracer, to clarify the meaning of the isophotometric tracings of galaxies made with this instrument and which are referred to later in this chapter. The optical system of this instrument automatically probes the entire plate area by making a series of closely spaced parallel scans. For each scan of the image a corresponding coded parallel line is recorded, forming a contour map of the scanned area. Contours produced show the quantitative density values at all points based on the calibration of a single data point. The code in the recorded lines indicates precisely the amount of density change in known increments. For increasing density, we obtain a blank-dots-line tracing, while for decreasing density, we obtain a line-dots-blank-line-dots-blank tracing. Each symbol in sequence represents a density increment and is is continuously plotted until the density in the image changes by that amount. After one run, the pen lifts from the paper, and both the plate table and the recording table return to the start, while at the same time, the recording pen steps in the Y direction and the next scan is commenced. The X magnification scale ranges from 1 to 2000 and the Y ranges from 1 to 3000; each of these scales may be set independently. The pen can space lines 125 microns apart or any multiple

Magnification: 50X in x and y.

Magnification: 200X in x and 50X in

Isophotes of NGC 4111 made on a Joyce Loebl Isodensitracer.

from 1 to 31 of this value. The mode in which the pen writes is controlled by the movement of an optical attenuator. This consists of a 9-inch continuous wedge whose density increases linearly from one end to another. When two beams of light, one passing through the image and the other through the attenuator, are of unequal intensity, a servomechanism physically moves the attenuator until the light intensity difference is zero. This wedge movement, which is an analog output of the image density, is encoded and fed into the isophote pen solenoid. The size of the density increment can be controlled by interchanging 5 optical attenuators giving a variation in the density steps of from 0.0125 to 1.0D. On the suggestion of Mr Loebl, a plate of NGC 4111 was sent to the United States and the accompanying diagram shows the tracings obtained from the isodensitracer. The density steps were approximately 0.02D and a comparison with the isophotes obtained using the Hilger microphotometer clearly reveals the superior resolution of the Joyce-Loebl instrument.

3. Photometry of NGC 4111 in the B Wavelength Range

The complete plate material used in the study of NGC 4111 is listed in table 1; the JGT was stopped down to 32 inches throughout the work which is the aperture for no vignetting.

TABLE 1

PLATE	TELESCOPE	OBJECT	EMULSION	FILTER	DATE	EXPOSURE(MIN.)
N1	SLT	NGC 4111	OaO	B(P)	7/8.4.64	10
N2	SLT	NGC 4111	OaO	B(P)	7/8.4.64	55
N3	SLT	NGC 4111	OaD	V(P)	7/8.4.64	10
N4	SLT	NGC 4111	OaD	V(P)	6/7.3.64	60
N5	JGT	NGC 4111	OaO	B(S)	25/26.4.64	10
N6	JGT	NGC 4111	OaO	B(S)	12/13.4.64	60
N7	JGT	NGC 4111	OaD	V(S)	12/13.4.64	12
N8	JGT	NGC 4111	OaD	V(S)	13/14.4.64	90
N9	JGT	NGC 4258	OaF	V(S)	1/2.5.64	46

PLATE MATERIAL

Isophotes have been obtained for all these plates, but the photometric parameters have only been evaluated using the JGT plates, in view of its larger plate scale and better resolution. Isophotes of plates taken with the SLT are shown for comparison on Figures 22,23,26 and 27.

NGC 4111 ($\alpha=12^h04^m.5$, $\delta=+43^o21'(1950)$) is an elliptical galaxy type E7 on the Hubble classification and a type $SA(r)O^+$ in de Vaucouleurs classification (de Vaucouleurs 1959, 1962). The SAO means a lenticular with an absence of bar structure, probably because it is viewed edge-on, the (r) means it belongs to the ringed family as opposed to the spiral (s) and the $^+$ means it is in the early subdivision of the SAO. In the following section, the derivation and listing of the

parameters is made for NGC 4111 using the B and V magnitudes; the arrangement of the data and graphs is based on de Vaucouleurs' papers on the photometry of bright southern galaxies photographed between 1952 and 1956 with the 30-inch and 74-inch reflectors of Mount Stromlo.

For an ideal object with circular isophotes, the luminosity emitted between r and r+dr is $2\pi I(r)rdr$ and the total luminosity emitted between the centre and r is

$$L_T = 2\pi \int_0^r I(r)\, r\, dr.$$

For an elliptical galaxy with semi-axes a and b, the total luminosity may be evaluated numerically according to

$$L_T = \pi \sum_0^\infty (a_{i+1} b_{i+1} - a_i b_i) I_{i+\frac{1}{2}} = \pi \sum_0^\infty P_i$$

where I is the brightness of the isophote of semi-axes a and b. The fraction of the total luminosity emitted between o and r is $k(r) = L_r/L_T$. For elliptical isophotes with semi-axes a and b, the luminosity profile I (a) is supplemented by the ellipticity curve b/a(a), and the relative integrated luminosity curve k(a) then defines the effective semi-major axis a_e where k(a) =1/2. The equivalent effective radius $r_e = \sqrt{a_e b_e}$.r* can be defined by $r^* = \sqrt{A/\pi}$ where A is the total area of the isophote. The equivalent luminosity profile and the relative integrated luminosity profile are log I against r* and k(r) against r* respectively. The reduced luminosity profile is defined by the reduced variables

$J=I/I_e$ and $\alpha=a/a_e$. In addition to the effective dimensions r^*_e, defined by $k=1/2$, dimensions r^*_1 and r^*_3 defined by the quartiles of the relative integrated luminosity curve $k(a_1)=1/4$ and $k(a_3)=3/4$, are introduced to define two concentration indices $C^*_{21} = r^*_e/r^*_1$, $C^*_{32} = r^*_3/r^*_e$.

The galaxy, in addition to the tabulated parameters, is described by

(1) A set of isophotes

(2) The luminosity profiles along the principal axes, and a mean luminosity profile $\log I(a) = 1/2 \left[\log I(a) + \log I(-a)\right]$

(3) An ellipticity curve

(4) A relative integrated luminosity curve

(5) A table of mean luminosity distribution and integrated luminosity.

The isophotes of the inner and outer regions of NGC 4111 taken with the JGT on plates N5 and N6 respectively are shown on Figures 13 and 14, while the isophotes obtained with the SLT plates are shown in Figures 22 and 23, together with their corresponding log I values. The major axis is in position angle $\theta=59^o\pm3^o$. The luminosity profiles of the major and minor axes are shown in Figures 15 and 16 together with the mean luminosity profiles of these axes in Figure 17. The ellipticity curve in Figure 18 shows for $10" < b/a < 90"$ that $\langle b/a \rangle = q = 0.30$.

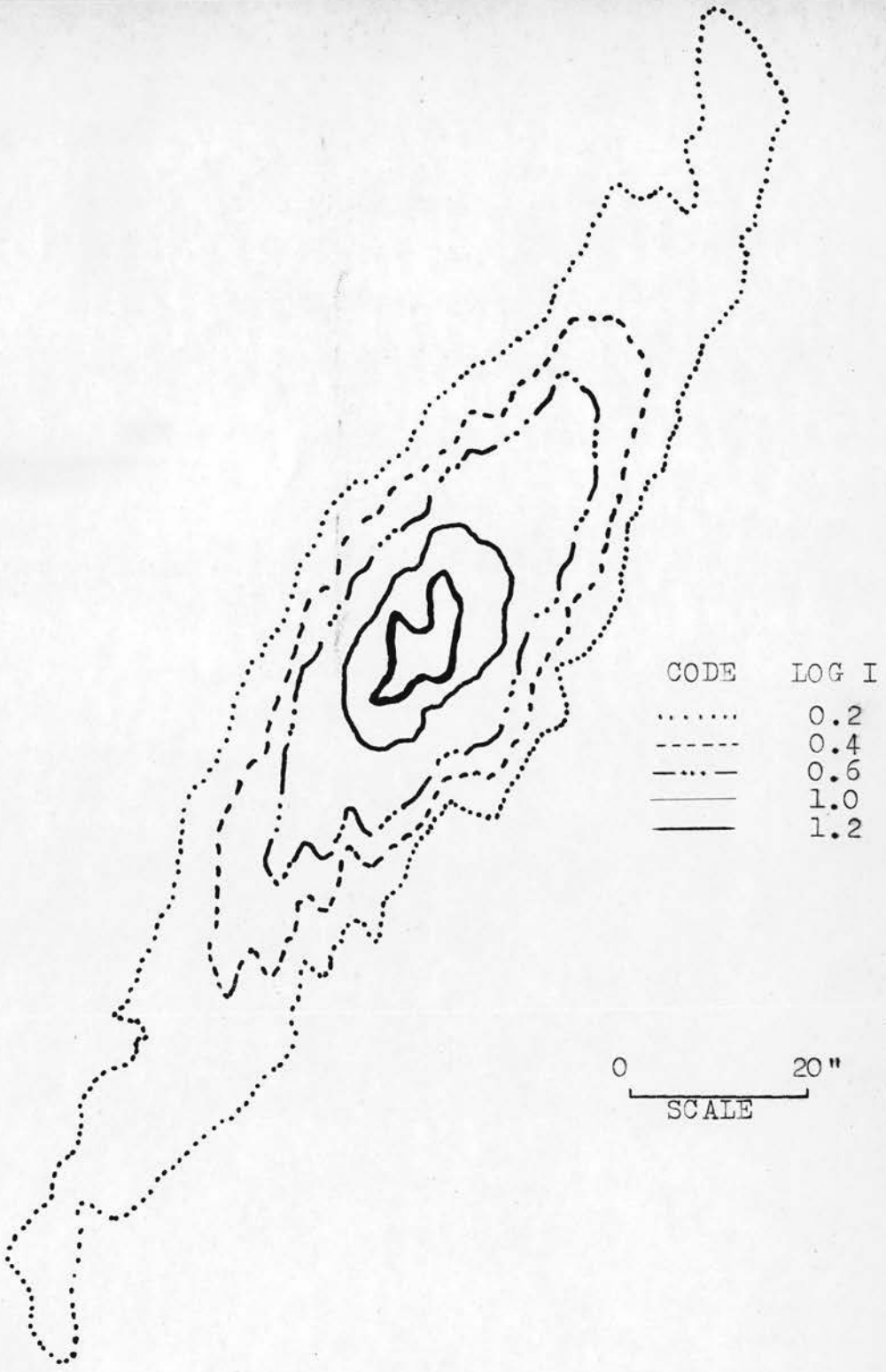

Fig. 13 --- Isophotes of the inner regions of NGC 4111.

B-FILTER. PLATE N5.

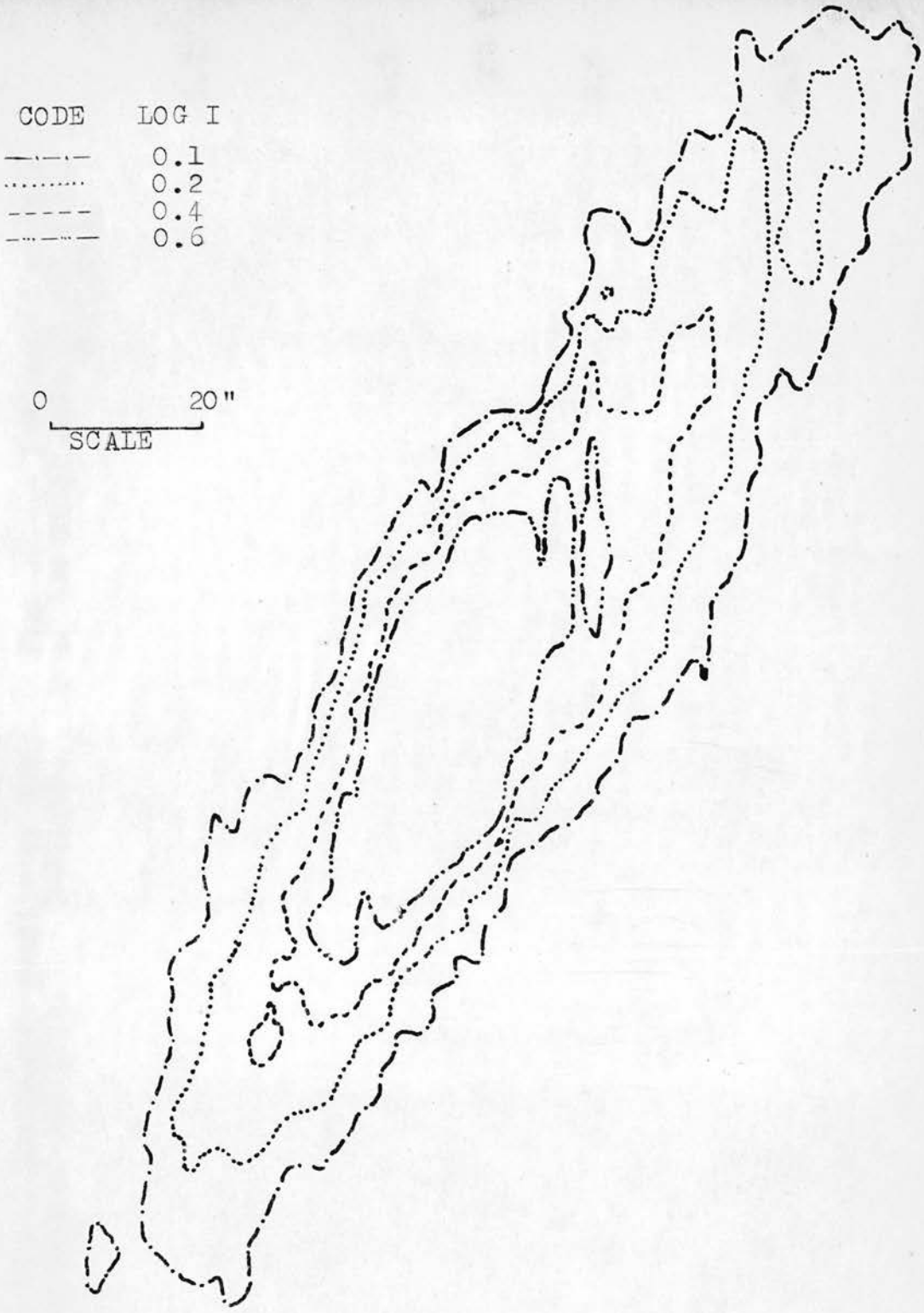

Fig. 14 --- Isophotes of the outer regions of NGC 4111.
B-FILTER. PLATE N6.

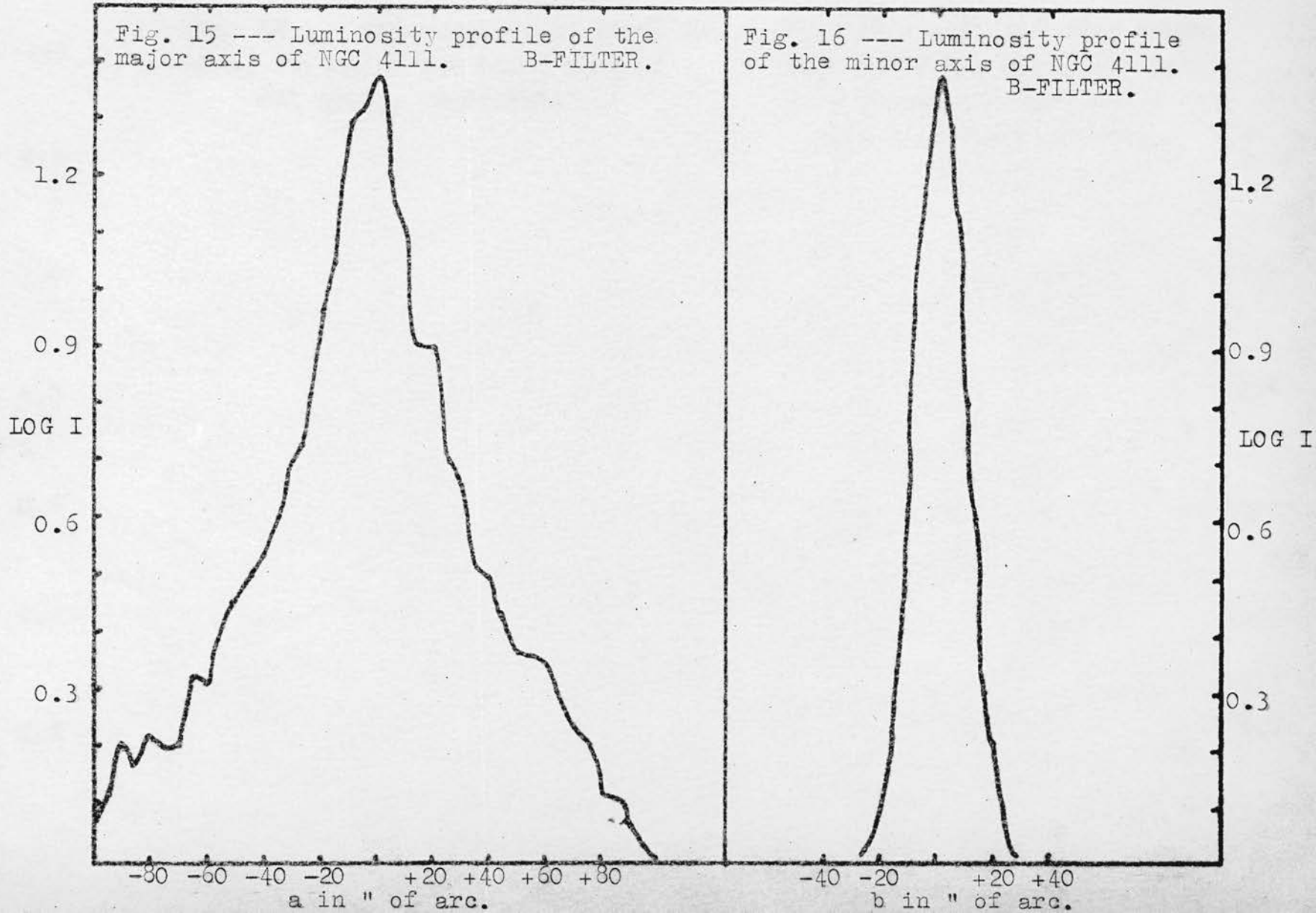
Fig. 15 --- Luminosity profile of the major axis of NGC 4111. B-FILTER.
1.2
0.9
LOG I
0.6
0.3
-80 -60 -40 -20 +20 +40 +60 +80
a in " of arc.
Fig. 16 --- Luminosity profile of the minor axis of NGC 4111. B-FILTER.
1.2
0.9
LOG I
0.6
0.3
-40 -20 +20 +40
b in " of arc.

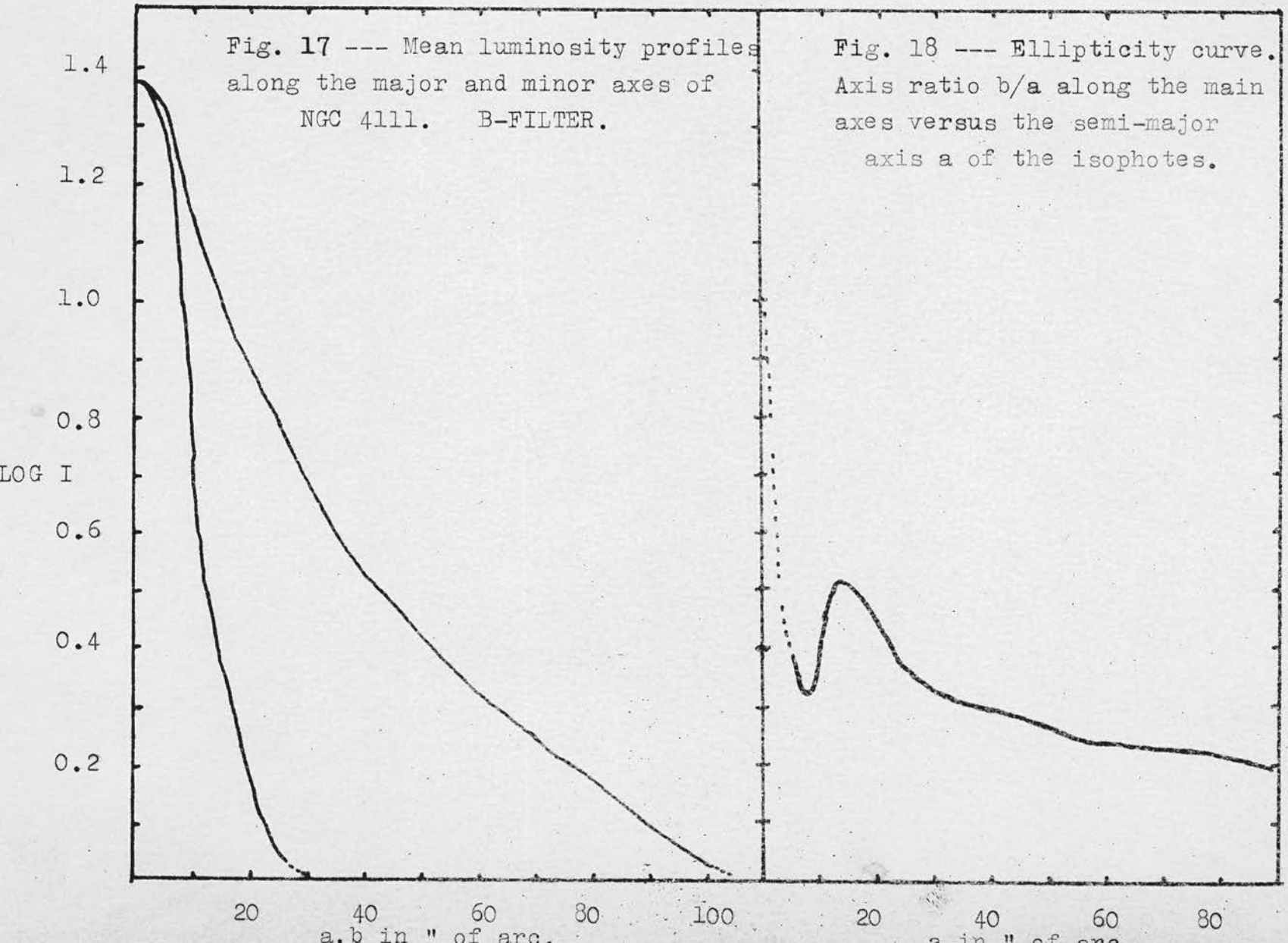

Fig. 17 --- Mean luminosity profiles along the major and minor axes of NGC 4111. B-FILTER.

Fig. 18 --- Ellipticity curve. Axis ratio b/a along the main axes versus the semi-major axis a of the isophotes.

These isophotes which have been obtained are, however, uncorrected for instrumental profile; the correction to the major axis can be determined by solving the equations of the form derived in part six of chapter two:-

$$M(x) = \int_{-\infty}^{+\infty} T(y)I(x-y)dy$$

where M is the measured distribution,

T is the true distribution and

I is the instrumental profile.

If a mathematical function could be found to represent both M(x) and I(x-y), the equation could be solved using one of the methods suggested by van de Hulst (1946). The numerical values of the luminosity must be displaced so that the maximum of the galaxy corresponds with the maximum of the instrumental profile. The equation for M(x) is obtained by the following method:-

x/12.5 (x measured along major axis)	log I	x	x.log I	x^2.log I
0	2.10	-8	-16.8	134.40
1	2.15	-7	-15.05	105.35
2	2.21	-6	-13.26	79.56
3	2.32	-5	-11.60	58.00
4	2.44	-4	-9.76	39.04
5	2.58	-3	-7.74	23.22
6	2.80	-2	-5.60	11.20
7	3.10	-1	-3.10	3.10
8	3.38	0	0	0
9	3.12	1	3.12	3.12
10	2.83	2	5.66	11.32
11	2.66	3	7.98	23.94

12		2.50	4	10.00	40.00
13		2.37	5	11.85	59.25
14		2.20	6	13.20	79.20
15		2.14	7	14.98	104.86
16		2.08	8	16.64	133.12
	$\sum \log I$ =	42.98			
	$\sum x \log I$ =			0.44	
	$\sum x^2 . \log I$ =				888.69

$M = A + \sum x . \log I / \sum \log I = 0.013$

$\sigma^2 = \sum x^2 \log I / \sum \log I - (M-A)^2$

$\sigma = 4.5472$, $2\sigma^2 = 41.3534$ and

$M(x) = 3.7808\ e^{-x^2/41.35}$.

In a similar manner we obtain for $I(x-y) = 2.809\ e^{-(x-y)^2/10.56}$.

We require to find f(y) from the equation

$$3.7\ e^{-x^2/41.3} = \int_{-\infty}^{+\infty} f(y) .\ 2.809\ e^{-(x-y)^2/10.56}\ dy.$$

Attempts were made to obtain a solution for this equation using Hermite polynomials defined by $e^{2xy-x^2} = \sum_{n=0}^{\infty} (H_n(y)/n!)x^n$ and their property of orthogonality, but an inadmissible solution for T(y) resulted. Another attempt was made for the solution for T(y) as a power series:-

Let $\mu_n = \int_{-\infty}^{+\infty} z^n\ h(z)dz$ where $z=x-y$.

Since the instrumental profile function h(z) is symmetrical, all odd values of μ are zero. The measured distribution $M(x) = \sum_n c_n x^n$ and $T(x-z)=T(y)= \sum_n c_n P_n(y)$.

$P_n(y)$ is a polynomial of the n th degree where $P_n(y) =$

$$-\sum \binom{n}{m} \lambda_{n-m}\, y^m \qquad \text{--------(1);}$$

the coefficients λ_j are derived from

$$\sum_k \lambda_{l-k} \binom{l}{k} (-1)^k \mu_k = \begin{cases} 1 \text{ for } l=0 \\ 0 \text{ for } l \neq 0 \end{cases} \qquad \text{--------(2).}$$

The moments of $h(z) = 2.809\, e^{-x^2/10.56}$ are

$\mu_0 = 16.182$ $\qquad$ $\lambda_0 = 0.0618$

$\mu_2 = 85.465$ $\qquad$ $\lambda_2 = 0.3264$

$\mu_4 = 1354.1020$ $\qquad$ $\lambda_4 = 5.1725$.

Solving equations (1) and (2) gives the following polynomials for P(y):-

$$P_0(y) = 1,$$

$$P_2(y) = y^2 - 3.5692,$$

$$P_4(y) = y^4 - 31.68y^2 + 83.6975.$$

$$M(x) = 3.7808\left(1 - x^2/41.3 + \left(x^4/(41.3)^2\right)(1/3!) - \left(x^6/(41.3)^3\right)(1/4!) \ldots\right)$$

Whence $c_0 = 3.7808$, $c_2 = 0.09143$, $c_4 = 0.00036$, $c_6 = 0.0000022$

This gives $T(y) = 3.7808 - 0.09143(y^2 - 3.5692) + (y^4 - 31.68y^2 + 83.6975)(0.0063)$ . . . .

Substitution of y in the above equation gives

$f(0) = 4.1372$ $\quad$ $f(2) = 3.7270$ $\quad$ $f(4) = 2.2966$

$f(1) = 4.0347$ $\quad$ $f(3) = 3.2143$ $\quad$ $f(5) = 1.5737$.

These values produce the following result on the luminosity values of the major axis of NGC 4111. The central intensity

must be increased by log I=0.62=1.564 magnitudes, while at a point 15" from the centre, the increase in magnitude is only 0.37. This compares with a correction, derived by Redman and Shirley (1938), on the 36-inch Newtonian Reflector at the Solar Physics Observatory, Cambridge, of 0.4 magnitudes in log I for the nucleus of NGC 3379. The surface brightness gradient from the centre outwards is much greater in stellar images than in the galaxy, therefore it is to be expected that the distortion of the galaxy is serious only near the nucleus. The following table gives the mean luminosity distribution in NGC 4111; the values in column 1 are corrected for instrumental profile.

TABLE 2 MEAN LUMINOSITY DISTRIBUTION

LogI	I	A	ΔA	P=$\bar{I}$.ΔA	ΣP	k(a)	r*	a	b/a	∝	J	Log J
2.00	100	0	0	0	0	0	0	0	1	0	9.3	0.96
			58.5	35.5								
1.66	45.9	58.5			35.5	0.137	4.33	7.5	0.33	0.35	4.2	0.62
			194.5	5.60								
1.21	16.2	252			8675	0.34	8.94	12.5	0.52	0.59	1.51	0.18
			690	6720								
0.7	5.01	942			15395	0.608	17.6	30	0.33	1.42	0.47	1.670
			706	2750								
0.5	3.16	1648			18145	0.712	22.9	42.5	0.29	2.01	0.29	1.46
			770	2165								
0.4	2.51	2418			20310	0.795	26.7	55	0.25	2.50	0.24	1.38
			1591	2415								
0.2	1.58	4009			22525	0.882	36.2	75	0.23	3.53	0.14	31.15
			2251	1005								
0.1	1.25	6260			25530	1.00	44.6	95	0.22	4.47	0.12	1.08

L_T=25530 and log L_T=4.4065.

$m_{sky} - m_{galaxy} = 2.5 \log L_T$ (de Vaucouleurs 1948) and this gives

$$m_{galaxy} = m_{sky} - 2.5 \log L_T .$$

Throughout this work, de Vaucouleurs' (1960) value for the sky background has been used; it is the mean sky brightness μ_s = 22.18mag.sec.$^{-2}$. Thus m_{galaxy} = 22.18-11.00 = 11.18 and so the total apparent photographic magnitude = 11.18 . The maximum dimensions are 190" × 45" = 7.2kpc. × 1.7kpc., the scale factor being 1' = 2.3kpc. using V = 832km./sec.(Humanson, Mayall, Sandage 1956) and H, the Hubble Constant = 100km./sec./Mpc. (Sandage 1962). The distance modulus is m-M = 29.60 and the absolute magnitude is -18.42 .

TABLE 3

PHOTOMETRIC PARAMETERS OF NGC 4111 IN THE B WAVELENGTH RANGE

Apparent distance modulus	m-M=29.60
Integrated luminosity (sky units per square second)	L_T=25530
Adopted sky unit (pg. mag. per square second)	μ_s=22.18
Total apparent magnitude(pg.)	m_T=11.18
Absolute magnitude	M_T=18.42
Absolute luminosity ($\odot$ =1)	log$\mathcal{L}$=9.308
Mean axis ratio $\langle b/a \rangle$, (10" < a < 90"). . . .	q=0.30±0.02

Parameters at k=1/4

Semi-major axis . . . . . a_1=10".4=0.4kpc.

Axis ratio . . . . . b/a=0.45

Equivalent radius . . . . . r_1*=6".9=0.26kpc.

Parameters at k=1/2(effective)

Semi-major axis . . . . . a_e=21".2=0.8kpc.

Axis ratio . . . . . b/a=0.40

Equivalent radius . . . . . r_e*=13".4=0.51kpc.

Mean surface brightness (mag. per square second). . . . . μ'_e=18.01

Parameters at k=3/4

Semi-major axis . . . . . a_3=46".3=1.76kpc.

Axis ratio . . . . . b/a=0.28

Equivalent radius . . . . . r_3*=23".7=0.90kpc.

Concentration indices . . . . . C_{21}=1.94

C_{32}=1.76

Gradient of exponential component. . . G(a)=-0.70min.$^{-1}$=-0.30kpc^{-1}.

Gradient of exponential component. . . G(b)=-3.60min.$^{-1}$=-1.55kpc^{-1}.

Equivalent gradient of exponential component. . G(r*)=-2.4min.$^{-1}$=-1.04kpc^{-1}.

The mean luminosity profiles shown in Figure 17 exhibit an approximate exponential decay outside the nuclear regions. Gradients G(a)=dlogI/da=-0.70min.$^{-1}$ and G(b)=dlogI/db=-3.6min.$^{-1}$

are derived from the mean luminosity profiles while $G(r^*) = d\log I/dr^* = -2.4 \text{min.}^{-1}$ is derived from the equivalent luminosity profile $\log I = f(r^*)$, which is plotted in Figure 20; it is much smoother than either of the mean luminosity profiles. The relative integrated luminosity curves k(a) against a and k(r) against r* are plotted in Figures 19 and 21 respectively. It should be stressed that the parameters in table 3 are based on an adopted value of 22.18 mag.sec.$^{-2}$ for the mean sky brightness. μ_e', the mean surface brightness inside the effective isophote is given by $\mu_e' = m_T + 5\log r_e^* + 1.995$, and for NGC 4111, this value is found to be 18.01 mag.sec.$^{-2}$. It was originally intended to determine the brightness of the sky photo-electrically in terms of known B magnitudes of stars in the vicinity of the fields in which the galaxies were located. However, photo-electric equipment was not available when the photographic observational programme was carried out.

4. Photometry of NGC 4111 in the V Wavelength Range

The corresponding set of results for plates N7 and N8 are described at this stage. The isophotes are shown in Figures 24 and 25, together with their corresponding log I values, while Figures 26 and 27 show the isophotes obtained with the SLT for NGC 4111 in V . A striking feature of the isophotes is the slight rotation of the major axes with increasing luminosity value. The major axis is in position angle $58^\circ \pm 3^\circ$; the luminosity profiles along the principal axes

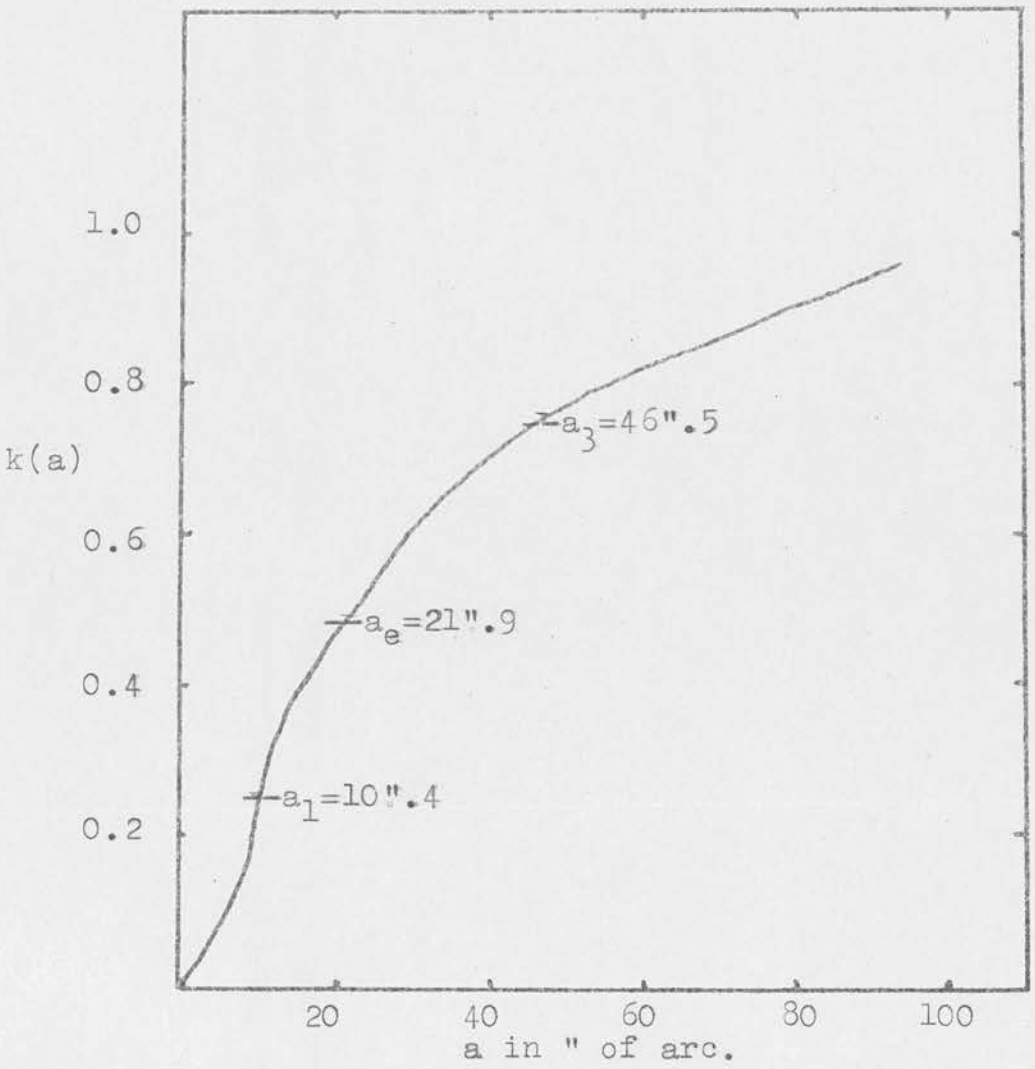

Fig. 19 --- Relative integrated luminosity curve.
NGC 4111. B-FILTER.

Fig. 20 --- Equivalent luminosity profile for NGC 4111. B-FILTER.

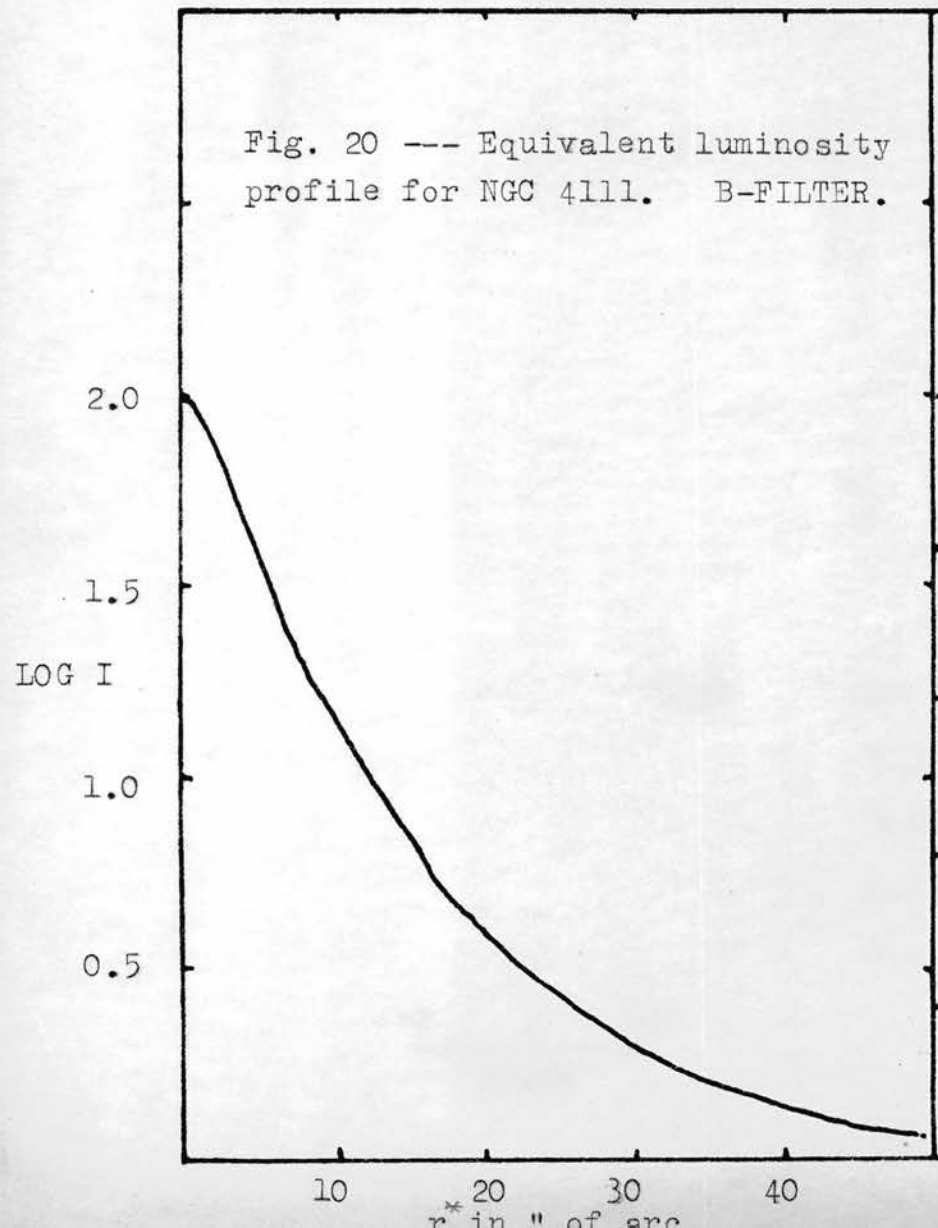

Fig. 21 --- Relative integrated luminosity k(r) versus equivalent radius r .

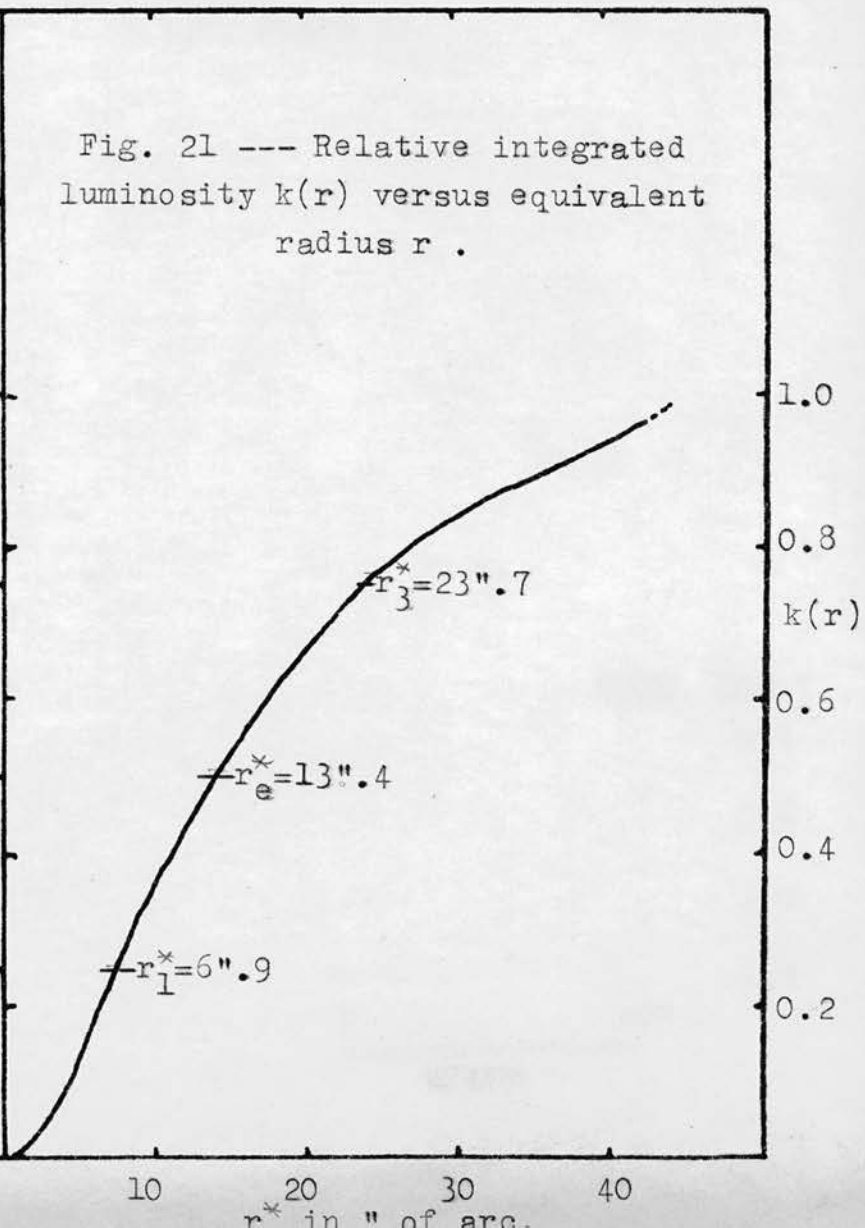

Fig. 23 --- Isophotes of outer regions of NGC 4111. B-FILTER. SLT PLATE N2.

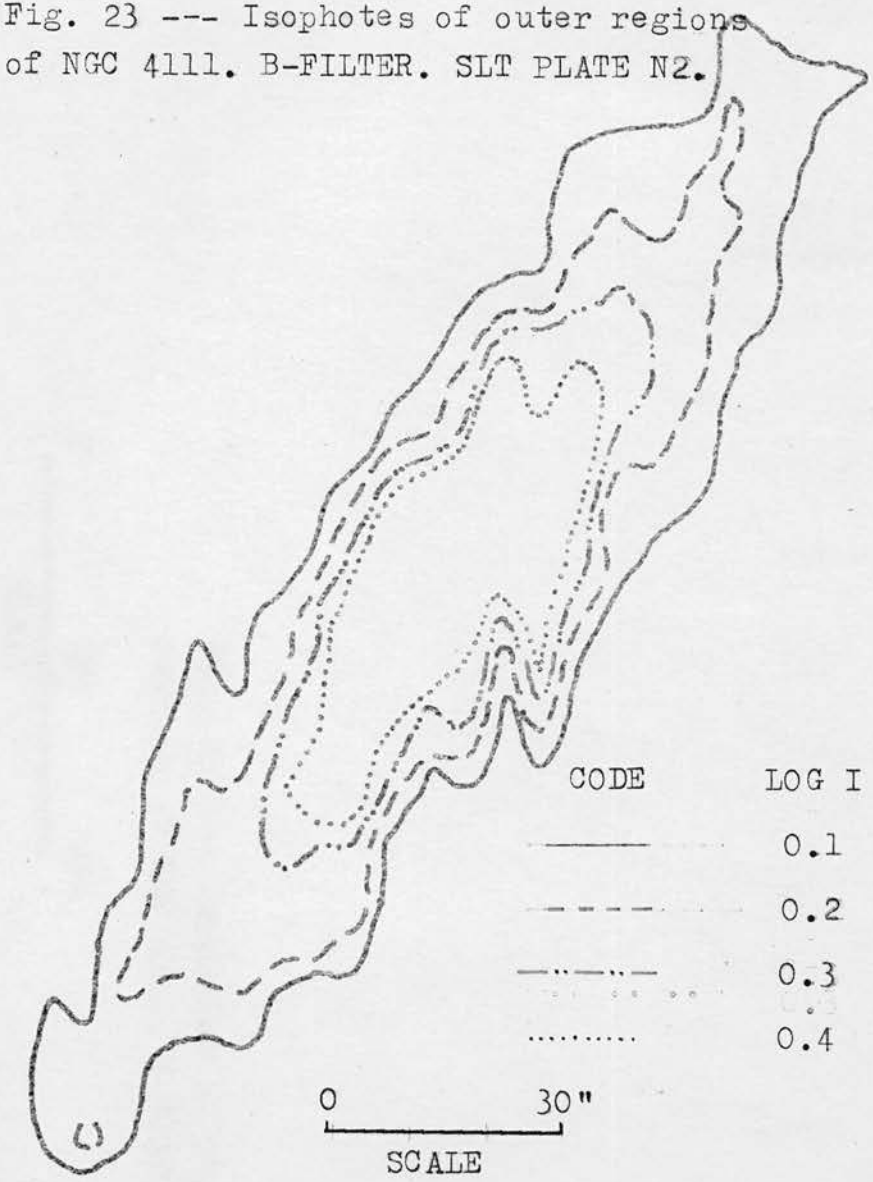

Fig. 22 --- Isophotes of inner regions of NGC 4111. V-FILTER. S.L.T. PLATE N1.

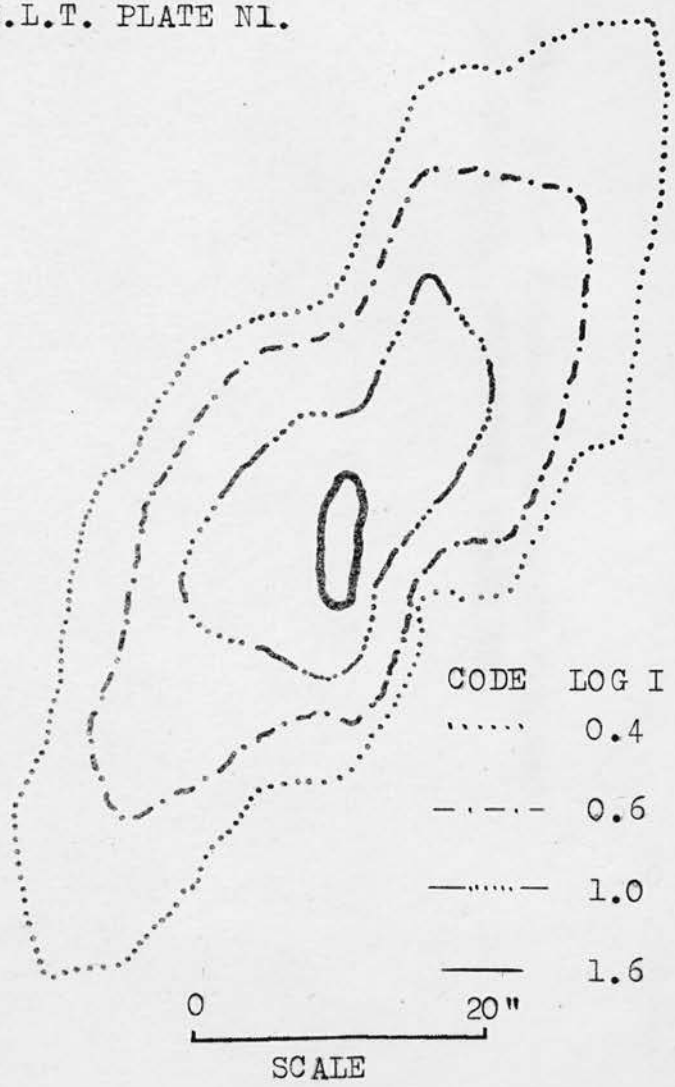

Fig. 25 --- Isophotes of outer regions of NGC 4111. V-FILTER. PLATE N8.

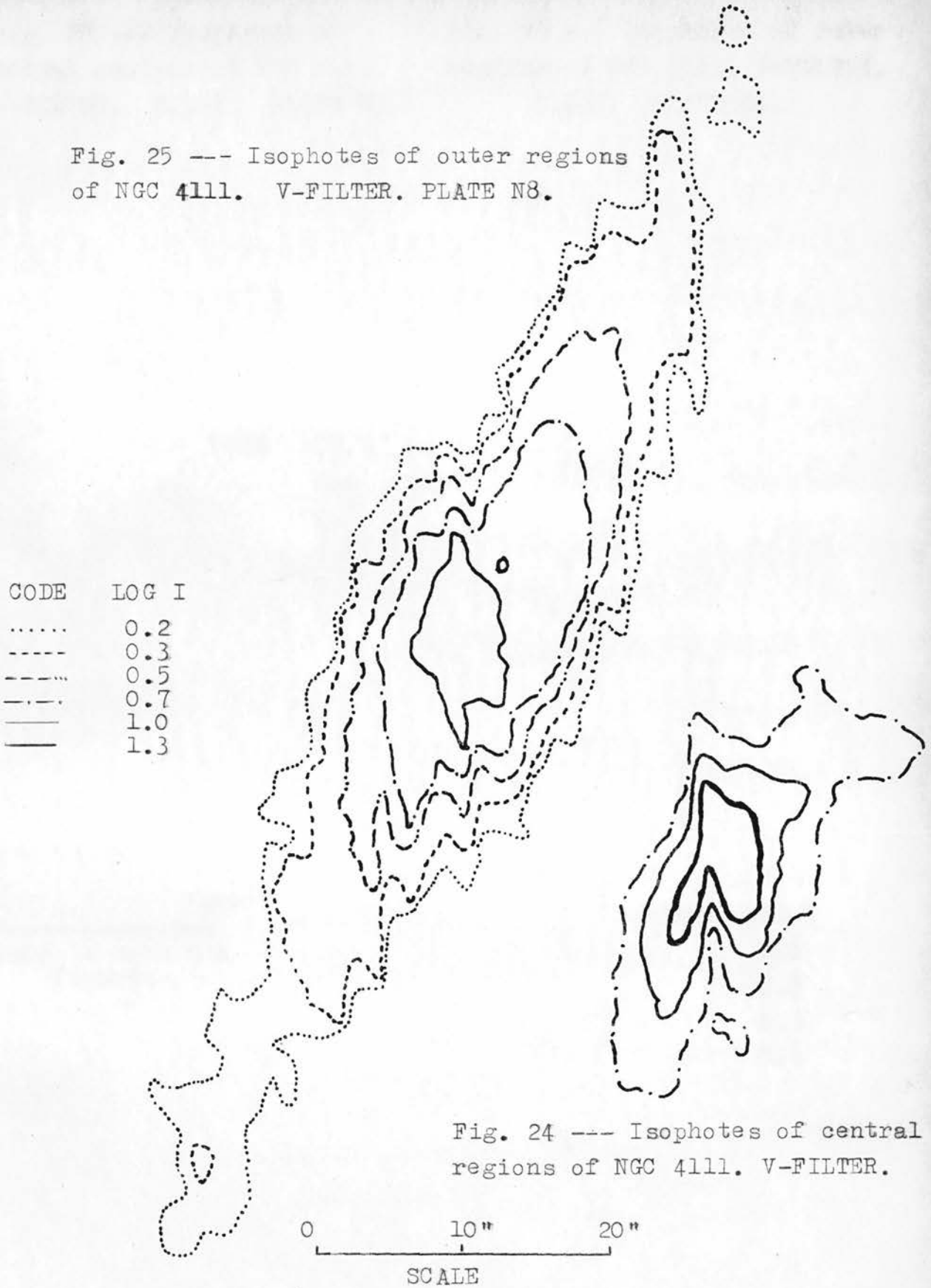

Fig. 24 --- Isophotes of central regions of NGC 4111. V-FILTER.

Fig. 26 --- Isophotes of central regions of NGC 4111. V-FILTER. S.L.T. PLATE N3.

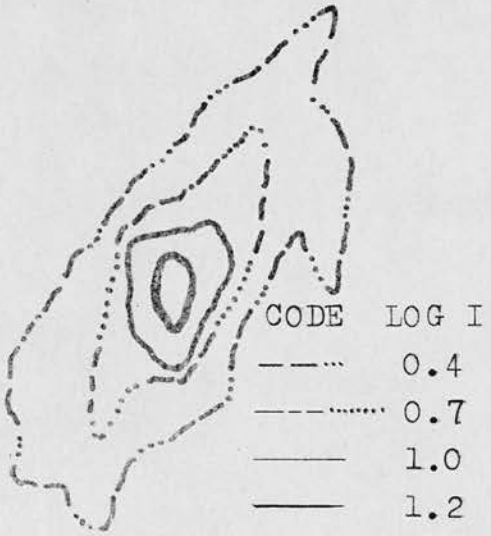

Fig. 27 --- Isophotes of outer regions of NGC 4111. V-FILTER. S.L.T. PLATE N4.

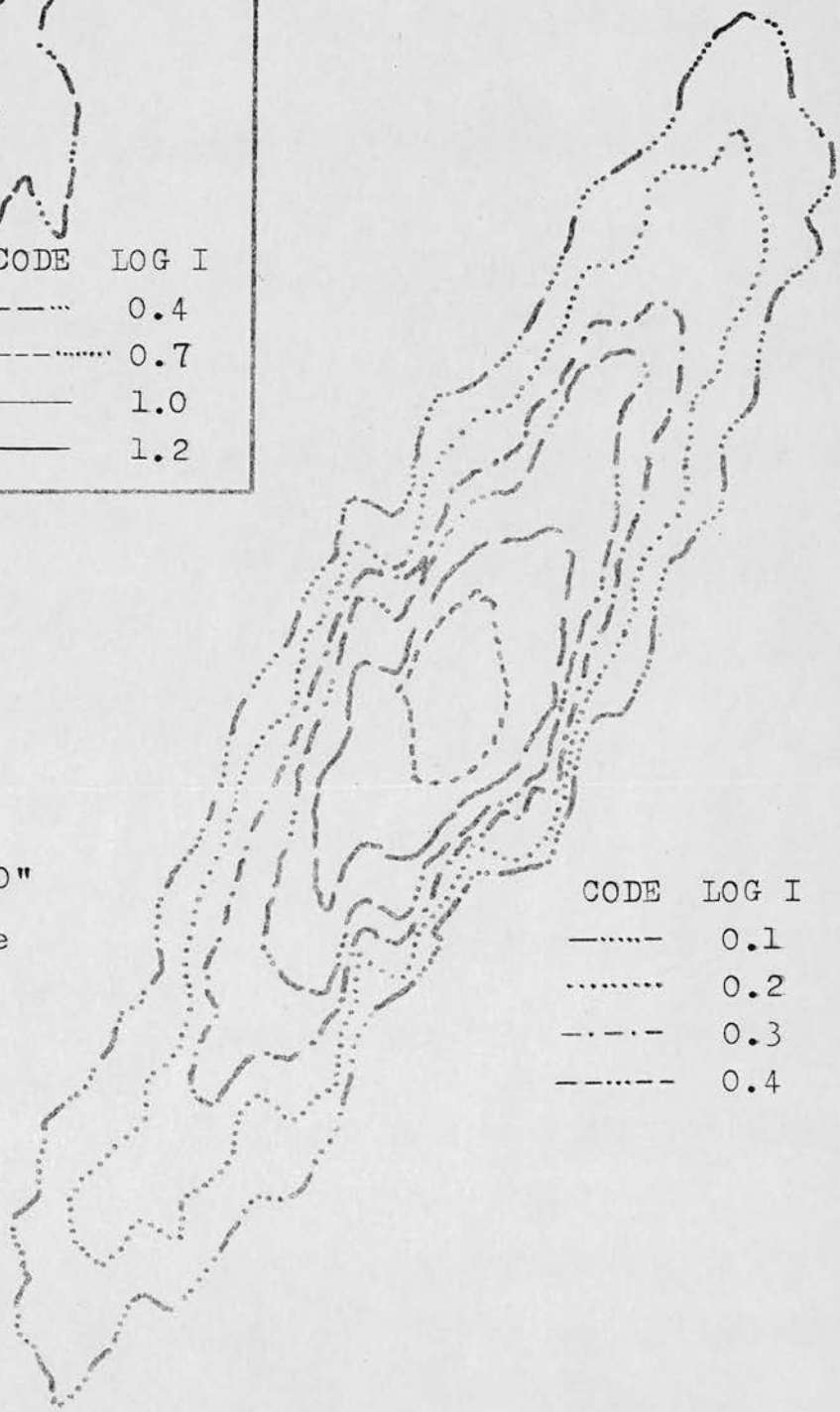

0 40"

Scale in both the figures.

are shown in Figures 28 and 29 and the mean luminosity profiles are shown in Figure 30. In Figure 31, the ellipticity curve is plotted and it gives a value for q =0.34 for 10" $<\langle b/a \rangle <$ 80". Table 4 gives the summarized mean luminosity distribution of NGC 4111 in V, corrected for instrumental profile.

TABLE 4 MEAN LUMINOSITY DISTRIBUTION OF NGC 4111

logI	I	A	ΔA	$P=\bar{I}\Delta A$	P	k(a)	r*	a	b/a	$\propto$	J	log J
1.84	69.0	0			0	0	0	0	1	0	9.3	0.96
			38	2040								
1.60	39.8	38			2040	0.01	1.10	4	0.75	0.21	5.3	0.72
			119	3800								
1.40	25.0	157			5840	0.27	7.05	10	0.50	0.54	3.4	0.53
			87	1640								
1.20	15.8	244			7480	0.35	8.8	113	0.46	0.70	2.1	0.32
			86	1080								
1.00	10.0	330			8560	0.40	10.3	15	0.46	0.81	1.36	0.13
			300	2430								
0.80	6.3	630			10990	0.51	14.3	20	0.50	1.08	0.85	1.93
			679	3450								
0.60	3.9	1309			14440	0.67	22.0	32	0.41	1.73	0.52	1.71
			711	2280								
0.40	2.5	2020			16720	0.78	25.4	46	0.31	2.5	0.34	1.53
			1300	2626								
0.20	1.58	3320			19346	0.90	32.4	62	0.27	3.35	0.21	1.32
			1450	2080								
0.10	1.26	4770			21396	1.00	39.0	80	0.24	4.32	0.17	1.23

A is in square seconds of arc.

From the total luminosity, we calculate m_T = 10.56 assuming a value of 21.6 mag.sec.$^{-2}$ for the mean sky brightness

Fig. 28 --- Luminosity profile of the major axis of NGC 4111. V-FILTER.

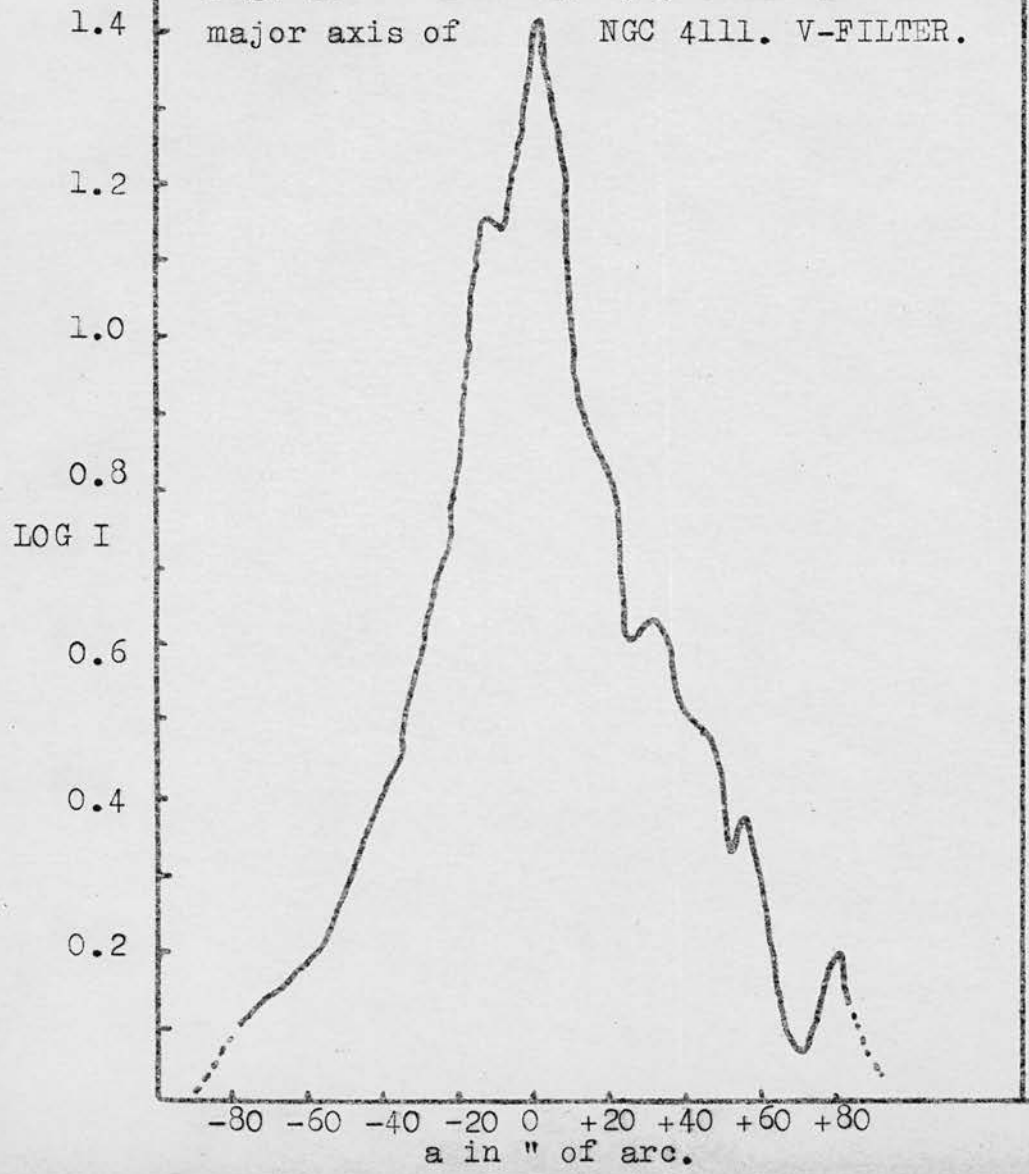

Fig. 29 --- Luminosity profile of the minor axis of NGC 4111. V-FILTER.

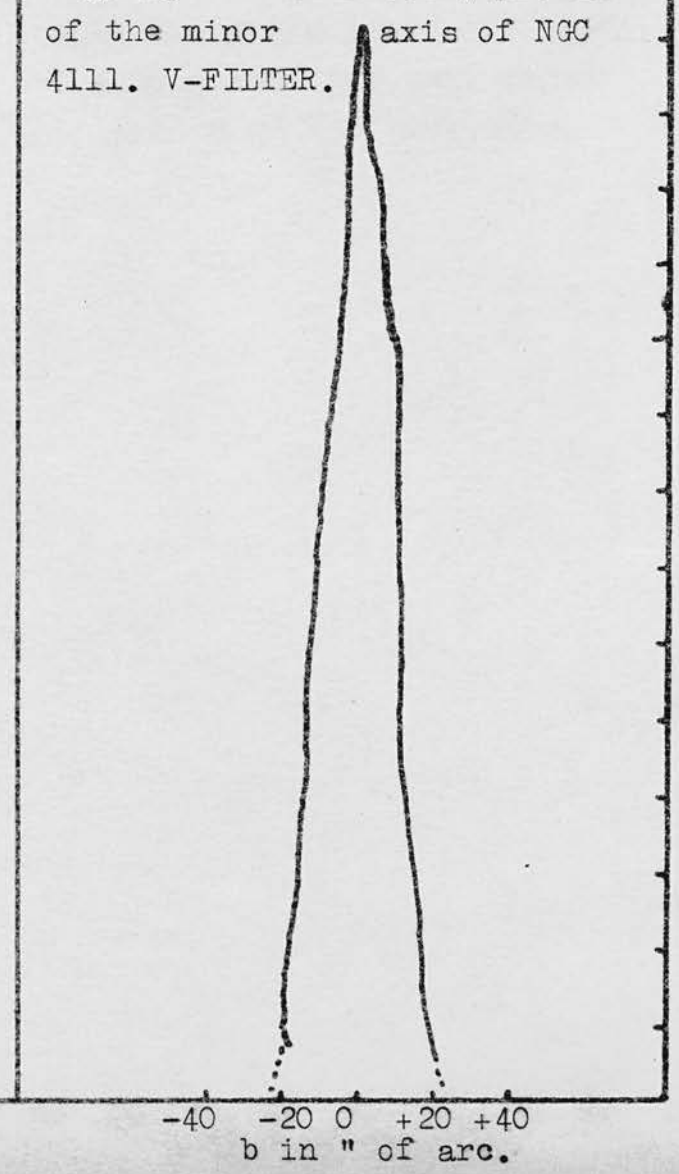

Fig. 30 --- Mean luminosity profiles along the major and minor axes of NGC 4111. V-FILTER.

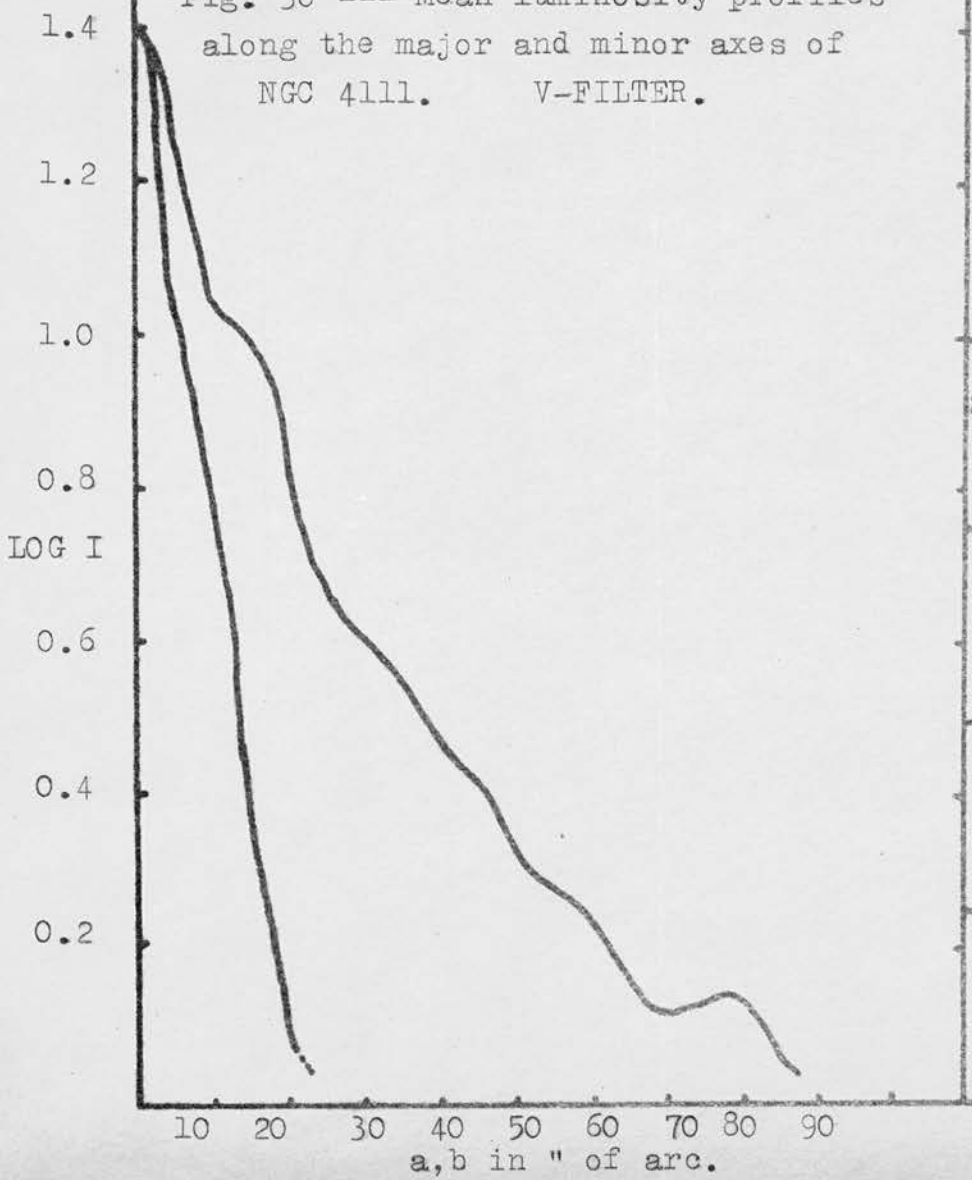

Fig. 31 --- Ellipticity curve. Axis ratio b/a along the main axes versus the semi-major axis a of the isophotes.

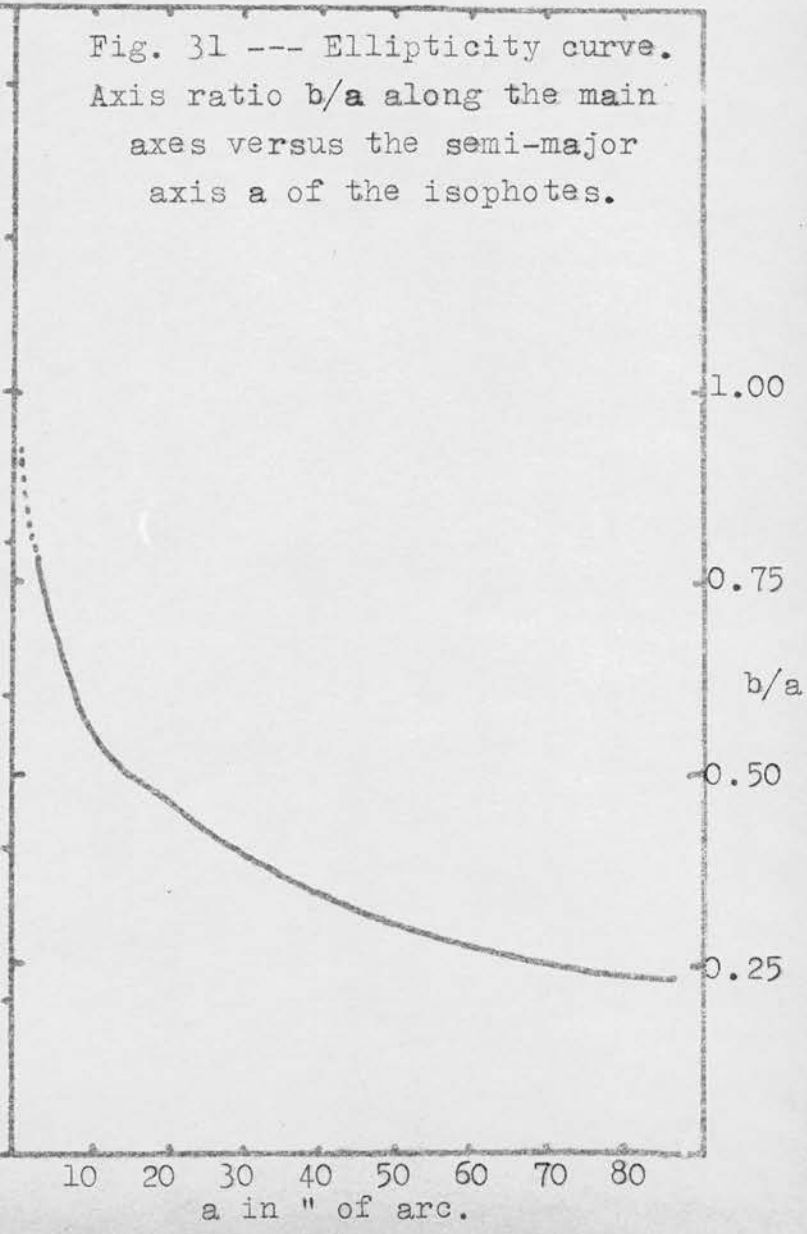

in V (de Vaucouleurs 1960) and the absolute magnitude is -19.04 . Figures 32 and 33 show the equivalent luminosity profile and the relative integrated luminosity curve; Figure 34 also defines the latter curve and gives a value of r_e^*=13.5 for the equivalent effective radius. For a > 20", b > 5" and r* > 10", the luminosity distribution is approximately exponential with mean gradients G(a)=-0.74min.$^{-1}$=-0.32kpc.$^{-1}$, G(b)=-3.9min.$^{-1}$=-1.70kpc.$^{-1}$, G(r*)=-2.04min.$^{-1}$=-0.89kpc.$^{-1}$.

TABLE 5

PHOTOMETRIC PARAMETERS OF NGC 4111 IN THE V WAVELENGTH RANGE

Apparent distance modulus	m-M=29.60
Integrated luminosity(sky units per square second)	L_T=21396
Adopted sky unit(pg. mag. sec.$^{-2}$)	μ_s=21.60
Total apparent magnitude (pg.)	m_T=10.58
Absolute magnitude	M_T=-19.02
Absolute luminosity (⊙=1)	log L=9.54
Major axis position angle	$\theta=58^o \pm 3^o$
Mean axis ratio $\langle b/a \rangle$, (10"<a<80")	q=0.34 0.02
Gradient of exponential component	G(a)=-0.74min.$^{-1}$=-0.32kpc.$^{-1}$.
Gradient of exponential component	G(b)=-3.90min.$^{-1}$=-1.70kpc.$^{-1}$.
Equivalent gradient of exponential component	G(r*)=-2.04min.$^{-1}$=-0.89kpc.$^{-1}$.
Parameters at k=1/4	
Semi-major axis	a_1=9".2=0.34 kpc.
Axis ratio	b/a=0.53
Equivalent radius	r_1^*=5".6=0.21 kpc.

Fig. 32 --- Equivalent luminosity profile for NGC 4111. V-FILTER.

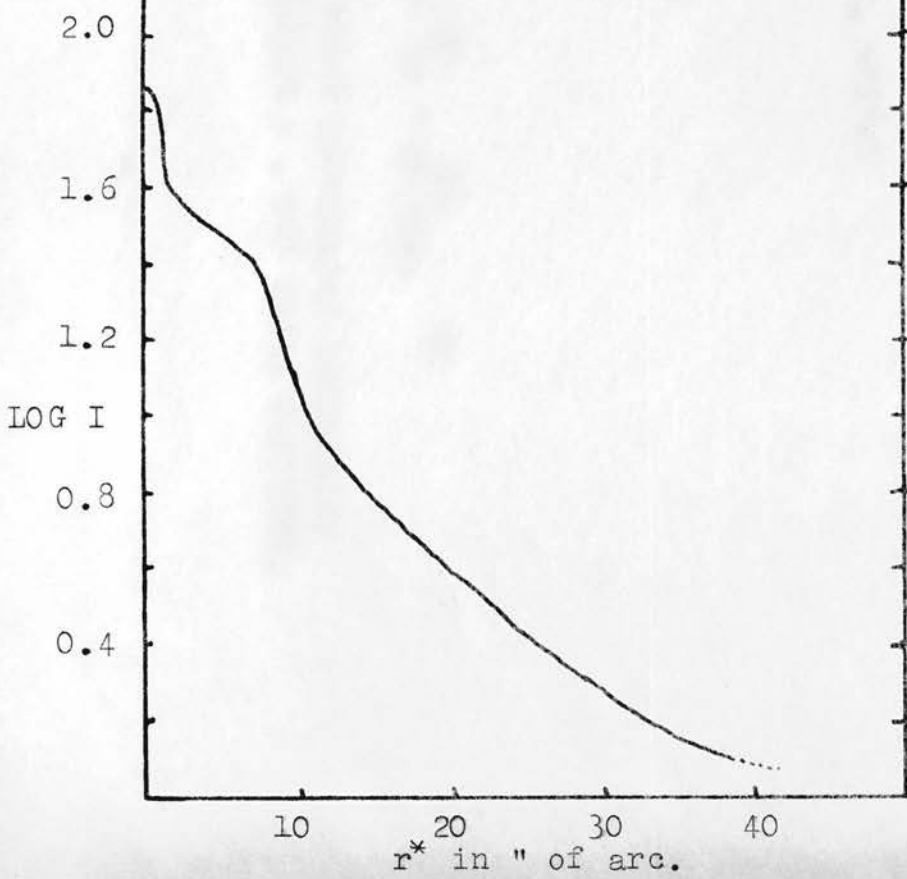

Fig. 33 --- Relative integrated luminosity curve: k(a) against a.

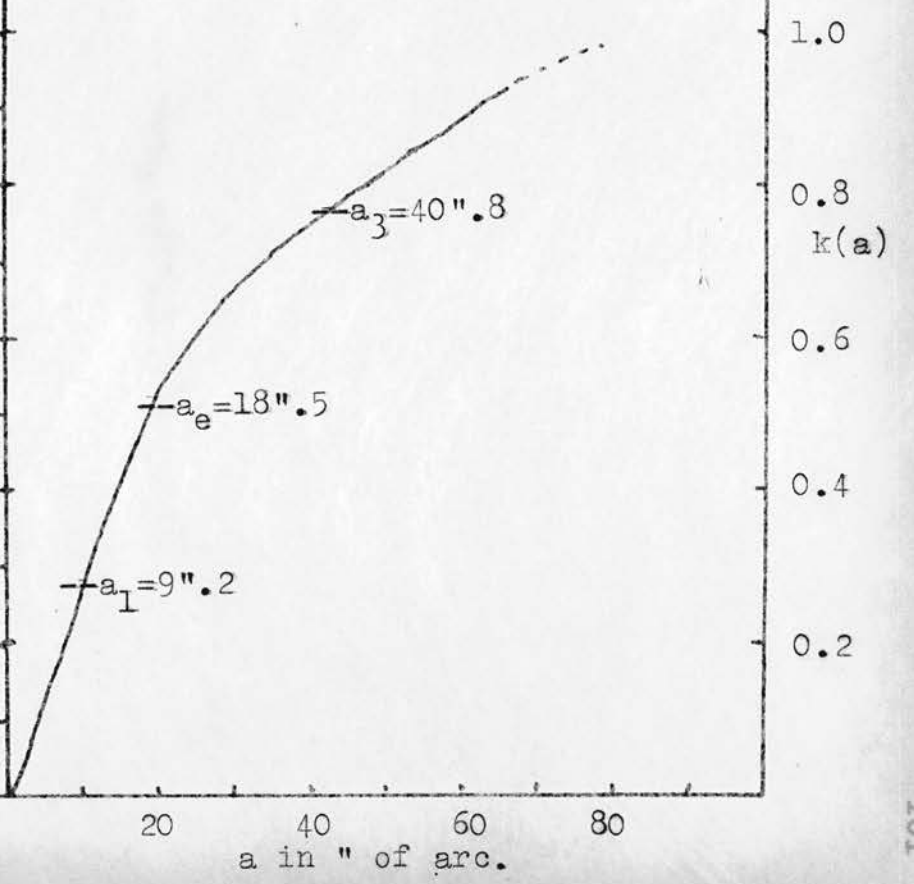

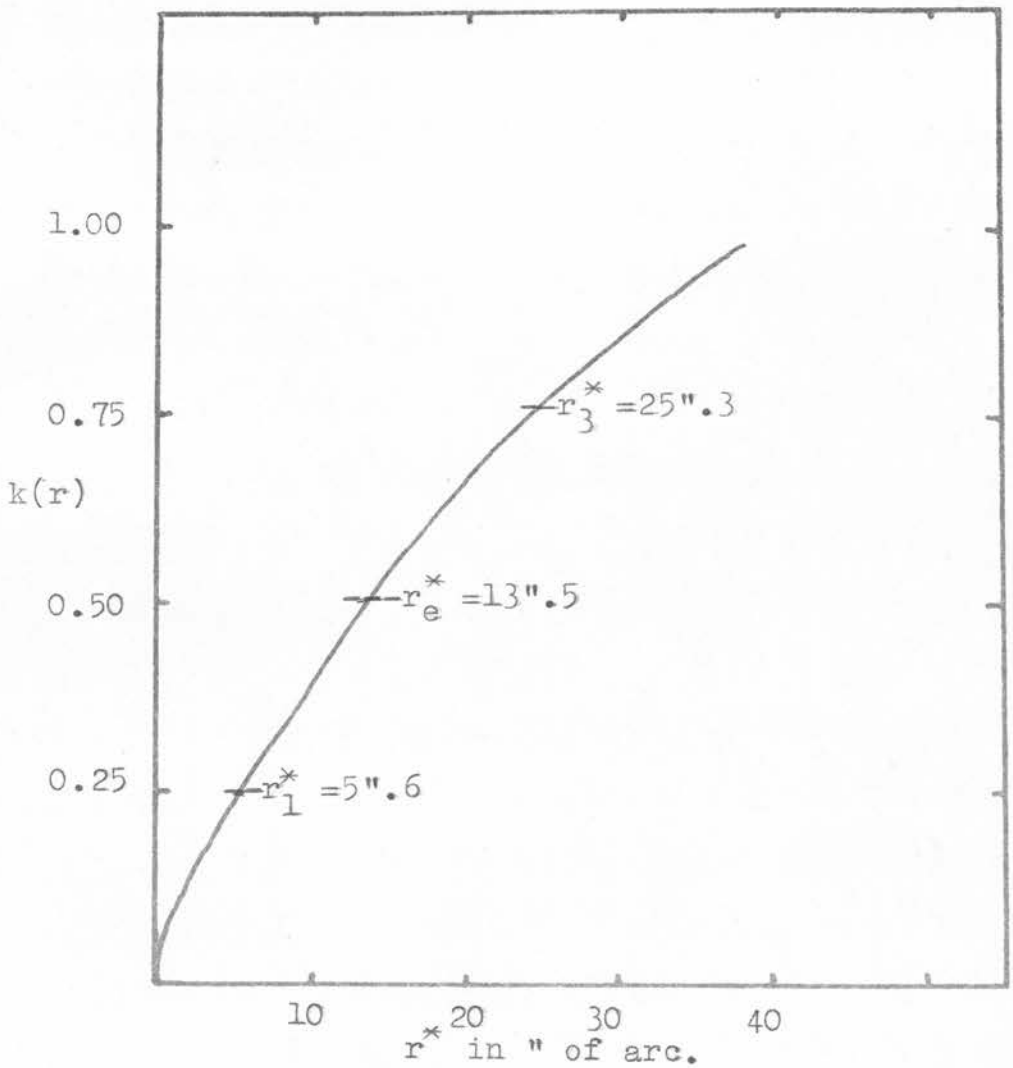

Fig. 34 --- Relative integrated luminosity profile: k(r) against r^*. NGC 4111. V-FILTER.

Parameters at k=1/2

Semi-major axis . . . . . a_e=18".5=0.70 kpc.

Axis ratio . . . . . b/a=0.44

Equivalent radius . . . . . r_e*=13".5=0.51 kpc.

Mean surface brightness . . . . . μ'_e=18.22mag.sec.$^{-2}$

Parameters at k=3/4

Semi-major axis . . . . . .a_3=40".8=1.55 kpc.

Axis ratio . . . . . b/a=0.35

Equivalent radius . . . . . .r_3*=25".3=0.96 kpc.

Concentration indices . . . . . C_{21}=2.4

. . . . . C_{32}=1.86

From the two lists of parameters, we are able to deduce that B-V = 0.60 mag., corresponding with van Houten's (1961) value for B-V of 0.92 mag. at the central nucleus of NGC 4111.

At the I.A.U. meeting in Berkeley in 1961, a working sub-committee on galaxy photometry was formed, with Professor Stibbs as one of its founder members, with a view to standardizing the photometric measurements of different observers. The parameters listed in Tables 3 and 5 are the first set of parameters which have been determined for this galaxy. Accordingly, it is not possible to make a definitive comparison between the work presented in this thesis and the work of other investigators which has centred on the determination

of the integrated apparent magnitude of the object. As already mentioned, a direct comparison between the St Andrews magnitudes and the magnitudes obtained by other investigators cannot be made at this stage on account of the absence of information on the intensity of the sky background.

5. Photometry of NGC 4258

Photometry of NGC 4258 was performed with the JGT, but only one plate was found suitable, plate N9 as described in the table 1.

NGC 4258 ($\alpha = 12^h16^m.5$, $\delta = 47^o35'$(1950)) is an Sb galaxy on the Hubble classification while de Vaucouleurs classifies it as a type SAB(s)bc (de Vaucouleurs 1959). SAB means the galaxy is intermediate between the ordinary spiral type SA and the barred spiral type SB. (s) means a spiral type, and bc denotes the half way point between b, the intermediate class and c, the late class.

The isophotes obtained from plate N9 are shown in Figure 35 and the luminosity profiles in Figures 36 and 37. Figures 38 and 39 show respectively the mean luminosity profiles along the principal axes and the ellipticity curve. Outside the central region the mean axis ratio in the range $1' < a < 6'$ is $q = \langle b/a \rangle = 0.44 \pm 0.02$. Assuming for spiral galaxies that the true ellipticity for surfaces of constant

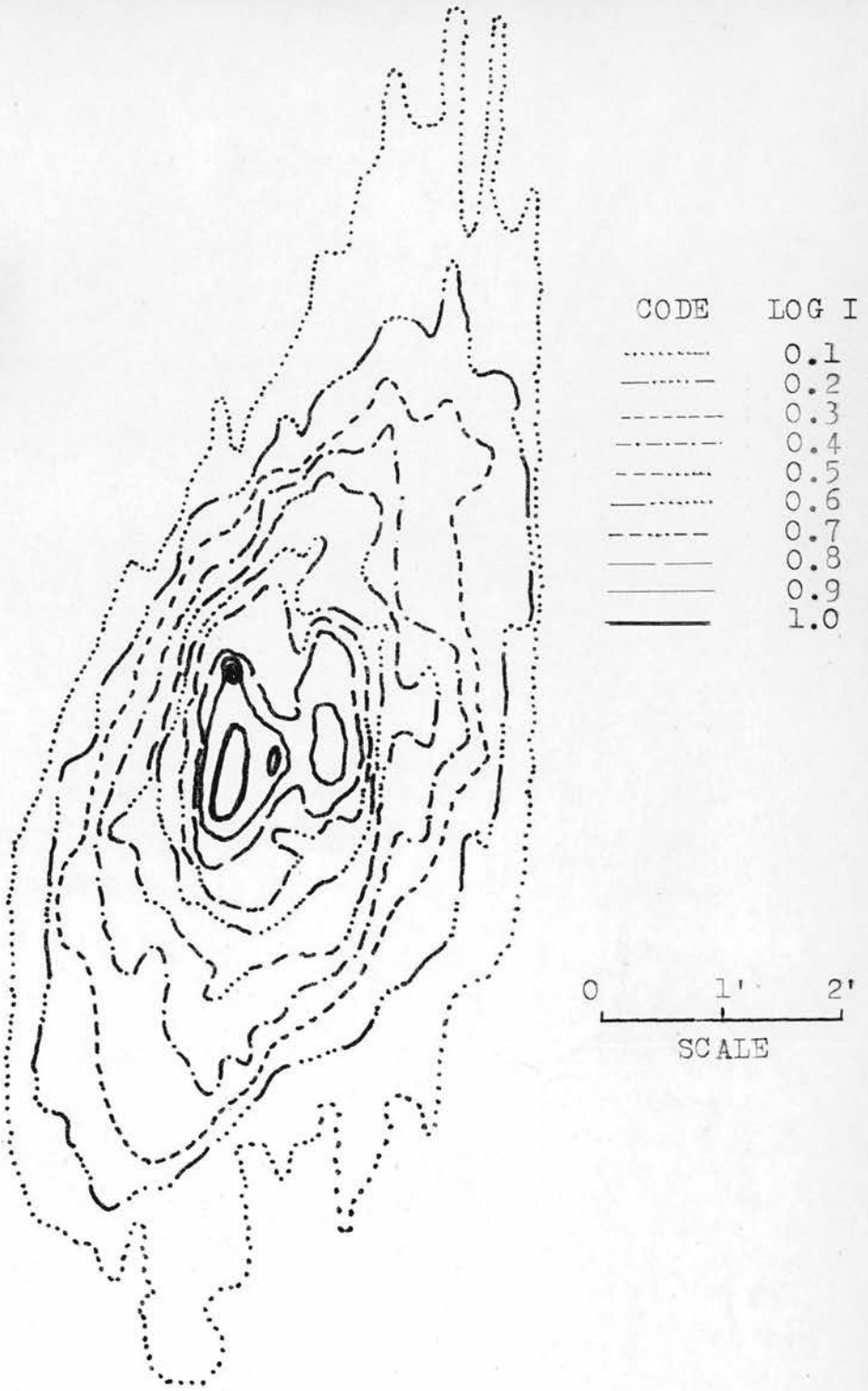

Fig. 35 --- Isophotes of NGC 4258. V-FILTER.
PLATE N9.

Fig. 36 --- Luminosity profile of the major axis of NGC 4258. V-FILTER.

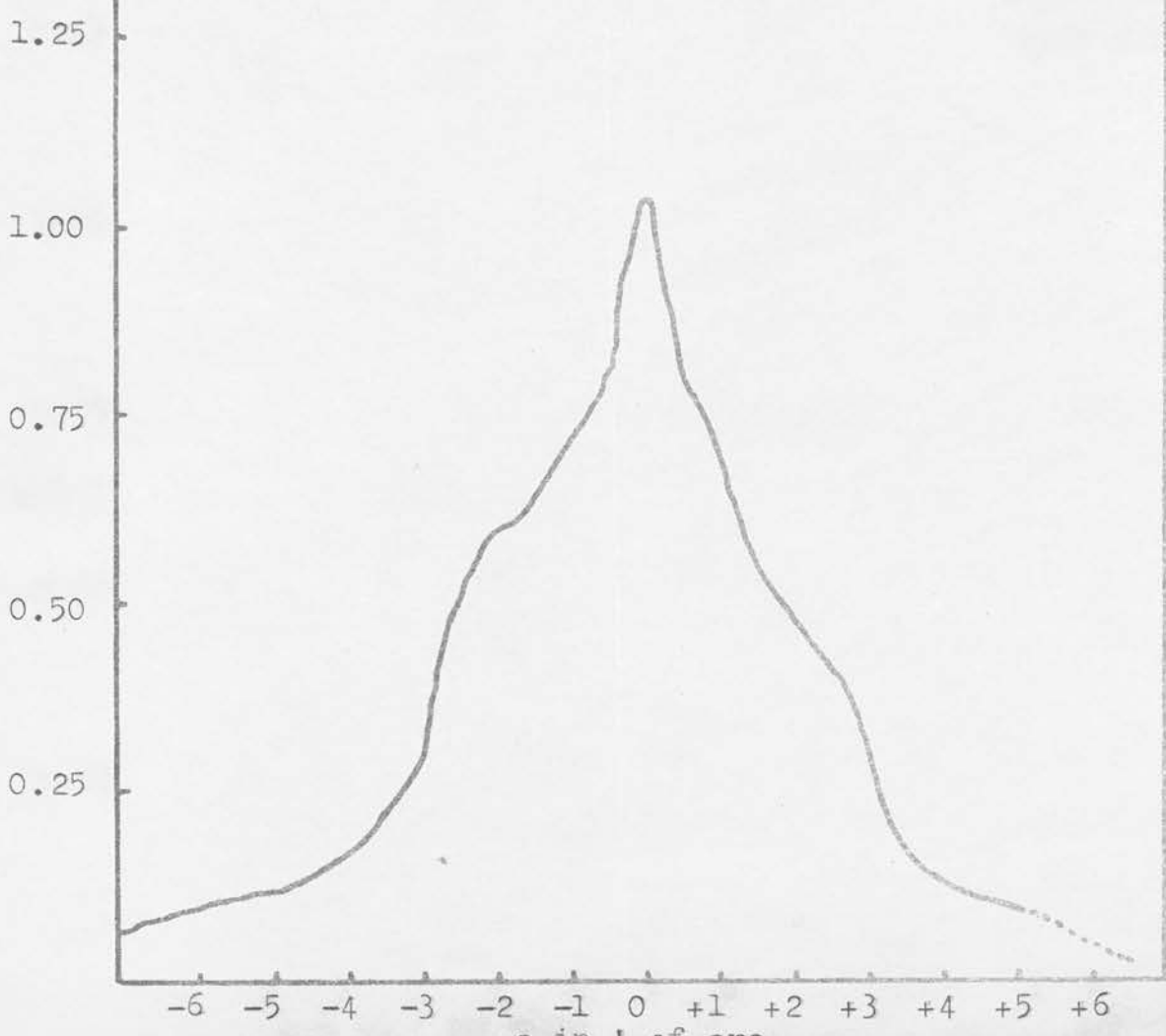

Fig. 37 --- Luminosity profile of the minor axis of NGC 4258. V-FILTER.

Fig. 38 --- Mean luminosity profiles along main axes. NGC 4258. V-FILTER.

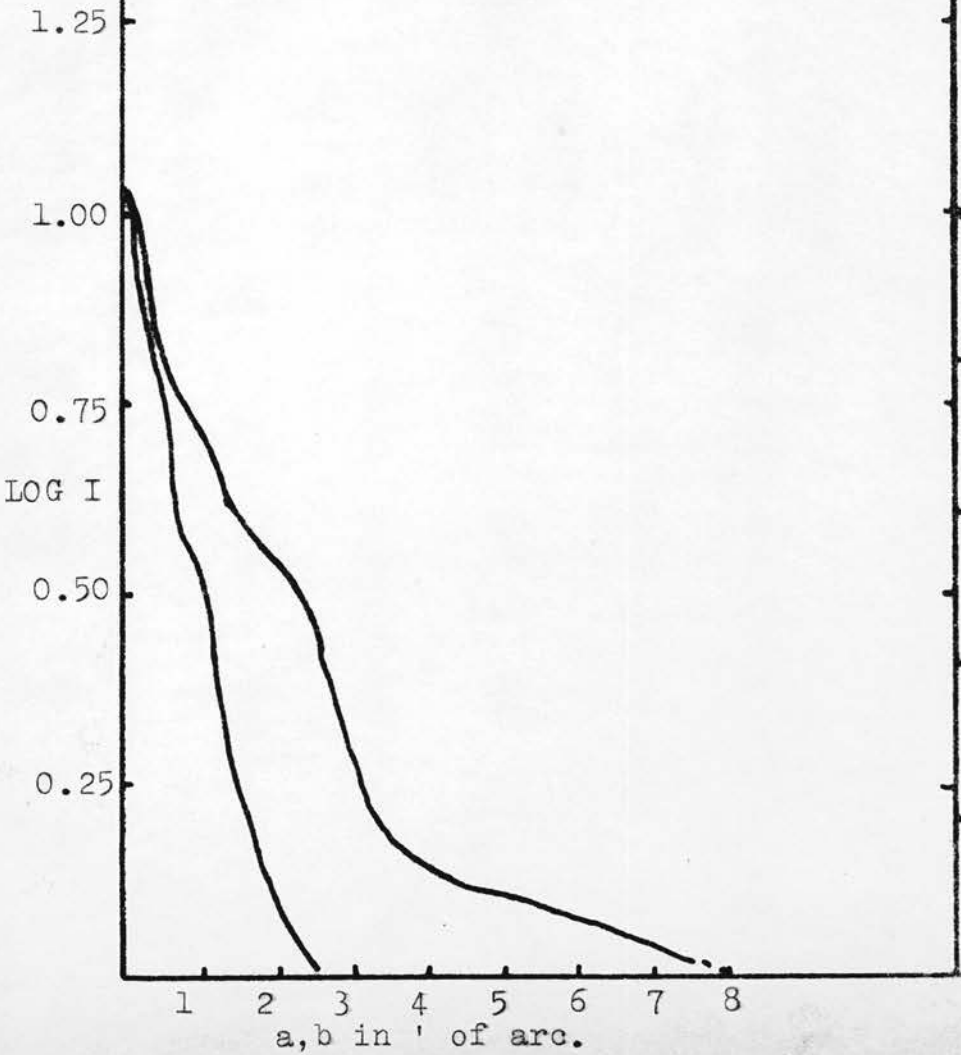

Fig. 39 --- Ellipticity curve. Axis ratio b/a along the main axes versus mean semi-major axis a of the isophotes.

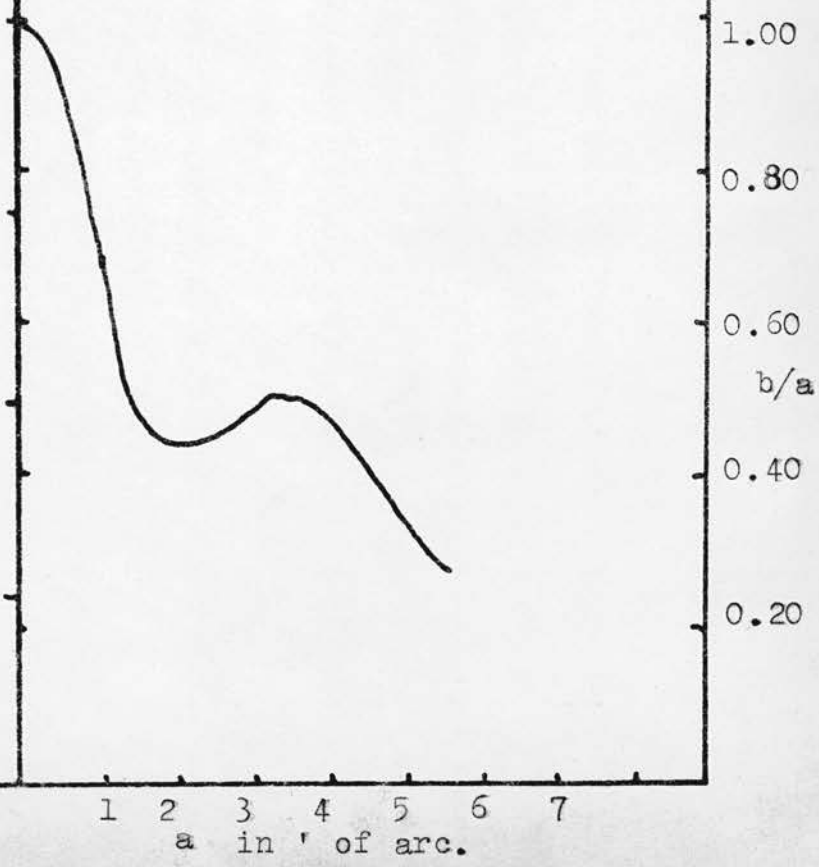

luminosity is ρ =0.2 (Holmberg 1946), the inclination of the principal plane of NGC 4258 is given by $\sin^2 i=(q^2-\rho^2)/(1-\rho^2)=0.156$ and $i=23^\circ 30' \pm 2^\circ$. Figures 40 and 41 show the equivalent luminosity profile and the relative integrated luminosity profile respectively, and table 6 gives the mean luminosity distribution. The other parameters described in the photometry of NGC 4111 are given in the classified list of parameters in table 7. The distance modulus m-M is calculated using a value for the red-shift of 494km./sec(Humanson et al 1956).

TABLE 6 MEAN LUMINOSITY DISTRIBUTION IN NGC 4258

logI	I	A	ΔA	P=I×ΔA	ΣP	k(a)	r*	a	b/a	α	J	logJ
1.35	13	0			0	0	0	0	1	0	4.96	0.70
			0.195	2.25								
1.00	10	0.195			2.25	0.032	0.25	0.25	1	0.10	3.8	0.58
			0.55	4.45								
0.8	6.3	0.7			6.7	0.095	0.46	0.50	0.95	0.20	2.4	0.38
			2.4	9.8								
0.6	3.9	3.1			16.5	0.23	0.99	1.4	0.50	0.56	1.48	0.17
			6.7	21.0								
0.4	2.5	9.8			37.5	0.53	1.76	2.6	0.45	1.04	0.95	1.97
			6.2	12.4								
0.2	1.5	16.0			49.9	0.70	2.25	3.2	0.50	1.28	0.57	1.76
			15.0	21.0								
00.1	1.25	31.0			70.9	1.0	3.14	5.2	0.37	2.08	0.47	1.67

A in square minutes

Fig. 40 --- Equivalent luminosity profile for NGC 4258. V-FILTER.

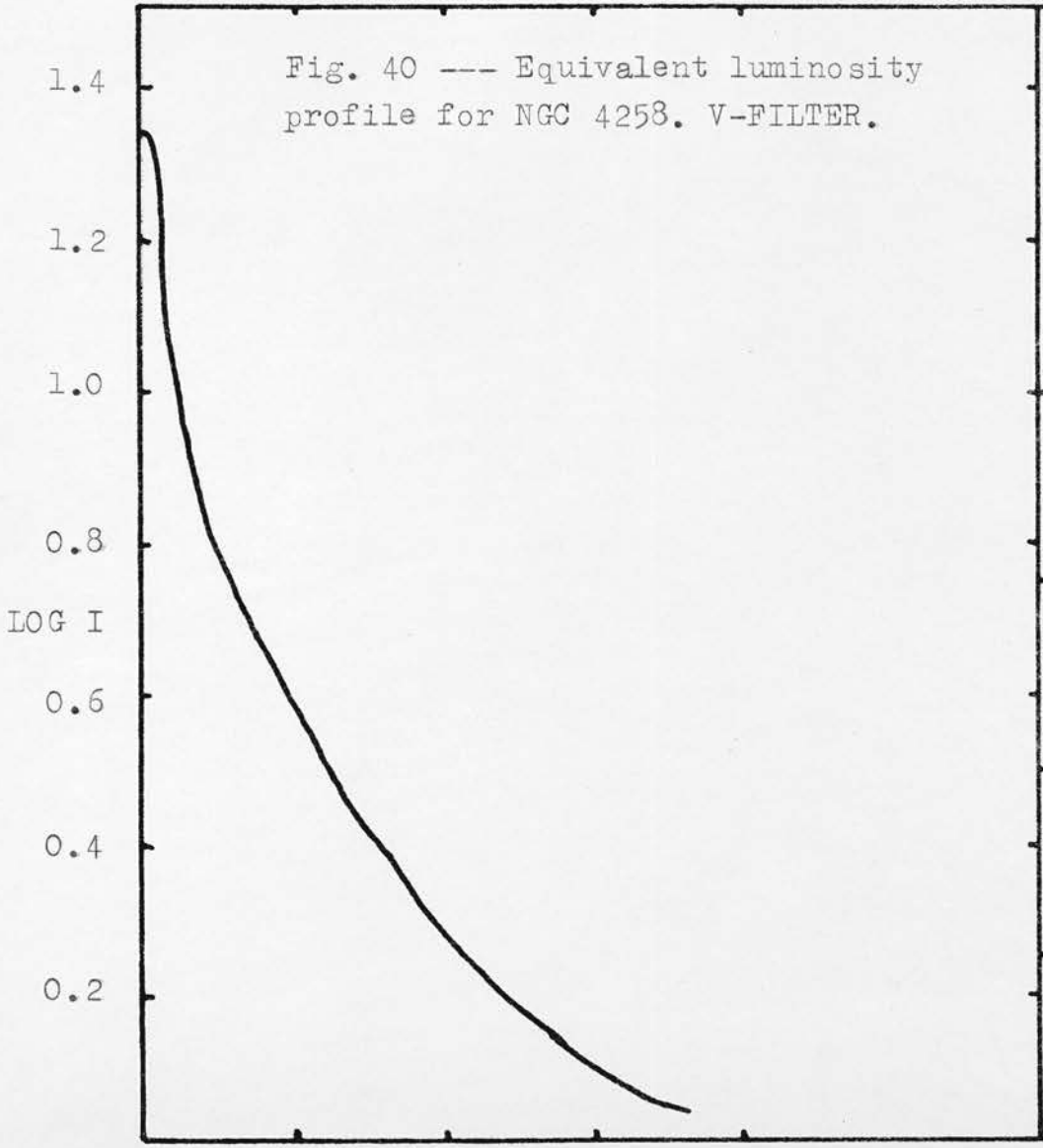

Fig. 41 --- Relative integrated luminosity curve:- k(r) against r^*.

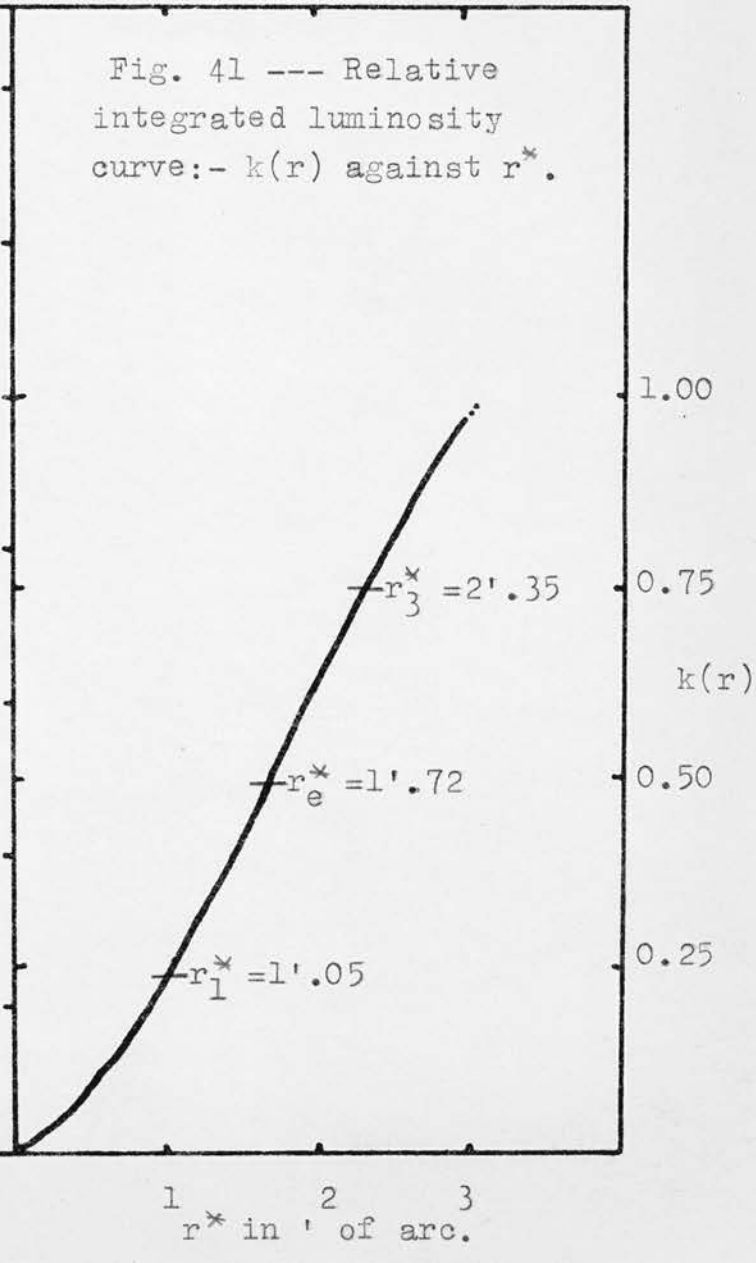

TABLE 7

PARAMETERS OF NGC 4258 IN THE V WAVELENGTH

Apparent distance modulus.		m-M=28.47
Integrated luminosity(units per square minute).	L_T	=70.9
Adopted sky unit(mag.min.$^{-2}$)	μ_s	=12.72
Total apparent magnitude.	m_T	=8.22
Absolute magnitude.	M_T	=20.25
Absolute luminosity($\odot$=1). . . . . .log		=10.40
Major position angle.	θ	=72°+3°
Mean axis ratio $\langle b/a \rangle$ (1'<a<6'). . . .	q	=0.44 0.02
Inclination.	i	=23°.5+2°
Parameters at k=1/4		
Semi-major axis.	a_1	=1'.1=0.158kpc.
Axis ratio. . . . . b/a		=0.45
Equivalent radius. . . . . .r_1*		=1'.05=0.150kpc
Parameters at k=1/2		
Semi-major axis. . . . . .a_e		=2'.5=0.36kpc
Axis ratio. . . . . b/a		=0.46
Equivalent radius . . . . . r_e*		=1'.72=0.246kpc
Mean surface brightness (mag.sec.$^{-2}$).	μ_e'	=20.3
Parameters at k=3/4		
Semi-major axis. . . . . .a_3		=3'.7=0.53kpc
Axis ratio. . . . . .b/a		=0.42
Equivalent radius. . . . . .r_3*		=2.35=0.35kpc

Concentration indices. . . . . $C_{21}=1.64$

$C_{32}=1.37$

Equivalent Gradient of exponential component. . . . $G(r^*)=0.28\text{min.}^{-1}=1.94\text{kpc}^{-1}$.

The value of $m_T=8.66$ is higher than de Vaucouleurs value (1959). This can possibly be explained by the fact that since the sensitivity of the OaF emulsion, which was used with the V-filter, falls off at around 500A° greater than the OaD emulsion normally used with the V-filter for V photometry, the resultant effective wavelength range is increased by around 500 A° and the total magnitude is therefore greater. Furthermore, the sky brightness over the longer wavelength region will vary, not necessarily by the same amount as that experienced by the galaxy, hence the adopted value of 12.72 mag.min.$^{-2}$ is subject to error. The use of an OaF plate with a V-filter for the photometry of NGC 4258 was dictated by the plate supply position when the observational work on the object was carried out. A new batch of OaD plates manufactured by Kodak(London) was available at the time, and these new plates were found to be so excessive in their grain, and so chemically fogged as to be unsuitable for precise photometry. Accordingly, it was decided to select the OaF plates which gave the best resolution of the spiral arms to enable a study to be made of the photometry of an object with detailed spiral structure.

CHAPTER IV

1. Introduction

Photographic surface photometry with interference filters makes it possible to carry out the photometry of objects without the disturbing influence of the sky background. This arises from the fact that if the luminosity of an object, such as a planetary nebula, is confined to emission lines, the resolution of the lines by means of an interference filter enables an adequate exposure to be obtained of such a nebula with only a very small fraction of the flux from the sky background which would produce appreciable sky fog in an exposure with an ordinary filter. In this chapter, an account is given of the surface photometry of two planetary nebulae with contrasting distributions of intensity. The work is essentially a test of the methods already described in the previous chapter for the surface photometry of galaxies.

Photographic photometry was performed on NGC 6720 and NGC 6543 in the emission lines $H\beta$ and N_1+N_2 using the Grubb Parson interference filters described in chapter II. The plate material used for the photometry of these objects is listed in Table 1.

TABLE 1.

PLATE MATERIAL FOR PHOTOMETRY OF NGC 6543 AND NGC 6720

PLATE	OBJECT	TELESCOPE	EMULSN.	FILTER	DATE	EXPOSURE
PN1	NGC 6543	JGT	OaO	N_1+N_2	12/13.5.1964	2^m.
PN2	NGC 6543	JGT	OaO	H	12/13.5.1964	4^m.
PN3	NGC 6720	JGT	OaO	N_1+N_2	19/20.5.1964	60^m.
PN4	NGC 6720	JGT	OaO	H	1/2 .6.1964	40^m.

NGC 6543($\alpha=17^h58^m.8, \delta=+66^o38'(1950)$) is a planetary nebula with diameter 22 seconds of arc and is slightly elliptical in shape, while the planetary NGC 6720($\alpha=18^h57^m.7$, $\delta=+32^o58'(1950)$) with dimensions of 83×59 seconds of arc has a ringed structure, from which it derives its usual description as the Ring Nebula.

In this work, it proved possible to take more than one exposure of a particular object on each plate, since, when using an interference filter which only lets through a very small wavelength range of the spectrum, the sky background is not detectable, and so difficulties of pre and post-exposure encountered in the work of the previous chapter did not arise. In fact, exposures of several minutes were necessary to produce a measurable density on the plate after exposure of a plate behind an interference filter to a sky which was so bright that only first magnitude stars were visible to the naked eye.

The procedure followed for each object has been to obtain images with the same exposure times in Hβ and N_1+N_2

on the same plate. The only difficulty in the photometry of a planetary nebula is that for similar quantities of radiation in N_1+N_2 and Hβ reaching the photographic plate, it will appear that more Hβ radiation has been emitted from the nebula than has N_1+N_2. This is because the sensitivity of the OaO plates is already falling off slowly over the wavelength range $4864A^o < \lambda < 5012A^o$ and therefore OaJ plates would probably have been better suited to this work.

2. Isophotes

The isophotes of NGC 6543, shown in Figures 1 and 2, are found to give the dimensions as 37×24 seconds of arc compared with the accepted dimensions of 22 seconds diameter. We have seen how, in the case of NGC 4111, the instrumental profile distortion of a nebular image is serious only around the central nucleus, but with NGC 6543, where the total dimensions are of the same order of magnitude as those of the nucleus of NGC 4111, the instrumental distortion acts over the complete area of the planetary nebula, thus smoothing out the luminosity profile and making the dimensions appear greater. The isophotes of the N_1+N_2 exposure show the elliptical shape of the nebula rather better than those of the Hβ exposure; there was no need to make more than one exposure for each set of isophotes since the intensity range in this work is increased due to the elimination of the contribution to the intensity of the sky fog.

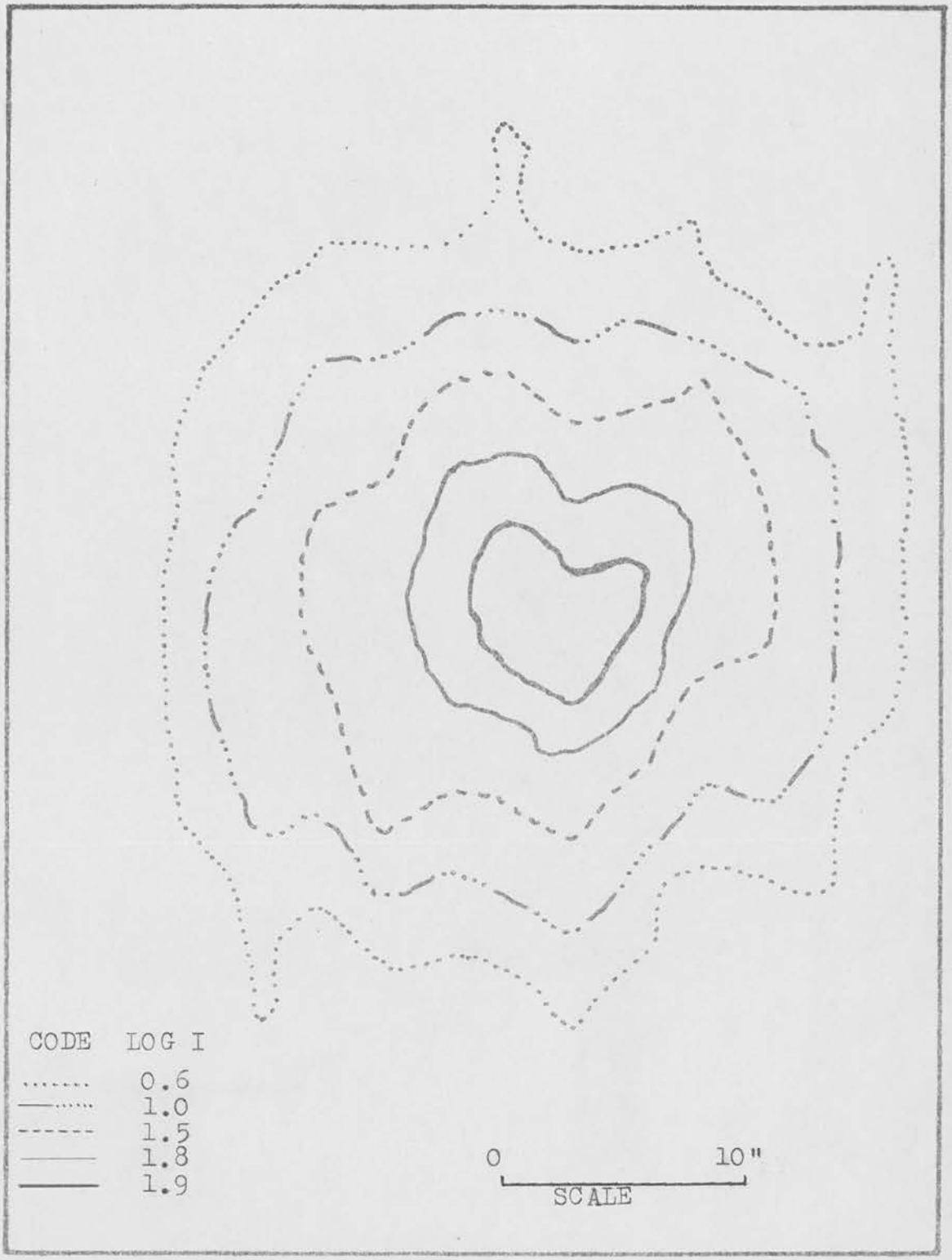

Fig. 1 --- Isophotes of NGC 6543. H_{β}-FILTER. PLATE PN2.

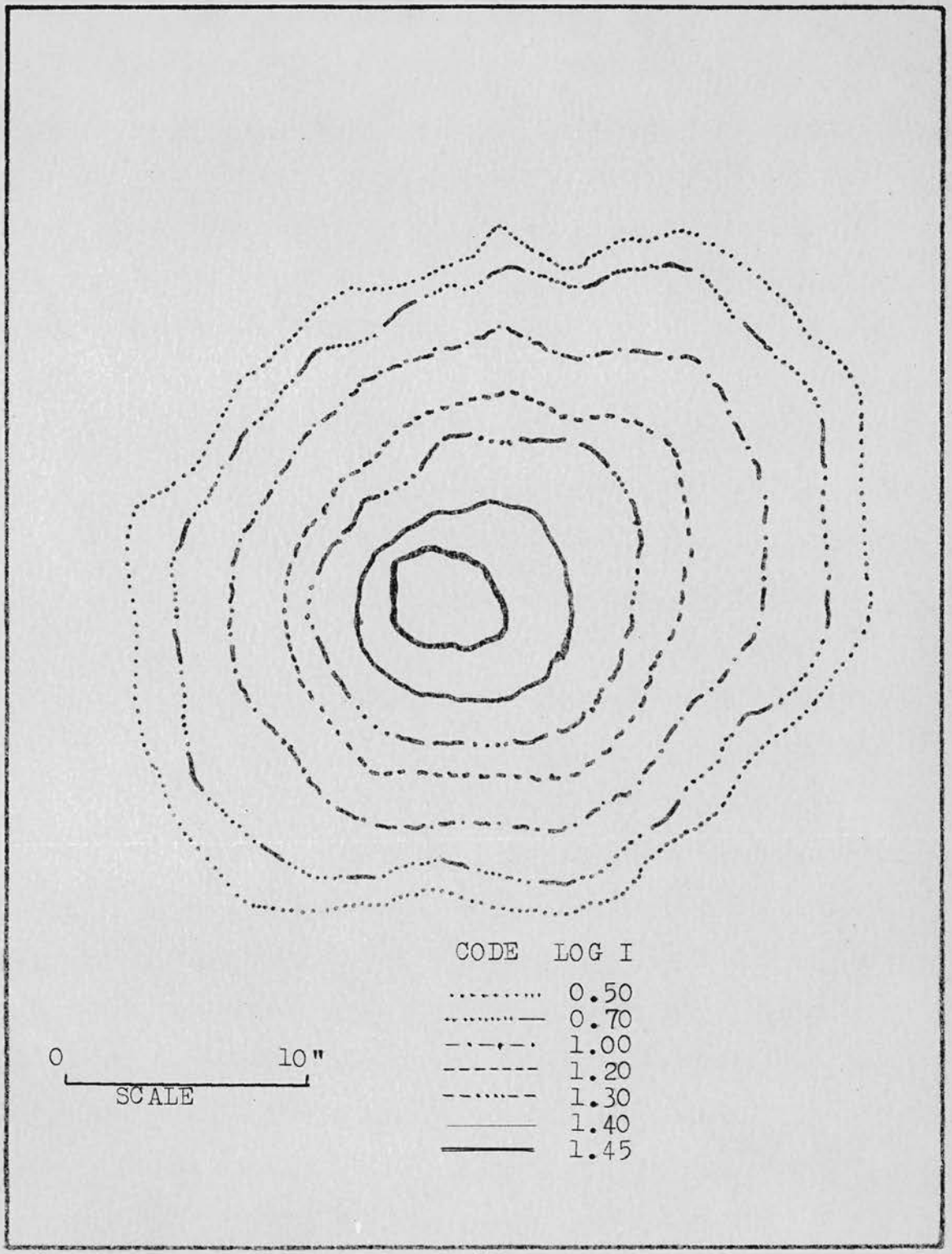

Fig. 2 --- Isophotes of NGC 6543. N_1N_2-FILTER. PLATE PN1.

In Figures 3 and 4 are found the isophotes for NGC 6720 in Hβ and N_1+N_2 respectively; the interesting feature is the characteristic sharp luminosity gradient at each end of the minor axis of the nebula. The approximate dimensions are 75×62 seconds for the Hβ image and 90×70 seconds of arc for the N_1+N_2 image; these values, together with the higher surface brightness found in the N_1+N_2 image compared with the Hβ image, suggested that NGC 6720 is richer in N_1+N_2 radiation than in Hβ.

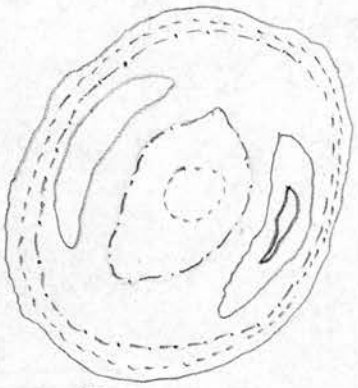

Figure 5. Isophotes of NGC 6720 obtained with Dr Koelbloed's isophotometer.

The isophotes obtained in Amsterdam on plate PN3 with Dr Koelbloed's isophotometer are shown in Figure 5. They are, of course, on a much smaller scale than those obtained using the Hilger microphotometer, because Dr Koelbloed's machine had only the one magnification scale whereas the isophotes obtained from the Hilger tracings may be constructed on any desired scale. The dark slide and clear plate readings were noted, and also the distances from the dark slide to those slits remaining open during a run. These distances were then converted to transmissions, opacities and densities; the corresponding intensities were then read off from the characteristic curve. In Figure 5, the composite result of four runs is shown: the isophotes compare favourably with those obtained in St Andrews, but a critical comparison is not possible between the two sets of

Fig. 3 --- Isophotes of NGC 6720. H_{β}-FILTER. PLATE PN4.

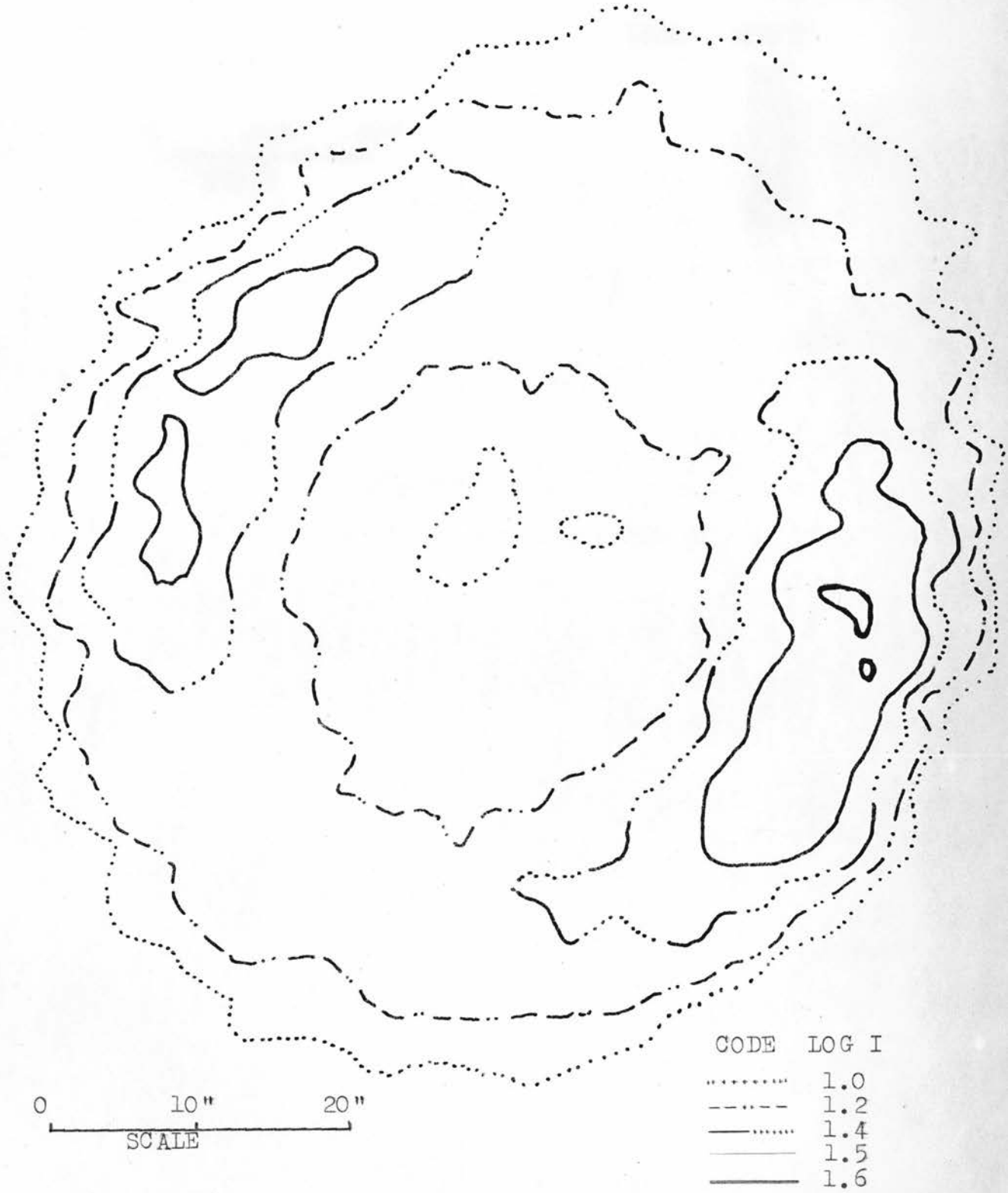

Fig. 4 --- Isophotes of NGC 6720. N_1N_2-FILTER. PLATE PN3.

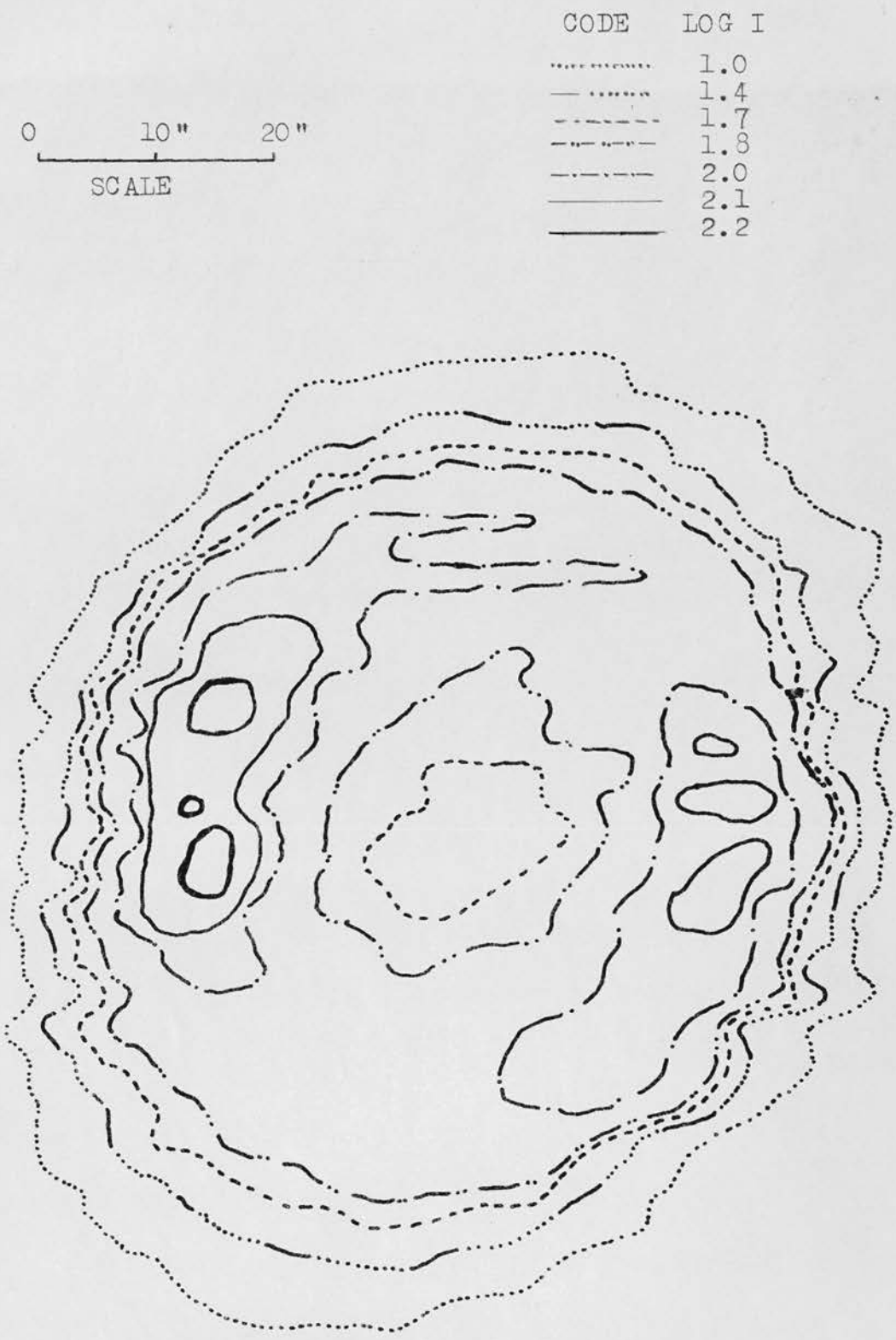

isophotes because the resolution of Dr Koelbloed's isophotometer is not sufficiently good in areas which have a steep luminosity gradient, such as at the edge of the minor axis of NGC 6720.

The object of the work on the two planetary nebulae was not to attempt to derive detailed information on the physical conditions in the nebulae from a study of the ratio of the number of photons in the forbidden oxygen lines and the hydrogen lines, but to examine the photometric difficulties in the isophotometry of these objects as a prelude to further work either photographically or photo-electrically. In principle, it is possible to use photographically determined isophotes to deduce the ratio of the number of photons from a knowledge of the peak transmission of the filters as well as the wavelength/sensitivity of the photographic emulsion used. On the other hand, the photo-electric method would appear to be more satisfactory because the number of photons could be calibrated in terms of the luminosity of standard stars or artificial energy sources.

CONCLUDING REMARKS

The photometric investigations described in this thesis were undertaken in order to establish reliable methods for the processing and measurement of photographic data obtained with the Cassegrain Schmidt telescopes of the University Observatory, and to examine in detail methods for the reduction of the data. The investigations cover the initial phase of an extensive programme of photographic work at the University Observatory on the photometry of galaxies and nebulosities which will be supplemented by photo-electric methods using equipment being designed in the Electronics Laboratory. The isophotometry will be greatly facilitated by the aquisition for the Instrument Laboratory of the isodensitracer described in chapter III. The methods of reduction and analyses described in this thesis were necessarily limited by the instrumentation available in the Laboratory during the time in which the work was undertaken.

ACKNOWLEDGEMENTS

The writer is deeply indebted to Professor D.W.N. Stibbs for the continual encouragement, the helpful suggestions and many valuable criticisms which he willingly gave during his supervision of the work for this thesis. Grateful acknowledgement is due to Dr D. Koelbloed of the Astronomical Institute of the University of Amsterdam for permission to use his new isophotometer while still in the developmental stage; also to our late colleague, Mr W. Fraser, who gave knowledgeable assistance in some practical and theoretical aspects of the photographic process. Finally, thanks are due to other members of the academic and technical staff who offered occasional advice on some aspects of the work.

The study was performed during the writer's tenure of a Department of Scientific and Industrial Research Studentship.

REFERENCES

Holmberg,E. 1946, Medd. Lund. Obs., Vol. 2,117.

Houten,C.J.van 1961, B.A.N.15,1.

Hulst,H.C.van der 1946, B.A.N. 10,75.

Humanson,M.L., Mayall,N.U. and Sandage,A.R. 1956, A.J. 61,97.

Mohler,O.C. and Pierce,A.K. 1957, Ap.J. 125,285.

Redman,R.O. and Shirley,E.G. 1936, M.N.R.A.S. 96,588.

----------. 1938, M.N.R.A.S. 98,613.

Sandage,A.R. 1962, Problems of Extra-galactic Research, I.A.U. Symposium No. 15(New York:Macmillan),p.359.

Vaucouleurs,G.de 1948, Ann. d'ap., 11,247.

----------. 1959, Handbuch der Physik(Berlin:-Springer-Verlag), 53,275.

----------. 1960, Ap.J.131,574.

----------. 1962, Ap.J.Supp. 8,31.

Vaucouleurs,G.de and Page,J. 1962, Ap.J. 136,107.